



Universidad de Granada



Dinámica Ambiental  
UNIVERSIDAD DE GRANADA

Instituto Interuniversitario de Investigación del Sistema Tierra en  
Andalucía (IISTA)

Programa de Doctorado de Dinámica de Flujos Biogeoquímicos y sus  
Aplicaciones

Universidad de Granada

**Alongshore sediment transport on curvilinear coasts  
and implications on shoreline evolution**

**Doctoral Thesis**

Alejandro López Ruiz  
Advisor: Miguel Ortega Sánchez  
April 2014

Editor: Editorial de la Universidad de Granada  
Autor: Alejandro López Ruiz  
D.L.: GR 1928-2014  
ISBN: 978-84-9083-099-4

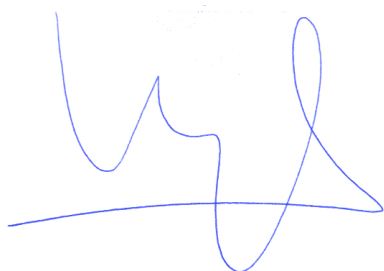




El doctorando **Alejandro López Ruiz** y el director de la tesis **Miguel Ortega Sánchez**, garantizamos, al firmar esta tesis doctoral, que el trabajo ha sido realizado por el doctorando bajo la dirección de los directores de la tesis y hasta donde nuestro conocimiento alcanza, en la realización del trabajo, se han respetado los derechos de otros autores a ser citados, cuando se han utilizado sus resultados o publicaciones.

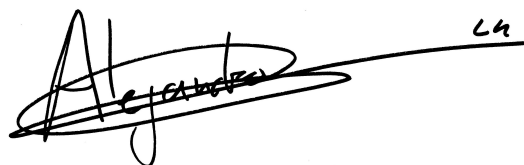
Granada, a 9 de abril de 2014.

Director de la tesis:



Fdo.: Miguel Ortega Sánchez

Doctorando:



Fdo.: Alejandro López Ruiz



# Agradecimientos

---

Este trabajo no hubiese sido posible sin la ayuda de muchas personas a las que quiero expresar mi gratitud.

El primer lugar, quiero agradecer a mi director de Tesis, Miguel Ortega, toda la ayuda y la formación recibidas, su dedicación, su paciencia y sus consejos. Todo empezó hace 6 años en las clases de la Escuela, y espero que sigamos trabajando juntos en el futuro. Quiero darle las gracias a Miguel Losada por todo lo que he aprendido de él, tanto en los malos como en los buenos momentos, y por hacerme pensar y darle una vuelta de rosca más a las cosas.

Gracias a toda la gente del Grupo de Dinámica de Flujos Ambientales por su paciencia y la ayuda recibida. Mi gratitud también a Stefano Lanzoni y a Mario Putti por su hospitalidad, dedicación e interés durante mi estancia en la Universidad de Padua. Tenemos trabajo pendiente.

Agradezco al Ministerio de Educación, Política Social y Deporte la concesión de una ayuda FPU.

Además de a mis copañeros y mentores, quiero darle las gracias a muchas personas que han contribuido a mantener mi ánimo y las ganas de ir a trabajar cada día, sirviéndome de un apoyo sin el que hubiera sido imposible llegar hasta aquí.

A mis padres Paco y María Dolores por su apoyo, cariño y comprensión. Como ya dijo mi hermano, son los mejores padres que se puede tener. A mi hermano Paco, por toda su ayuda y motivación, por enseñarme tanto. Sin él nunca me hubiese picado la curiosidad de la investigación. Aunque ahora vivas en Cádiz siempre te tengo cerca.

A los Rafas y a Alfonso. Sin ellos esto hubiese sido mucho más difícil y sobre todo aburrido. Gracias por estar siempre ahí, os quiero. También quiero darle las gracias a todos los que habéis hecho la vida en el CEAMA más divertida y agradable: Carmen, Pedro, Javi, ... Sin los ratos de charlas no hubiese sido lo mismo. A Chosé, y por supuesto a todos mis amigos de la carrera. Aunque estéis por el mundo y nos hayáis dejado huérfanos os sigo teniendo cerca.

Y sobre todo, a Alicia, por toda la felicidad que me das. A ella le dedico este trabajo.



*Para Alicia*



# Resumen

---

Las costas que pueden encontrarse alrededor del mundo suelen ser rectilíneas o tener una curvatura suave. Además, suelen presentar muchos tipos de morfologías de distintas dimensiones que se superponen a la alineación media de la playa. En esta Tesis se estudia la morfodinámica de costas con curvatura suave (en las que el radio de curvatura es mayor de 1000 m) y los procesos físicos relacionados en la formación de morfologías rítmicas en la línea de costa. Entre esas morfologías, este trabajo se centra en las ondulaciones de línea de costa (*shoreline undulations, SU*), que se definen como morfologías de media a gran escala que tienen dimensiones que oscilan entre cientos y miles de metros en la dirección de la alineación media de la costa y entre decenas y cientos de metros en la dirección transversal a la costa.

Para ello se ha definido una metodología paso a paso. Primero, los lugares donde estas SU aparecen han sido identificados y caracterizados a lo largo de 50.000 km de costa en 15 países, almacenando diferentes datos que han sido recogidos en una base de datos europea. Tras el análisis de la información obtenida, se ha concluido que las SU están muy relacionadas con al menos una de las siguientes peculiaridades: (1) una costa con una alineación media curva; (2) un cambio brusco en la alineación media; y (3) la presencia de obstáculos artificiales en las cercanías. También están relacionadas con un clima marítimo caracterizado por un oleaje de bajo contenido energético y condiciones micro o mesomareales.

El segundo paso es la identificación y cuantificación de los efectos que las costas curvilíneas tienen en los patrones de propagación del oleaje. Esto se ha realizado utilizando observaciones *in situ* registradas mediante video imágenes y con los resultados de un modelo numérico. Tras el análisis de los resultados, se ha concluido que la presencia de batimetrías curvilíneas provoca importantes variaciones longitudinales en el contenido energético y en el ángulo del oleaje. Estas dos variables tienen un papel clave en el transporte longitudinal de sedimentos.

El tercer paso es la adaptación de una expresión del transporte longitudinal de sedimentos para que éste considere los procesos físicos propios de costas curvilíneas, como los efectos en la propagación del oleaje de una batimetría curvilínea o las variaciones longitudinales en las características de la playa (pendiente, ángulo de la línea de costa o tamaño del sedimento). Esta aproximación ha sido concebida como una herramienta sencilla para su uso en la ingeniería de costas, que a su vez permita entender cómo las diferentes variables ambientales, hidrodinámicas y morfológicas afectan e interactúan con la evolución morfológica de la costa. Se ha realizado también un esfuerzo para evitar restricciones en cuanto a los valores que pueden tomar las variables analizadas.



Para obtener una expresión analítica del transporte longitudinal de sedimentos se han escogido dos modelos sencillos para la refracción del oleaje, obteniendo así dos expresiones distintas. Sin embargo, podría utilizarse cualquier otra solución para la refracción mediante una integración numérica.

El siguiente paso es el análisis del comportamiento y las implicaciones de la expresión del transporte de sedimentos obtenida anteriormente, así como de sus consecuencias en la hidrodinámica (setup y ondas de borde). Para ello, se han realizado diferentes experimentos numéricos con distintas configuraciones de playa y condiciones del oleaje. Los resultados muestran tres tendencias distintas en la línea de costa para playas con ondulaciones: migración de las ondulaciones cuando hay cambios en la dirección del oleaje en profundidades indefinidas, aumento de la amplitud para incrementos en la altura de ola o el periodo del oleaje, y asimetrías y cambios en la longitud de onda para costas con variaciones longitudinales de la pendiente. Los resultados también indican que el setup asociado a este tipo de playas puede favorecer la formación de ondulaciones en la costa.

El quinto paso es la definición de un modelo de evolución morfológica basado en la expresión del transporte longitudinal de sedimentos obtenida en esta Tesis: el modelo oneline. El análisis analítico de este modelo permite comparar los resultados obtenidos en este trabajo con las aproximaciones publicadas recientemente por otros autores. Este análisis muestra que al contrario que con esas aproximaciones, con el enfoque de esta Tesis las morfologías de la línea de costa en costas curvilíneas pueden aparecer sin la presencia de oleaje con gran oblicuidad.

Finalmente, el último paso de la metodología es la aplicación de una solución numérica del modelo de una línea desarrollado en la fase anterior a distintas localizaciones en las que se han identificado ondulaciones en la costa. Los resultados del modelo reproducen correctamente la situación, amplitud y longitud de onda de las ondulaciones observadas en dos frentes de flechas litorales situadas en el estuario del Guadalquivir (Huelva) y en la Bahía de Santander. Las asimetrías observadas en el sistema punta-bahía de la playa de Carchuna (Granada) también se han reproducido satisfactoriamente. Además, resultados preliminares obtenidos en un tramo de costa adyacente a la desembocadura del río Guadalfeo (Granada), muestran que tanto un déficit en el sedimento disponible como la presencia de irregularidades en la batimetría pueden desencadenar la formación de ondulaciones en la línea de costa.

# Abstract

---

Coastlines around the world are frequently rectilinear or weakly curved; they exhibit a wide range of shoreline morphological features of different dimensions superimposed. This Thesis studies the morphodynamics of weakly curvilinear coasts (radius of curvature greater than 1000 m) and the physical processes involved in the development of rhythmic shoreline features. Among these features, this work focuses on shoreline undulations, which are defined as medium to large spatial-scale shoreline features that have along-shore dimensions ranging from hundreds to thousands of meters and cross-shore widths from tens to hundreds of meters.

This is accomplished using a sequential methodology. First, the locations where these shoreline undulations develop are identified and characterized. For that, these features were identified along 50,000 kms and 15 countries, and different fields of data were collected and included into an European database. Results show that shoreline undulations are strongly related to the presence of at least one of the following peculiarities: (1) a curvilinear mean alignment of the coast; (2) a sudden change in the beach alignment; and (3) the presence of artificial or natural obstacles nearby. The wave climate that favors their appearance is characterized by mild waves and micro or mesotidal conditions.

The second step is the identification and quantification of the effects that these types of coasts have on the wave propagation patterns. This is accomplished through field evidences from video imagery and results of a numerical wave propagation model. After the analysis of the results, it is concluded that the presence of curvilinear bathymetries trigger significant alongshore variations in wave energy and wave angle. Both variables are of major importance for the alongshore sediment transport.

The third step is the update of an expression for the alongshore sediment transport to include the main characteristic processes involved on curvilinear coasts, as the effect of a curvilinear bathymetry on wave propagation or the alongshore variations on coast characteristics, i.e. beach slope, shoreline angle or sediment size. This approach was conceived as a simple coastal engineering tool to understand how the different environmental, hydrodynamical and morphological variables affect and interact with the shoreline morphology evolution. An effort was made to avoid restrictions on the variables analyzed. To develop the analytical formulation for the alongshore sediment transport, two different simple models for wave refraction were chosen obtaining two final expressions, but any other solution for wave refraction could be used.

The following step is the analysis of the implications of the alongshore sediment transport expression previously obtained. Numerical experiments with different beach and

wave climate characteristics are performed, and the hydrodynamical consequences are also examined. Three different shoreline tendencies were obtained for undulating shorelines: migration for changes in deep-water wave angle; amplitude growth for increases in wave height or wave period and changes in shoreline geometry; and wavelength changes and asymmetries for coasts with alongshore changes in beach slope. The results also indicate that wave setup may enhance the formation of undulating shoreline features.

The fifth step is the definition of a morphological evolution model based on the along-shore sediment transport expression: a one-line type model. An analytical analysis of this model is used to compare the results derived with the presented alongshore sediment transport expression with other recent works. This analysis shows that, unlike these works, with our approach shoreline features develop on curvilinear coasts without the presence of waves with great obliquity respect to the shore.

Finally, the last step of the methodology is the application of a numerical solution of the one-line model developed in this Thesis to different specific locations exhibiting shoreline undulations. The results of the model are in good agreement with nature in terms of location, amplitude and wavelength of the undulations for two prograding spit fronts in the Guadalquivir Estuary (Southern Spain) and the Santander Bay (Northern Spain). The asymmetries of a horn-embayment system in Carchuna Beach (Southern Spain) are also reproduced. Moreover, preliminary results on a track of coast near a river mouth indicate that both deficits in the available sediment and irregularities in the bathymetry may trigger the formation of shoreline undulations.

# Contents

---

<b>Contents</b>	<b>xi</b>
<b>List of Figures</b>	<b>xv</b>
<b>List of Tables</b>	<b>xxi</b>
<b>1 Introduction</b>	<b>1</b>
1.1 Coastline morphology . . . . .	1
1.2 Physical processes . . . . .	2
1.3 Objectives . . . . .	3
1.3.1 Main objective . . . . .	3
1.3.2 Specific objectives . . . . .	4
1.4 Outline of the Thesis . . . . .	4
1.5 Publications derived from this Thesis . . . . .	5
<b>2 Shoreline undulations</b>	<b>7</b>
2.1 Definition . . . . .	7
2.2 Examples . . . . .	8
2.3 European database . . . . .	9
2.3.1 Material and methods . . . . .	10
2.3.2 Results . . . . .	13
2.3.2.1 Regional analysis . . . . .	13
2.3.2.2 Series of undulations and type of coast . . . . .	16
2.3.2.3 Constraints . . . . .	17
2.3.2.4 Geometric analysis . . . . .	18
2.3.3 Spain: a country-scale example of the database . . . . .	20
2.3.4 Discussion . . . . .	22
2.3.4.1 Geometry and shape of the shoreline undulations . . . . .	22
2.3.4.2 Influence of the tides and waves . . . . .	22
2.3.4.3 Forming materials . . . . .	25
2.3.5 Conclusions derived from the European database . . . . .	26
<b>3 Curvilinear coasts (I): effects on wave propagation</b>	<b>27</b>
3.1 Introduction . . . . .	27
3.2 Evidences on nature . . . . .	28
3.3 Numerical results . . . . .	30

3.3.1	Surf zone width variations . . . . .	30
3.3.1.1	Prograding spit front . . . . .	31
3.3.1.2	Undulating coast . . . . .	33
3.3.2	Wave angle variations . . . . .	34
3.3.2.1	Prograding spit front . . . . .	34
3.3.2.2	Undulating coast . . . . .	36
3.4	Conclusions . . . . .	36
<b>4</b>	<b>Curvilinear coasts (II): alongshore sediment transport</b>	<b>39</b>
4.1	Framework and assumptions . . . . .	39
4.2	An updated expression for the AST . . . . .	42
4.3	First approach . . . . .	44
4.3.1	Surf zone width-dependent sediment transport . . . . .	45
4.4	Second approach . . . . .	46
4.4.1	Surf zone wave angle approximation . . . . .	48
4.4.2	Surf zone wave height . . . . .	51
4.4.3	Specific solution for alongshore sediment transport . . . . .	53
<b>5</b>	<b>Implications on coastal evolution (I): shoreline movements and hydrodynamics</b>	<b>55</b>
5.1	Numerical experiments and overall procedure . . . . .	55
5.2	Results . . . . .	56
5.2.1	Deep-water wave angle . . . . .	57
5.2.2	Wave period . . . . .	58
5.2.3	Deep-water wave height . . . . .	59
5.2.4	Shoreline geometry . . . . .	60
5.2.5	Beach slope and sediment size . . . . .	60
5.3	Discussion . . . . .	61
5.3.1	Erosion-deposition patterns . . . . .	62
5.4	Consequences on nearshore coastal morphodynamics . . . . .	64
5.4.1	Wave energy dissipation and setup . . . . .	64
5.4.2	Edge waves . . . . .	66
<b>6</b>	<b>Implications on coastal evolution (II): shoreline modeling</b>	<b>67</b>
6.1	Online modeling . . . . .	67
6.1.1	Hypothesis and governing equation . . . . .	68
6.2	Diffusivity analysis . . . . .	70
6.2.1	Diffusivity of the first approach for the alongshore sediment transport . . . . .	70
6.2.2	Diffusivity of the second approach for the alongshore sediment transport . . . . .	71
6.2.3	Conclusions . . . . .	73
<b>7</b>	<b>Applications</b>	<b>75</b>
7.1	Introduction . . . . .	75
7.2	Application to undulations on prograding spit fronts . . . . .	75
7.2.1	Circular spit front: Doñana . . . . .	76
7.2.1.1	Study zone . . . . .	76

7.2.1.2	Shoreline simulations . . . . .	77
7.2.1.3	Analysis of the results . . . . .	79
7.2.2	Elliptical spit front: El Puntal . . . . .	80
7.2.2.1	Study zone . . . . .	80
7.2.2.2	Shoreline features events . . . . .	81
7.2.3	Comparison with observations . . . . .	83
7.3	Application to a horn-embayment system . . . . .	84
7.3.1	Carchuna beach system . . . . .	84
7.3.1.1	Coastal morphology . . . . .	84
7.3.1.2	Submarine geomorphology and sediments . . . . .	84
7.3.1.3	Oceanographic regime . . . . .	86
7.3.2	Influence of the submarine canyon on wave propagation . . . . .	86
7.3.2.1	Bathymetric scenarios . . . . .	86
7.3.2.2	Numerical model . . . . .	87
7.3.2.3	General energy distribution and littoral drift trends . . . . .	89
7.3.2.4	Influence of the canyon . . . . .	90
7.3.2.5	Influence of the submerged IPW undulations . . . . .	92
7.3.2.6	Conclusions . . . . .	93
7.3.3	Interaction between the submarine and coastline morphologies . . . . .	94
7.4	Application to an erosional stretch of coast . . . . .	96
<b>8</b>	<b>Conclusions and future research</b>	<b>99</b>
8.1	Main conclusions . . . . .	99
8.2	Future research . . . . .	102
<b>A</b>	<b>Wave climate simulation</b>	<b>109</b>
A.1	Significant wave height . . . . .	110
A.1.1	Non-stationary distribution function . . . . .	110
A.1.2	Temporal dependence . . . . .	111
A.1.2.1	Markov model of first order . . . . .	112
A.1.2.2	Markov model of second and higher orders . . . . .	112
A.1.3	Application to the Gulf of Cádiz . . . . .	112
A.2	Peak wave period and mean wave angle . . . . .	114
A.2.1	Non-stationary distribution functions and normalization of the variables . . . . .	114
A.2.1.1	Peak period . . . . .	114
A.2.1.2	Mean direction . . . . .	114
A.2.1.3	Normalization of the variables . . . . .	115
A.2.2	Vector Autoregressive (VAR) Model . . . . .	115
	<b>Bibliography</b>	<b>117</b>



# List of Figures

---

1.1	Coastline features on curvilinear coasts: a) Sandy spit of Sylt Island, Germany; b) Shoreline undulations in Créances, France; c) Beach cusps in Trafalgar Beach, Spain (Ortega-Sánchez et al., 2008b); d) Large-scale cusate features in Carchuna Beach, Spain. White lines in b) and d) show the shape of the shoreline undulations and the large-scale cusate features, respectively. The triangles indicate the location of the geographical coordinates shown. Images for a), b) and d) are courtesy of Google Earth. . . . .	3
2.1	Shoreline undulations on prograding spit fronts: a) Sylt Island Spit, Germany; b) Cape Lookout Spit, North Carolina, USA; c) Arçay Spit, France; d) Sandy Hook Spit, USA; e) Doñana Spit, Spain; f) El Puntal Spit, Spain [courtesy of Google Earth and Apple Inc.]. The white dashed lines highlight the geometry of the features. . . . .	9
2.2	Examples of sites exhibiting SU related to coasts with a sudden change in the beach orientation or with the presence of a constraint: a) Beach close to Créances, France; b) Pellaro, Southern Italy; c) Coast of Pénestin, France; d) Calahonda, Málaga, Spain; e) Marbella, Málaga; f) Termini, Italy [courtesy of Google Earth and Apple Inc.]. The white dashed lines highlight the geometry of these undulations. . . . .	10
2.3	Coastline of the European and Northern African countries that were analysed (grey line). . . . .	11
2.4	General geometry of a series of shoreline undulations. $a$ - amplitude; $\lambda$ - wavelength; $a_c$ - amplitude of the crest; $a_s$ - amplitude of the sine; $\lambda_c$ - wavelength of the crest; $\lambda_s$ - wavelength of the sine. . . . .	12
2.5	Sites where shoreline undulations were identified. The legend of the figure corresponds to the number of individual shoreline undulations at each site. . . . .	14
2.6	Regions (1 to 15) within the area of study that were divided to describe the collected data. . . . .	15
2.7	Relationship between the number of undulations and the number of sites. The line corresponds to the fitting of the data to a cubic function. . . . .	16
2.8	Sites where SU are characterised by lengths lower than 500 m. The diameter of the circles is proportional to the number of undulations at a given site. . . . .	16
2.9	Number of sites as a function of the number of undulations and the type of coast. . . . .	17



2.10	Sites with constraints located at a distance of less than 5 m and the average length of the shoreline undulations. . . . .	18
2.11	SU classified according to the range of wavelengths (a) and amplitudes (b). .	19
2.12	Fitting of average wavelength and amplitude. $\sigma$ - standard deviation. . . . .	19
2.13	Symmetry with respect to the amplitude of the crest and sine of the SU. . . .	21
2.14	Maps showing different geometric (a, b) and maritime (c-f) information for the Spanish coast. . . . .	23
2.15	Distribution of the shoreline undulations superimposed over the tidal range.	25
2.16	Number of undulations as a function of the tidal range. A total of 20 sites are located at areas with tidal ranges exceeding 5.5 m. . . . .	25
3.1	Carchuna Beach system: H1-H6 denote the horns of the features and the blue circle represents the location of the cameras [courtesy of Apple Inc.] . .	28
3.2	Snapshot of Carchuna Beach on March 14th, 2012 at 13h: a) Non-filtered image; b) Filtered image, where yellow and red colors identify the surf zone.	30
3.3	Rectified snapshot of the H3-H4 embayment (Carchuna Beach) for February 2nd, 2004 at 8h. Solid line: local beach alignment; dashed lines: normal to shore direction; dash-dotted lines: wave front; arrows: wave direction. . .	30
3.4	Wave propagation on Pocinki's circular island: evolution of the ratio of deep-water wave height and breaking wave height for waves approaching from the left of the figure (Pocinki, 1950). . . . .	31
3.5	Results of the SWAN model for the elliptical spit front: a) $H_s$ for $\alpha_0 = 60^\circ$ ; b) $H_s$ for $\alpha_0 = 30^\circ$ ; c) $H_s$ for $\alpha_0 = 0^\circ$ ; d) $H_s$ for $\alpha_0 = -30^\circ$ ; e) $H_s$ for $\alpha_0 = -60^\circ$ ; f) Variation of the nondimensional surf zone width for different deep-water wave angles: $\alpha_0 = 60^\circ$ (blue line), $\alpha_0 = 30^\circ$ (green line), $\alpha_0 = 0^\circ$ (red line), $\alpha_0 = -30^\circ$ (black line), and $\alpha_0 = -60^\circ$ (grey line). . . . .	32
3.6	Wave energy pattern at the prograding front of a spit: a) energy divergence associated with low-angle wave approach; b) energy concentration associated with normal to positive wave angle values. The angles of incidence are measured counterclockwise from the positive Y-axis. . . . .	33
3.7	Results of the SWAN model for an undulation coast: a) $H_s$ for $\alpha_0 = 0^\circ$ ; b) $H_s$ for $\alpha_0 = 30^\circ$ ; c) $H_s$ for $\alpha_0 = 60^\circ$ ; d) Variation of the nondimensional surf zone width for different deep-water wave angles: $\alpha_0 = 0^\circ$ (blue line), $\alpha_0 = 30^\circ$ (green line), $\alpha_0 = 60^\circ$ (red line). . . . .	34
3.8	Results of the SWAN model for the elliptical spit front: a) $\theta$ for $\alpha_0 = 60^\circ$ ; b) $\theta$ for $\alpha_0 = 30^\circ$ ; c) $\theta$ for $\alpha_0 = 0^\circ$ ; d) $\theta$ for $\alpha_0 = -30^\circ$ ; e) $\theta$ for $\alpha_0 = -60^\circ$ ; f) Variation of the nearshore wave angle respect to the cross-shore direction for different deep-water wave angles: $\alpha_0 = 60^\circ$ (blue line), $\alpha_0 = 30^\circ$ (green line), $\alpha_0 = 0^\circ$ (red line), $\alpha_0 = -30^\circ$ (black line), and $\alpha_0 = -60^\circ$ (grey line). . . .	35
3.9	Results of the SWAN model for an undulation coast: a) $\theta$ for $\alpha_0 = 0^\circ$ ; b) $\theta$ for $\alpha_0 = 30^\circ$ ; c) $\theta$ for $\alpha_0 = 60^\circ$ ; d) Variation of the nearshore wave angle respect to the cross-shore direction for different deep-water wave angles: $\alpha_0 = 0^\circ$ (blue line), $\alpha_0 = 30^\circ$ (green line), $\alpha_0 = 60^\circ$ (red line). . . . .	36

4.1	Scheme of the bathymetric framework showing the amplitude $a$ of the SU in global coordinates $X$ and $Y$ . In the cases considered, $h_1 = 10$ m and $h_2 = 20$ m. The axis distances are non-dimensionalized by the wavelength of the SU $\lambda$ . . . . .	40
4.2	Definition of the main variables as a function of the local coordinates $s$ and $y$ , where $\alpha_{0p}$ is the deep water wave angle respect to to the global coordinates $X, Y$ , $\theta(s, y)$ is the local nearshore wave angle, $b(s)$ is the distance between the shoreline and the breaking line in the $y$ direction (surf zone width), and $\phi(s)$ is the local shoreline angle. Solid lines show the $(X, Y)$ directions, whereas the dashed lines show the local $(s, y)$ directions. . . . .	42
4.3	Relative alongshore sediment transport for the modified Inman and Bagnold (1963) formula, the CERC formula and the Ozasa and Brampton (1980) formula. Three cases were defined, depending on the shape of the surf zone: (a) surf zone width maximum on $\phi(s) = 0^\circ$ ; (b) surf zone width maximum on $\phi(s) = 30^\circ$ ; (c) constant surf zone width. . . . .	47
4.4	Wave angle of the SWAN model (black line), first angle approach (green line), second angle approach (blue line) and root-mean-square error (RMSE), correlation coefficient (R) and skill (S) between the approximations and the model results for different combinations of deep-water wave angle $\alpha_{0p}$ and wave period $T$ . . . . .	50
4.5	Wave ray paths and propagation coefficient ( $K_p$ ) for an undulating bathymetry: a) ray paths for $T = 12$ s and $\alpha_{0p} = 0^\circ$ (solid lines) and $\alpha_{0p} = 30^\circ$ (dashed lines); b) $K_p$ for $T = 12$ s and $\alpha_{0p} = 0, 15, 30, 45, 60^\circ$ (colored lines); c) ray paths for $\alpha_{0p} = 30^\circ$ and $T = 9$ s (solid lines) and $T = 12$ s (dashed lines); d) $K_p$ for $\alpha_{0p} = 30^\circ$ and $T = 6, 9, 12$ s (colored lines). The color scale shows the depth of the domain. . . . .	51
4.6	Alongshore wave angle variation for different $\lambda/a$ values (colours), with $T = 6$ s (solid lines) and $T = 12$ s (dashed lines) for different deep-water wave angles: a) $\alpha_{0p} = 0^\circ$ ; b) $\alpha_{0p} = 30^\circ$ ; c) $\alpha_{0p} = 60^\circ$ . Panel d) shows the results for $K_p$ for $\alpha_{0p}$ and $a/\lambda = 0.1, 0.05, 0.02, 0.01$ . . . . .	52
4.7	Upper panel: relative difference between $Q(s)$ of Eq. (4.28) and of Eq. (4.30). Lower panel: $\Psi_2(s)$ values depending on beach slope $\tan \beta$ and wave period $T$ . . . . .	54
5.1	Alongshore sediment transport $Q(s)$ , alongshore gradient of $Q(S)$ , surf zone width $b(s)$ , Iribarren number $Ir_b$ , and shoreline and beach slope for cases 03 (solid black lines), 10 (solid grey lines) and 11 (dashed black lines) in which $\alpha_{0p}$ varies. . . . .	57
5.2	Alongshore sediment transport $Q(s)$ , alongshore gradient of $Q(S)$ , surf zone width $b(s)$ , Iribarren number $Ir_b$ , and shoreline and beach slope for cases 01 (solid black lines), 03 (solid grey lines) and 09 (dashed black lines) in which $T$ varies. . . . .	58
5.3	Alongshore sediment transport $Q(s)$ , alongshore gradient of $Q(S)$ , surf zone width $b(s)$ , Iribarren number $Ir_b$ , and shoreline and beach slope for cases 02 (solid black lines), 03 (solid grey lines) and 04 (dashed black lines) in which $H_0$ varies. . . . .	59

5.4	Alongshore sediment transport $Q(s)$ , alongshore gradient of $Q(s)$ , surf zone width $b(s)$ , Iribarren number $Ir_b$ , and shoreline and beach slope for cases 05 (solid black lines), 03 (solid grey lines) and 06 (dashed black lines) in which $a/\lambda$ varies. . . . .	61
5.5	Alongshore sediment transport $Q(s)$ , alongshore gradient of $Q(s)$ , surf zone width $b(s)$ , Iribarren number $Ir_b$ , and shoreline (dotted line) and beach slope for cases 07 (solid black lines), 03 (solid grey lines) and 08 (dashed black lines) in which $K_\beta$ varies. . . . .	62
5.6	Alongshore energy dissipation per unit of wave crest and surf zone surface $D_{sz}$ , wave setup $\eta_s$ , surf zone width $b(s)$ (including setup), beach slope $\tan \beta$ , and shoreline for cases 07 (solid black lines), 03 (solid grey lines) and 08 (dashed black lines). . . . .	65
6.1	Scheme defined for the oneline model. . . . .	69
6.2	Non-dimensional diffusivity along a curvilinear shoreline for constant $b$ and $\alpha_0 = 0^\circ$ using the proposed formulation (Eq. 6.11) and the Ashton and Murray (2006a) expression (Eq. 6.8). . . . .	72
6.3	Non-dimensional diffusivity for the CERC formula (solid black lines), LR14 approach (solid grey lines) and Ashton and Murray (2006a) expression for cases 10 (upper panel) and 11 (intermediate panel). Shoreline is depicted in the lower panel. . . . .	73
7.1	Doñana spit, Southern Spain. The dashed lines indicete the shoreline undulations identified in the prograding spit front. . . . .	77
7.2	Some final shorelines for the Doñana spit after 2.5 years of wave climate forcing (colored lines). The black line represents the initial shoreline. . . . .	78
7.3	Some final shorelines for the Doñana spit after 5 years of wave climate forcing (colored lines). The black line represents the initial shoreline. . . . .	79
7.4	Distribution function of the first shoreline undulation amplitude obtained after the EOF analysis. . . . .	80
7.5	Distribution function of the first shoreline undulation amplitude obtained after the EOF analysis. . . . .	80
7.6	El Puntal spit, Nothern Spain. . . . .	81
7.7	Evolution of the coastline for the El Puntal spit after the growth stage of the undulations. Upper graph: longshore sediment transport (LST) (solid line) and LST derivative (dashed line). Lower graph: initial shoreline (black line), breaker line (grey line), intermediate shoreline (dashed line). . . . .	82
7.8	Evolution of the coastline for the El Puntal spit after the saturation stage of the undulations. Upper graph: longshore sediment transport (LST) (solid line) and LST derivative (dashed line). Lower graph: initial shoreline (black line), breaker line (grey line), intermediate shoreline (dashed line). . . . .	82
7.9	Evolution of the coastline for the El Puntal spit after the decay stage of the undulations. Upper graph: longshore sediment transport (LST) (solid line) and LST derivative (dashed line). Lower graph: initial shoreline (black line), breaker line (grey line), intermediate shoreline (dashed line). . . . .	83

7.10 Comparison between the obtained shorelines (red lines) and the plan view of the study cases: a) Doñana spit with an aerial photograph taken in 1956; b) El Puntal spit, with a satellite image taken in 2006. . . . .	83
7.11 Shaded-relief bathymetry of the study area, comprising the littoral and adjacent sedimentary wedges, indicating the location of the grids (the curvilinear coarse grid and the nested grid) used in the numerical model and moorings. The bathymetric contours are given in meters below the present sea level. . . . .	85
7.12 Scheme showing the main bathymetric elements. The blue line indicates the Carchuna Canyon. The green and red lines correspond to the western and eastern tributaries, respectively. The yellow dashed line indicates the position of the undulations of the IPW. The black dashed lines represent the mean alignment of the Carchuna Canyon and the tributaries. The numbers in parentheses indicate the scenarios in which the bathymetric element is present. . . . .	86
7.13 Bathymetries of scenarios 1, 2, 5, and 6 that were used for the wave propagation analyses (isobaths are in meters). . . . .	87
7.14 Comparison between the offshore WANA input wave data (the gray line), the propagated wave data measured by the ADCP (the dashed line), and the SWAN wave model results obtained for the same location of the ADCP (the black line). The wave model results correspond to the propagation over the real bathymetry (scenario 1) . . . . .	89
7.15 Graphs of the nearshore wave patterns for the actual bathymetry (sc1). Upper panel: W incoming waves (from the left lower corner of the figure). Lower panel: E incoming waves (from the right lower corner of the figure). Both cases correspond to storm conditions (a significant wave height of 4 m and a peak period of 10 s). . . . .	90
7.16 Graph of the evolution of the wave energy content for the actual bathymetry (sc1). The results correspond to an average period. The wave data were extracted for depths of 5 m and 8 m to avoid the influences of wave breaking and reflection near the shoreline. West refers to WSW waves. . . . .	91
7.17 Differences in the propagation coefficients between scenarios 1 and 2. Positive (negative) values indicate increases (decreases) in the wave energy. The discontinuous contour lines correspond to the isobaths for depths of 5 and 8 m. West refers to WSW waves. . . . .	91
7.18 Graph of the evolution of the wave energy content for the actual bathymetry (sc1) and the scenarios with the canyon tributaries (sc3, sc4, and sc5). West refers to WSW waves. . . . .	92
7.19 Alongshore evolution of the differences in the propagation coefficients between sc1 and sc6. Positive (negative) values indicate increases (decreases) in the wave height due to undulations. For clarity, the -15m bathymetric line, where the shape of the undulations is more pronounced, was included in the upper graph of the figure. West refers to WSW waves. . . . .	93

7.20	Alongshore evolution of the differences in the propagation coefficients between sc1-sc2 (the blue line) and sc1-sc6 (the red line). Positive (negative) values indicate increases (decreases) in the wave height due to the canyon (blue) or to the effect of undulations (red), respectively. West refers to WSW waves. . . . .	95
7.21	Upper panel: Initial shoreline for the one-line simulation (the solid black line) and surf zone width used during the simulation (the dashed blue line). Lower panel: Shoreline obtained after the simulation. . . . .	96
7.22	Plan view of the Guadalfeo river mouth, Granada, Southern Spain. Bathymetry (blue lines) and direction of the predominant waves are superposed. . . . .	97
7.23	Results obtained with the one line model for the Guadalfeo river mouth. . . .	97
A.1	Time evolution of $\mu_{LN}$ (blue), $\sigma_{LN}$ (green), $\xi_2$ (red) . . . . .	113

## List of Tables

---

2.1	Geometrical characteristics of shoreline undulations and/or shoreline sand waves identified on previous works found in the literature. . . . .	12
2.2	Main fields included in the general table that characterize the undulations. Maritime climate data corresponds only to sites where information was available to the authors. Some of the expanded fields of the table are: (1) Ocean/Sea: Mediterranean Sea, Atlantic Ocean, Bay of Biscay, English Channel, Irish Sea, North Sea, Skagerrak, Kattegat and Baltic Sea; (2) Type of coast: rectilinear, curvilinear and river mouth or estuary; (3) Obstacle: channelized river mouth, breakwater, pier, harbor and rocks. . . . .	13
5.1	Cases defined. For the beach slope: $\tan \beta = 0.01 + K_{\beta} \cos \left( \frac{2\pi}{\lambda} s \right)$ . . . . .	56
5.2	Shoreline movements found . . . . .	63
7.1	Bathymetric scenarios defined for Carchuna beach. . . . .	88
A.1	Fitted parameters of the copulas obtained with the NS-LN-GPD [4 1 1] distribution . . . . .	113



---

# Chapter 1

## Introduction

---

### 1.1 Coastline morphology

Coasts represent some of the most dynamic environments on earth, and 84% of the countries of the world have a coastline adjacent to open oceans, inland seas or both (Martínez et al., 2007). Coastlines develop a wide range of morphologies depending on many factors, such as forcing conditions, characteristics of the forming materials and regional geology (Carter et al., 1997; Woodroffe, 2002). Bird (2010) recently published an extensive, updated revision of worldwide coastal morphologies. Global and regional studies have identified and analyzed the main characteristics of such coastal morphologies (i.e., cliffs, beaches, estuaries, lagoons, etc.). Among them, beaches have been the most studied because of their social, economic and environmental interests (Davis and Fitzgerald, 2003). Beaches are frequently found on rectilinear or weakly curvilinear coasts, although they can also appear in other environments, such as estuaries, deltas or river mouths (Bird, 2010). From a morphological point of view, beaches have been intensively analyzed, with special attention given to both the beach form and profile (Dean and Dalrymple, 2002a) and morphological state (Masselink and Short, 1993).

Many studies also analyzed the generation, evolution and characteristics of secondary shoreline features (Coco and Murray, 2007) that many beaches exhibit. Secondary features can be parallel or perpendicular to the shoreline and may have different geometrical characteristics (Pethick, 1984). Recent attention has focused on shoreline undulations, which can be defined as medium to large spatial-scale shoreline features that have alongshore dimensions ranging from hundreds to thousands of meters and cross-shore widths from tens to hundreds of meters. SU are generally classified as rhythmic coastline features, although some examples are neither periodic nor regularly spaced (López-Ruiz et al., 2012a). SU are frequently associated with sudden changes in the orientation of the coast, such as at spits (Kaergaard and Fredsoe, 2013b), and are often located in proximity to human infrastructures (López-Ruiz et al., 2012b). Many authors have referred to SU as shoreline sand waves; however, shoreline sand waves are generally considered to be rhythmically spaced, and they migrate alongshore (Stewart and Davidson-Arnott, 1988; Davidson-Arnott and Heyningen, 2003).

The mechanism(s) behind the formation and the dynamics of SU are not well understood, but the working hypothesis adopted in recent years is that coastlines with a wave climate dominated by very oblique incidence instabilize and commonly feature large-



scale undulations (Ashton et al., 2001; Ashton and Murray, 2006a; Medellín et al., 2008). Recent advances reveal that variation in the alongshore sediment transport with the angle formed by the wave crests and the coastline plays a major role in the development of SU (López-Ruiz et al., 2012a), although a conclusive explanation for their formation does not currently exist. Therefore, the aim of this dissertation is to deepen the knowledge of the physical process involved in the morphodynamic evolution of stretches of coast where these features typically appear. Among these processes, those that affect the sediment transport such as wave propagation and changes in the beach characteristics are the most important, as they trigger the coastline evolution.

## 1.2 Physical processes

Sediment transport and coastline evolution are complex processes, and their basic governing physical mechanisms are still not completely understood. Questions regarding littoral processes and coastal management, such as how the coastline evolves over the short to long term scale with variations in hydrodynamics or beach conditions, are still open (Baquerizo and Losada, 2008).

In the last decade, several process-based approaches with different degrees of complexity have been developed to model coastline morphological features and shoreline evolution. The more complex models may still be considered to be at a relatively early stage of development due to their approximate description of the processes. For this reason, analytical or simple numerical approximations have also been proposed, as they are useful tools to identify and understand basic physical mechanisms. Some relevant works following these analytical or simple numerical approaches are the oneline and N-line models (Ashton and Murray, 2006a; Payo et al., 2008; Losada et al., 2011), in which the beach evolution is driven only by wave climate variations. Falqués and Calvete (2005) improved this type of models by accounting for the curvature of the shoreline features and by allowing the bathymetric perturbation of these features to extend a finite distance. However, these models typically do not consider factors such as variations in the sediment size, the beach slope and the type of wave breaking.

The influence of these morphological and hydrodynamical aspects on coastal evolution can be even more important on curvilinear coasts. Such coasts are very common around the world (Bird, 2010) and are present in areas with management interests, such as river mouths and spits. Moreover, they frequently lead to different coastline features, such as sandy spits (Petersen et al., 2008; Fig. 1.1a), shoreline undulations (Kaergaard et al., 2012; Fig. 1.1b), beach cusps (Ortega-Sánchez et al., 2008b; Fig. 1.1c) and large-scale cusped features (Ortega-Sánchez et al., 2003a; Fig. 1.1d).

There are some specific questions that remain unanswered related to the effects that hydrodynamic variables have on littoral processes on curvilinear coasts. Two examples are: (1) how the alongshore gradients in wave energy and dissipation rate and changes in the wave angle affect the morphodynamic evolution of curvilinear coasts, and (2) how the setup variations influence the development of circulation cells in horn-embayment systems. In addition, there are other elements that are rarely considered in simple approaches, such as the spatial variation (cross and alongshore) in beach characteristics,

i.e., beach slope, sediment size and shoreline orientation. Note that these variations can modify the sediment transport rate, which is responsible for the variations in beach morphology.

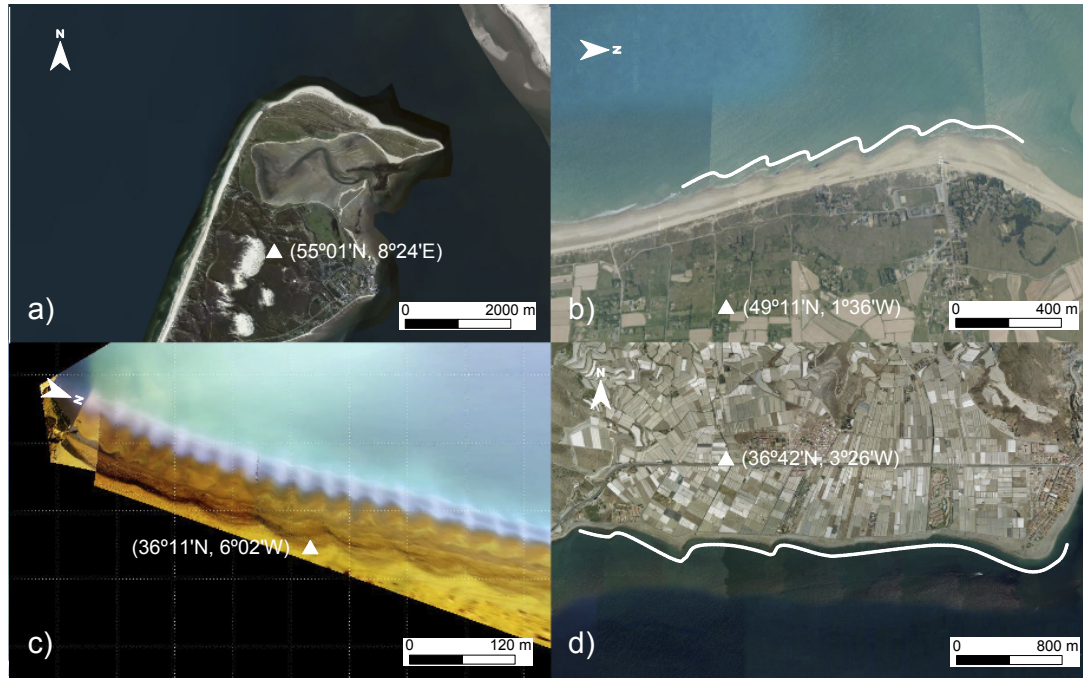


Figure 1.1: Coastline features on curvilinear coasts: a) Sandy spit of Sylt Island, Germany; b) Shoreline undulations in Créances, France; c) Beach cusps in Trafalgar Beach, Spain (Ortega-Sánchez et al., 2008b); d) Large-scale cusate features in Carchuna Beach, Spain. White lines in b) and d) show the shape of the shoreline undulations and the large-scale cusate features, respectively. The triangles indicate the location of the geographical coordinates shown. Images for a), b) and d) are courtesy of Google Earth.

Moreover, the effects of the wind and the persistence or intermittency of the sediment supply due to river discharges are not typically included in integrated models for beach evolution (Losada et al., 2011). Finally, it is not clear whether the shoreline features observed on curvilinear coasts, i.e., shoreline undulations, are evidence of the effects of previous hydrodynamic conditions on the beach morphology or whether they are due to small deficits in alongshore sediment transport. These factors and their interactions are not usually considered in beach evolution models, and hence, their importance has not been quantified.

This dissertation presents an analytical approach to quantify the importance of the variables described above for weakly curvilinear coasts. An updated formulation for alongshore sediment transport on weakly curvilinear coasts (radius of curvature greater than 1000 m) is presented, and the implications of the results for shoreline evolution are also discussed. This approach was conceived as a simple coastal engineering tool for understanding how the different environmental, hydrodynamical and morphological variables affect and interact with the shoreline morphology evolution.

## 1.3 Objectives

### 1.3.1 Main objective

The main objective of this Thesis is “to derive an updated formulation for the along-shore sediment transport rate on curvilinear coasts that will be used to study the morphological evolution of the coast”. An effort is done in avoiding restrictions on the hydrodynamics variables and keep all as analytical as possible.

### 1.3.2 Specific objectives

To achieve the main objective, a sequential methodology is defined. Every step of this methodology correspond to the following specific objectives:

1. To establish a formal definition of the shoreline undulations and find under what conditions they are more likely to occur and if there are a relationship between the presence of curvilinear bathymetries and the development of such undulations.
2. To analyze and quantify the effects of the presence of curvilinear coasts on wave propagation, mainly on the variables that drive the alongshore sediment transport.
3. To find an expression for the alongshore sediment transport that considers all the effects identified in the previous specific objective, and also other important characteristics in the morphodynamics of the sandy beaches (sediment size, beach slope, etc.).
4. To analyze how changes in the wave conditions and beach configurations modify the alongshore sediment transport defined and the potential evolution of the shoreline.
5. To define a morphological evolution model for the plan view of the coast (oneline type model) and compare it with other solutions obtained previously.
6. To apply this model to different locations with curvilinear coasts where rhythmical shoreline features develop to establish if the new processes considered in this work are decisive in the formation of such features.

## 1.4 Outline of the Thesis

Besides the motivation (Chapter 1) and conclusions (Chapter 8), this Thesis is organized in 6 main chapters. Each of them answers to one of the specific objectives outlined above.

In Chapter 2, a definition and some examples of shoreline undulations are given. An European database of these features is also presented. In this database, undulations over the coasts of 15 countries are identified, in combination with some geometric and hydrodynamical characteristics. After the statistical analysis of the data, it is concluded that the

presence of the shoreline undulations are usually related to the presence of curvilinear bathymetries.

Chapter 3 is devoted to the identification and quantification of the modification of the wave propagation patterns due to the presence of curvilinear coasts. Both field evidences and numerical results are presented, showing the significant alongshore variations in wave energy and wave angle that those coasts induce.

In chapter 4, the framework defined to update a widely used expression for alongshore sediment transport is presented. It is capable to account for the effects identified in the previous chapter. Two different analytical solutions are presented, depending on how the nearshore wave angle is approximated.

Chapter 5 presents some numerical experiments carried out to analyze the behavior of the approach for the sediment transport defined in Chapter 4. The implications of that approach on coastal evolution and hydrodynamics are also studied. Three different shoreline movements are found for undulating features: migration, amplitude growth and changes in wavelength and asymmetries.

In Chapter 6 the oneline model is presented and a analysis in terms of “diffusivities” is done. This analysis shows that, in contrast to other models, waves which approach the beach with a high angle are no necessary to the shoreline features to develop.

Chapter 7 is dedicated to the application of the oneline model to different locations. The short to mid-term shoreline evolution modeled show a good agreement with observations, supporting the hypothesis and framework defined trough the Thesis.

Finally, in Chapter 8 the main conclusions and the future research lines are drown.

## 1.5 Publications derived from this Thesis

### Refereed Journal Papers

- Magaña P, Lira A, **López-Ruiz A**, Ortega-Sánchez M and Losada M (2014). A public, open Western Europe database of shoreline undulations based on imagery. *Progress in Physical Geography (Under review)*.
- **López-Ruiz A**, Ortega-Sánchez M, Baquerizo A and Losada M (2014). A note on the alongshore sediment transport on curvilinear coasts and implications on coastline evolution. *Coastal Engineering*, 88C, 143-153. doi: 10.1016/j.coastaleng.2014.03.001.
- Ortega-Sánchez M, Lobo FJ, **López-Ruiz A**, Losada M and Fernández-Salas LM (2013). Influence of shelf-indenting canyons and infralittoral prograding wedges on the coastal morphology: the example of the Carchuna system (Southern Spain). *Marine Geology* 347, 107-122.
- **López-Ruiz A**, Ortega-Sánchez M, Baquerizo A and Losada MA (2012). Short and medium-term evolution of shoreline undulations on curvilinear coasts. *Geomorphology* 159-160, 189-200.

### Chapters in Books

- Ortega-Sánchez M, **López-Ruiz A**, Baquerizo A and Losada MA (2015). *Shoreline undulations*. In: Encyclopedia of Estuaries (Ed. Michael J. Kennish). Encyclopedia of Earth Sciences Series, Springer, doi: 10.1007/978-94-017-8801-4.

### International Peer-Reviewed Conferences

- **López-Ruiz A.** M, Ortega-Sánchez M, Baquerizo A, Navidad D and Losada MA (2012). Nonuniform alongshore sediment transport induced by coastline curvature. In: 33<sup>th</sup> International Conference on Coastal Engineering (ICCE). Electronic edition, Texas Digital Library, Santander (Spain).
- **López-Ruiz A**, Ortega-Sánchez M, Baquerizo A and Losada MA (2011). Short-term simulation of the evolution of a curvilinear coast. 5th International Short Conference on Applied Coastal Research (SCACR). RWTH Aachen University (Germany).

### Spanish Peer-Reviewed Conferences

- **López-Ruiz A**, Ortega-Sánchez M, Lobo FJ, Baquerizo A and Losada MA (2013). Morfología de la línea de costa inducida por ondulaciones de media escala en la plataforma: Carchuna (Granada). XII Jornadas Españolas de Ingeniería de Costas y Puertos. Cartagena, Spain. (*In Spanish*).
- **López-Ruiz A**, Ortega-Sánchez M, Baquerizo A and Losada MA (2011). Ondas de arena en costas curvilíneas. Aplicación al sistema litoral de Doñana. XI Jornadas Españolas de Ingeniería de Costas y Puertos. Las Palmas de Gran Canaria, Spain. (*In Spanish*).

---

## Chapter 2

# Shoreline undulations

---

In this chapter, a formal definition of the shoreline undulations is given. Some examples of these features on prograding spit fronts and discontinuous beaches are shown based on an european database. The aim of this database was to analyze the relationships between the presence and the geometry of the shoreline undulations and the characteristics of the local coast (mainly geometry and forcing agents).

### 2.1 Definition

Shoreline undulations (hereinafter SU) are defined as “medium to large spatial scale shoreline features with alongshore dimensions ranging from hundreds to thousands of meters and amplitudes from tens to hundreds of meters” (Ortega-Sánchez et al., 2015). They are generally classified under rhythmic coastline features, although many examples are neither periodic nor regularly spaced (López-Ruiz et al., 2012a).

SU can be episodically or persistently found along many shorelines all over the world, including regular rectilinear or weakly curved beaches and river mouths and estuaries. They are also frequently found associated to sudden changes in the orientation of the coast, prograding spits fronts (Kaergaard and Fredsoe, 2013b) and near human infrastructures. This work focuses mainly on the latter groups of coasts where there are irregularities in the nearshore bathymetry.

Many authors named this type of features as shoreline sand waves (Ashton et al., 2001; Falqués and Calvete, 2005), whereas the latter are generally considered rhythmically spaced and that migrate alongshore. It is generally assumed that when an undulation is present in the shoreline the bathymetry is approximately parallel down to a certain depth. Hence, the presence of these features could be related to the existence of a curvilinear bathymetry that may affect wave propagation processes. This assumption is adopted in what follows.

The mechanism(s) behind the formation of the SU is still not well understood. The main working hypothesis followed during last years is that coastlines with a wave climate dominated by very oblique incidence destabilize and commonly feature large scale undulations, suggesting that this instability could be the main mechanism responsible for the formation of regularly spaced shoreline undulations (Falqués and Calvete, 2005; Ashton

and Murray, 2006a). However, the variation of the alongshore sediment transport with the angle formed by the wave crests and the coastline as well as the surf zone width may play a major role in the development of SU (López-Ruiz et al., 2012a). This is of high importance in estuarine and river mouths, littoral spits, curved coastlines and close to human interventions (e.g., jetties) where the nearshore wave regimen is intensively modified. Whatever the case may be, detailed description of the nearshore hydrodynamics is required for modeling SU.

## 2.2 Examples

Preliminary observations of satellite imagery and aerial photography showed that SU are usually related with two different types of coasts: (1) sandy spits that develop on river mouths and estuaries, and (2) coast with a sudden change in the mean alignment or where an obstacle is present along the shoreline. Both cases have in common the presence of a curvilinear or at least irregular bathymetry.

The SU found at the first type of coasts (prograding spits fronts) can be permanent or associated with certain wave characteristics (Medellín et al., 2008). Some examples of permanent SU are: Sylt Island in the southern North Sea (Germany), where the SU have alongshore dimensions of 500 – 1000 m (Fig. 2.1a; Lindhorst et al., 2010); the spit on the west side of Cape Lookout (North Carolina, USA) with dimensions of 250 – 1000 m (Fig. 2.1b; Park and Wells, 2007); at the Arçay Spit (France) with lengths of 500 – 1000 m (Fig. 2.1c; Allard et al., 2008); and at Sandy Hook Spit (New York, USA) with lengths of 1000 – 2000 m (Fig. 2.1d; Nordstrom et al., 1978).

Two examples of SU in prograding spit fronts on the Spanish coast are the undulations found at Doñana (Fig. 2.1e), at the mouth of the River Guadalquivir (Gulf of Cádiz), and at the El Puntal Spit in Santander (Fig. 2.1f) (Medellín et al., 2008, 2009). In the first case these features are permanent (shoreline features are identified in the available aerial photographs) and have alongshore dimensions of 500 – 2000 m and cross-shore amplitudes of  $\simeq 150$  m. In contrast, at El Puntal spit, the SU are non-permanent and their presence depends mainly on the wave conditions (Medellín et al., 2008). In this location, when the SU develop they have alongshore dimensions of 125 – 150 m and cross-shore amplitude of  $\simeq 15$  m. In neither case has migration been observed.

The SU found at the second type of coasts (sudden change in the beach orientation, or where there is an obstacle or constraint) can be also permanent or associated with certain wave characteristics. However, they usually have a greater number of crests and troughs along the coast compared with the prograding spit fronts, and the alongshore and cross-shore dimensions are smaller. Fig. (2.2) shows some examples of this type of SU. Figs. (2.2a-c) present three locations where there is a sudden change in the alignment of the coast and SU develop. Those SU exhibit alongshore dimensions ranging between 100 and 200 m. Finally, Figs. (2.2d-f) depict other three examples of SU where there is an obstacle or constraint (small dykes in the three cases). In these cases, SU have alongshore dimensions of 50-100 m.





Figure 2.1: Shoreline undulations on prograding spit fronts: a) Sylt Island Spit, Germany; b) Cape Lookout Spit, North Carolina, USA; c) Arçay Spit, France; d) Sandy Hook Spit, USA; e) Doñana Spit, Spain; f) El Puntal Spit, Spain [courtesy of Google Earth and Apple Inc.]. The white dashed lines highlight the geometry of the features.

## 2.3 European database

To study whether the relationship between the presence of a curvilinear or discontinuous bathymetry and the development of SU is casual, we developed a european database of SU based on the analysis of a total of approximately 50.000 km of coast in Europe and Northern Africa. Different characteristics of the SU were collected and included in the database, such as the site wave climate or the geometry (dimensions, number or symmetry) of the undulations. This database is free, public and available for the scientific community and can be used to gain deeper insight into coastal morphodynamic processes. It can be consulted through this link: [http://gdfa.ugr.es/su\\_data/](http://gdfa.ugr.es/su_data/).





Figure 2.2: Examples of sites exhibiting SU related to coasts with a sudden change in the beach orientation or with the presence of a constraint: a) Beach close to Créances, France; b) Pellaro, Southern Italy; c) Coast of Pénestin, France; d) Calahonda, Málaga, Spain; e) Marbella, Málaga; f) Termini, Italy [courtesy of Google Earth and Apple Inc.]. The white dashed lines highlight the geometry of these undulations.

We analyzed the coastlines of Belgium, Denmark, France, Germany, Ireland, Italy, Netherlands, Portugal, Spain and the United Kingdom in Europe and Algeria and Morocco in North Africa to identify SU (Fig. 2.3). The North African countries were selected because of their proximity to Spain and readily available maritime information. A total of approximately 50.000 km of coast were investigated.

### 2.3.1 Material and methods

For the analysis, we used images from the Google Earth imagery database. Google Earth maps the earth by the superimposition of images obtained from satellite imagery, aerial photography and GIS 3D globe and is freely available. This company is actively updating their database with higher resolution datasets that have a much finer resolu-

tion than the original 15-30 m/pixel. Resolution for the sites analyzed in this work is  $< 1$  meter/pixel; certain images had a resolution on the order of cm/pixel.

Although ideally all images should correspond to low tide and similar conditions of the wave forcing (mainly wave height and period), this is not possible with the images that are available. Nevertheless, those variables are not significant for our analysis, which focuses on the identification and geometric characterization of the shoreline undulations but not on their dynamics or evolution in time. Moreover, possible wave variations between images are not significant for the presence of the SU, since they are more stable and have greater spatial scales than the regular shoreline features strongly affected by waves (i.e. Beach cusps).

Nevertheless, two main restrictions are still present in the use of Google Earth as a researching tool. First, high resolution images are not available for every spot in the world. In these cases, we made use high resolution images from other virtual globe tools, like Nokia HERE or Microsoft Bing. Second, inconsistency of remotely sensed image quality in Google Earth impedes consistent analysis. Because images from Google Earth are processed for visualization purposes, precise quantitative measurements and analysis is lost. This issue is also increased with the previous point, by using images from different virtual globes. These two remaining limitations made very difficult to consider automatic algorithms to get consistent results. Even more when the problem of automatic detection of shoreline features is not trivial Ortega-Sánchez et al. (2008b).



Figure 2.3: Coastline of the European and Northern African countries that were analysed (grey line).

Shorelines were visually analyzed and the undulations were identified based on the ratio  $a/\lambda$ , where  $a$  and  $\lambda$  are the length and width of the undulations, respectively (Fig.

Reference	$\lambda$ [m]	$a$ [m]	$a/\lambda$
Bruun (1954)	300-2000	60-80	$\sim 0.03-0.25$
Verhagen (1989)	2500-22000	30-500	$\sim 0.001-0.2$
Thevenot and Kraus (1995)	750	40	$\sim 0.053$
Schwartz (2006)	500-750	15-25	$\sim 0.02-0.05$
Medellín et al. (2008)	125-150	15	$\sim 0.1$
López-Ruiz et al. (2012a)	500-2000	150	$\sim 0.1-0.3$

Table 2.1: Geometrical characteristics of shoreline undulations and/or shoreline sand waves identified on previous works found in the literature.

2.4). To measure these distances, we used the ruler tool in combination with complementary software tools (i.e., time lapse or zoom) to assist in the image analysis. For this database, in certain cases, the series of undulations were estimated; therefore, this is independent.

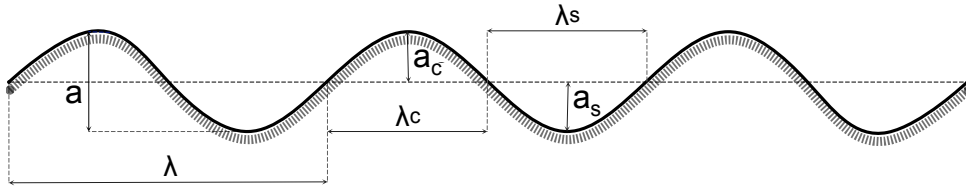


Figure 2.4: General geometry of a series of shoreline undulations.  $a$  - amplitude;  $\lambda$  - wavelength;  $a_c$  - amplitude of the crest;  $a_s$  - amplitude of the sine;  $\lambda_c$  - wavelength of the crest;  $\lambda_s$  - wavelength of the sine.

For each site where an SU was identified, different data were gathered and included in a general table (Table 2.2). We divided the data into four main categories: (1) general information, (2) geometry, (3) constraints and (4) maritime climate. Constraints are the presence of any artificial obstacles at the shoreline located near the SU. It was hypothesized that these obstacles might influence the undulations when they were at a distance lower than  $5\lambda$ , measured from the boundary of the SU closest to the constraint.

The information collected for the different sites was pre-processed using software for data analysis. Intervals were defined for certain variables ( $a$ ,  $\lambda$  and distance to the constraint), and correlations between groups of two and three variables were attended to, with special attention given to  $a/\lambda$ , with the results compared with published data. Subsequent analyses performed with the collected information were anticipated, so the most representative variables were analyzed:

- Country and adjacent water body (ocean/sea)
- Undulation wavelength

Group	Term	Unit	Range
General information	Name (Id)	Nominal	-
	Latitude	Coordinates	31.46° - 57.93°
	Longitude	Coordinates	-10.21° - 18.27°
	Location	Nominal	-
	Ocean	Nominal	-
	Year of image	-	2000-2012
Geometry	Number of undulations	-	1->15
	Wavelength $\lambda$	m	30-5000
	Amplitude $a$	m	4-500
	Length sine/crest $\lambda_s, \lambda_c$	m	10-3200
	Amplitude sine/crest $a_s, a_c$	m	2-300
Constraints	Type of coast	Nominal	-
	Obstacle	Nominal	-
	Distance to the obstacle	m	20-8000
Maritime climate	Significant wave height $H_S$	m	0.43-1.71
	Peak wave period $T_p$	s	3.75-10.39
	Tidal range	m	0.31-4.90
	Wave energy flux (module)	kW/m	0.53-13.91
	Wave energy flux (direction)	°	0-359

Table 2.2: Main fields included in the general table that characterize the undulations. Maritime climate data corresponds only to sites where information was available to the authors. Some of the expanded fields of the table are: (1) Ocean/Sea: Mediterranean Sea, Atlantic Ocean, Bay of Biscay, English Channel, Irish Sea, North Sea, Skagerrak, Kattegat and Baltic Sea; (2) Type of coast: rectilinear, curvilinear and river mouth or estuary; (3) Obstacle: channelized river mouth, breakwater, pier, harbor and rocks.

- Undulation amplitude
- Number of undulations at a given site (series of undulations)
- Symmetry
- Type of coast
- Constraints
- Tidal range
- Wave climate (only for Spanish coasts)

## 2.3.2 Results

A total of 294 sites exhibiting SU were identified (Fig. 2.5). The information included in the global database and the stored geographical information is offered as a PostGIS layer for the scientific community. Consequently, the information can be easily incorporated into GIS software such as QGIS or ArcGIS.

### 2.3.2.1 Regional analysis

The majority of the sites exhibiting SU were found in the Mediterranean Sea (107, 36.4%), whereas 55 (18.7%) were found in the Atlantic Ocean and 50 (17%) at the Kat-

tegat Strait (Baltic Sea). The remaining sites face local seas or straits, with proportions lower than 6%.

The country with the most sites is Denmark (64, 21.8%), followed by Spain (56, 19%) and Italy (51, 17.3%); the remaining countries have less than 9% of the sites identified as exhibiting SU, with only one case identified in Northern Ireland. To describe the collected data, we divided the study area into regions depending on the number of sites, global orientation and length of coastline and country boundary (Fig. 2.6). The average density ( $d$ ) for each region was defined as the number of sites divided by the length of the coastline ( $d = \text{sites/km}$ ).

Region 1 corresponds to the southern Mediterranean and Atlantic coast of Spain and Portugal and is characterized by a high number of sites ( $d = 1/23$ ), irrespective of whether their location is adjacent to the Mediterranean Sea or Atlantic Ocean. However, the number is much lower along the northern coast of Africa (Region 2), where the density decreases to  $1/164$ . This region exhibits sites with a wide variety in the number of undulations, whereas sites with only one SU are predominantly in the Atlantic region.

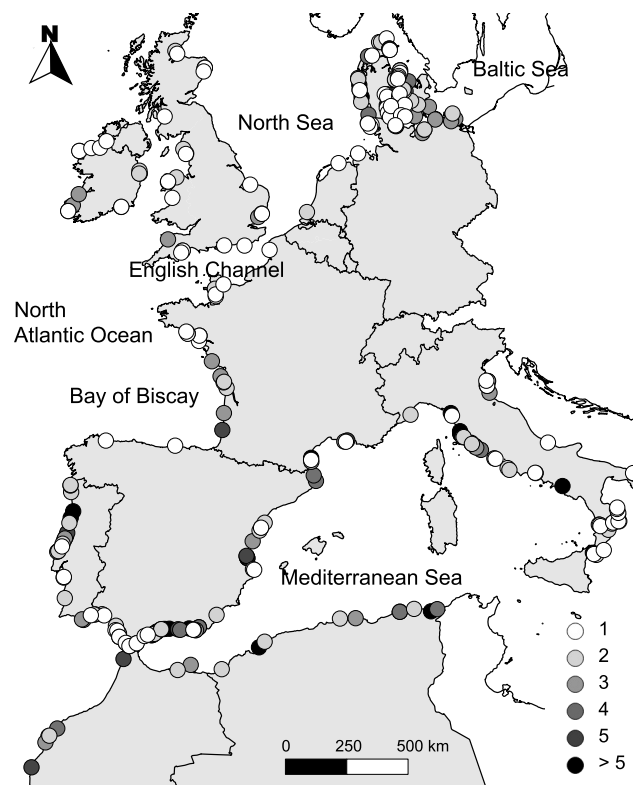


Figure 2.5: Sites where shoreline undulations were identified. The legend of the figure corresponds to the number of individual shoreline undulations at each site.

Region 3 corresponds to the N-S oriented coast of Portugal and contains frequent sites with SU ( $d = 1/59$ ) along with gaps that are remarkably visible at the southern end. The northern Spanish coast (Region 4) exhibits a strong reduction in the number of sites ( $d = 1/319$ ), with only two cases that have singular undulations. Region 5 corresponds to the southern part of the French coast where the coastline orientation turns from W-E to

almost N-S. The number of sites increases to a density of  $1/125$ , which is higher than in region 4 but lower than in regions 1 to 3, with a coastal gap in the region of Bretagne. Sites in the northern section of Region 5 exhibit only one SU, whereas in the southern section, sites are characterized by more than one SU. Sites were identified in Region 6 (stretch of the French coast facing the English Channel), increasing the density to  $1/59$ .

A major portion of United Kingdom is included in Region 7, except for an area located in the northeast that was defined as Region 9. UK sites are scarce, with a density of  $1/269$  and sites that have only one SU dominating. A similar situation is found for Ireland (Region 8) and Scotland (Region 9), where the presence of SU is not significant ( $d=1/251$  and  $d=1/135$ , respectively).

Region 10 corresponds to the coast of Holland and Germany and covers a total of  $\sim 2.000$  km of coast. However, despite of the length of the coast and the presence of long beaches, only four sites were found, resulting in the lowest density of all the regions ( $d=1/494$ ). Only one or two undulations were exhibited at each of the four sites.

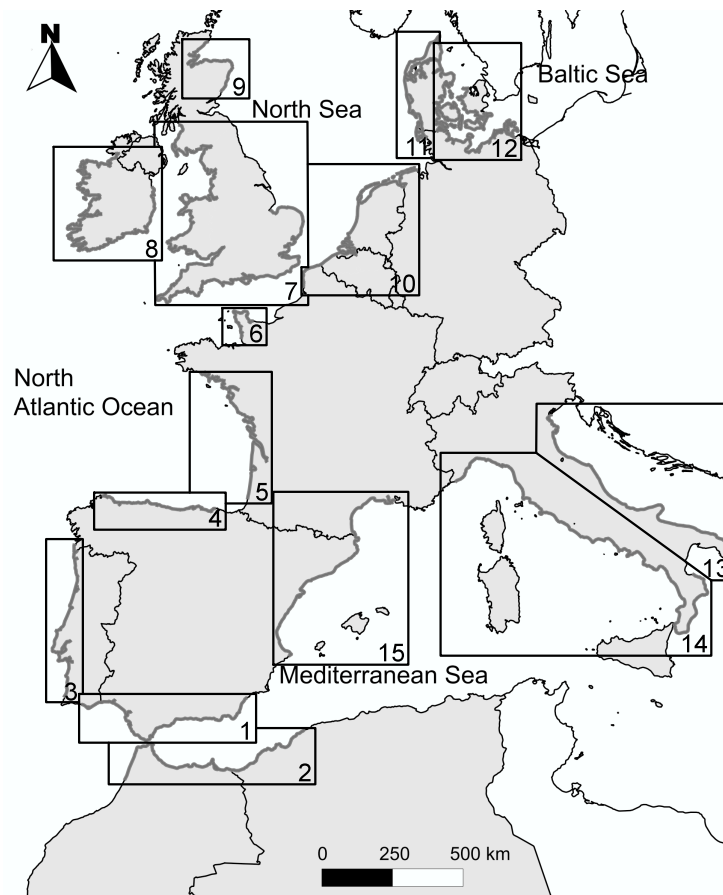


Figure 2.6: Regions (1 to 15) within the area of study that were divided to describe the collected data.

The western and eastern coasts of Denmark are included in Regions 11 and 12, respectively, and the SU density increases to values of  $d=1/103$  and  $d=1/70$ , indicating a change in conditions with respect to the nearby coasts of Holland and German. Additional sites have been identified in the eastern area of the country. Italian coasts facing the Adriatic

and Mediterranean seas are included in regions 13 and 14, respectively. Few undulations are present along the Adriatic Sea ( $d=1/110$ ), whereas the density increases along the Mediterranean side ( $d=1/44$ ). This behavior is similar what was observed on the Spanish Mediterranean coast, indicating that similar maritime climate conditions and geomorphic characteristics could be responsible for the high number of SU along both coastlines.

### 2.3.2.2 Series of undulations and type of coast

Certain sites only contained one shoreline undulation, whereas series of undulations were found at numerous sites, with certain sites exhibiting up to 15 individual SU (Figs. 2.7 and 2.8). Sites with only one undulation were predominant (99, 34%) followed by sites with two undulations (81, 28%), with sites containing one and two SU representing 62% of the total. The number of sites exhibiting more than two SU decreases rapidly until it reaches 5-6 SU when the number stabilizes. A cubic function fits the data with a high correlation (Fig. 2.7).

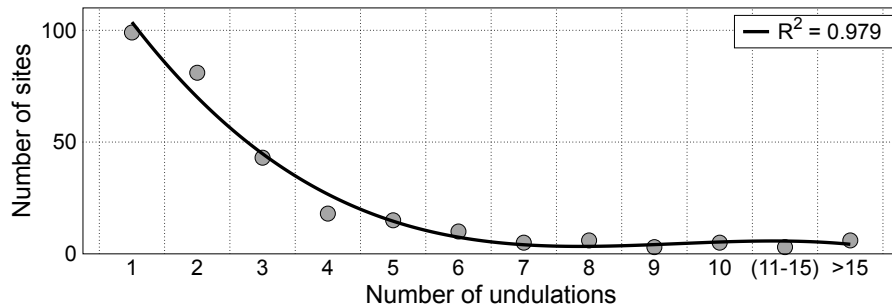


Figure 2.7: Relationship between the number of undulations and the number of sites. The line corresponds to the fitting of the data to a cubic function.

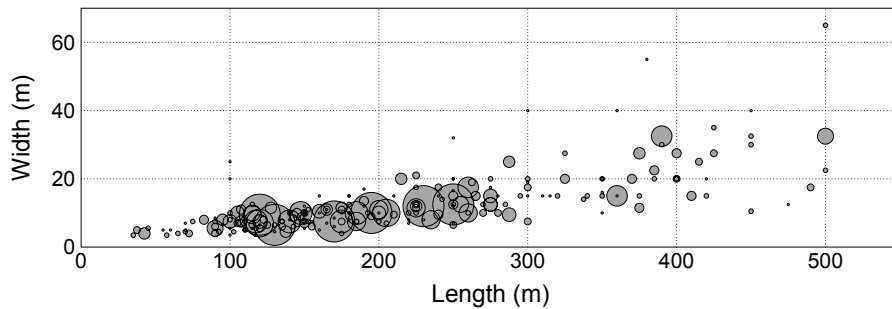


Figure 2.8: Sites where SU are characterised by lengths lower than 500 m. The diameter of the circles is proportional to the number of undulations at a given site.

Shoreline undulations with the longest lengths are found at sites characterized by only one or two undulations, whereas an increasing number of undulations generally indicates a shorter length. There is only one site with more than 3 SU that has lengths exceeding



1.000 m. Sites with 10 (or more) undulations have shorter lengths (<350 m). Fig. (2.8) depicts sites where the SU have average lengths lower than 500 m. In general, sites with a higher number of undulations have lengths lower than 250 m (on average) and widths that are usually below 30 m.

We also analyzed the number of undulations as a function of the type of coast (curved, rectilinear or at an outlet or river mouth). This division was based on the importance of the curvature in the generation of shoreline features, which was noted by numerous authors (Kaergaard and Fredsoe, 2013a; López-Ruiz et al., 2012a). A similar number of observations were identified for the three types of coast. However, when this variable is analyzed in combination with the number of undulations (Fig. 2.9), sites showing more than 6 undulations are not found at outlets or river mouths but are predominantly located along rectilinear coasts and sites with only one undulation are predominantly found at river mouths (43%) followed by curvilinear (36%) and rectilinear (20%) coasts.

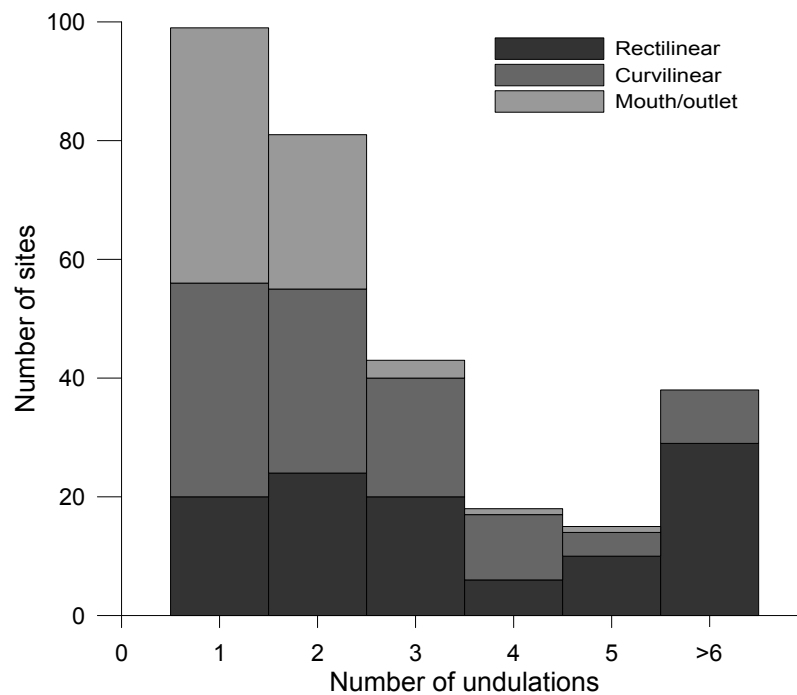


Figure 2.9: Number of sites as a function of the number of undulations and the type of coast.

### 2.3.2.3 Constraints

SU are morphological features of the shoreline. In theory, a quasi-rectilinear coastline with a constant alongshore sediment transport rate should be in equilibrium and no undulations would be expected. However, modifications of such an ideal situation could lead to the formation of SU, and such modifications can be produced by an artificial constraint at the coastline (Dean and Dalrymple, 2002a).

To analyze the impact of constraints (obstacles) on the development of SU, the presence of these constraint was identified both with the SU themselves. Dikes, jetties or any other artificial element located at a distance of  $5\lambda$  from to the nearest boundary of the



SU were considered. In cases of a series of undulations, the average length of the SU was used. Fig. (2.10) illustrates undulations where obstacles could have played a significant developmental role.

A total of 135 SU (45.9%) could have been influenced by constraints, with coastal jet-ties the predominant obstacle (39, 29%). Rocky shores are also found along with a high number of SU (34, 25%), followed by ports (29, 22%) and channelling at river mouths (24, 18%). When the distance to the obstacle is analyzed, 34% are located at a distance of  $\lambda$ , with almost 60% at a distance of  $2\lambda$ . These results indicate the strong influence that constraints have on the morphodynamic processes that generate shoreline undulations.

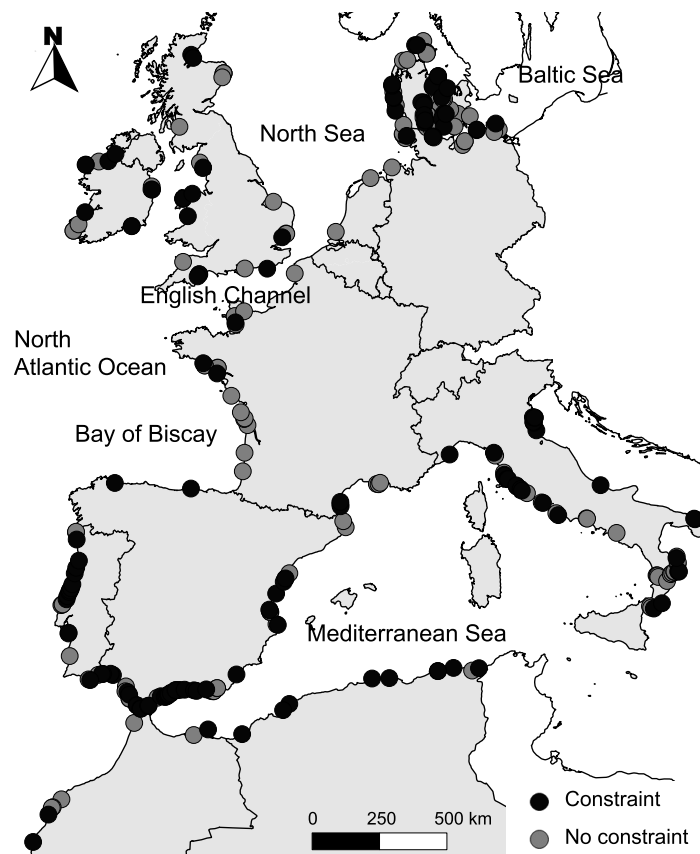


Figure 2.10: Sites with constraints located at a distance of less than 5 m and the average length of the shoreline undulations.

#### 2.3.2.4 Geometric analysis

The wavelength and amplitude of the SU were measured, and for the sites with series of undulations, the amplitude and wavelength of each undulation along with their average values were included in the database (Fig. 2.11). Amplitude and wavelength of the crest or sine of every undulation were also measured and incorporated to the database.

Focusing on the relationship between the length and width of the SU, the criterion used to identify the SU was the ratio  $a/\lambda \in (0.1 - 0.3)$  (Table 2.1). We now use the results from the database to investigate if there is a predominant relationship between those variables. Fig. (2.12) plots the fitting of  $\lambda$  and  $a$  using a linear relation (average values at every

site were considered). The best linear correlation is achieved using 240 data points, with a relation of  $a/\lambda \simeq 0.05$ . When the fitting is performed for different intervals of wavelength (Figure 2.12), lower correlations are obtained because of the increasing dispersal of the data. Additional tests with different intervals of  $a$  and  $\lambda$  were tested, but the correlations did not improve. Similar results are obtained if series with the same number of SU are analyzed. Our value of  $a/\lambda$  is the same as what was obtained by Thevenot and Kraus (1995) and in the range of the value obtained by Bruun (1954). However, the result is a bit displaced with respect to the results from the remaining authors included in Table (2.2). Nevertheless, we consider our results more representative because a higher number of sites and samples were included.

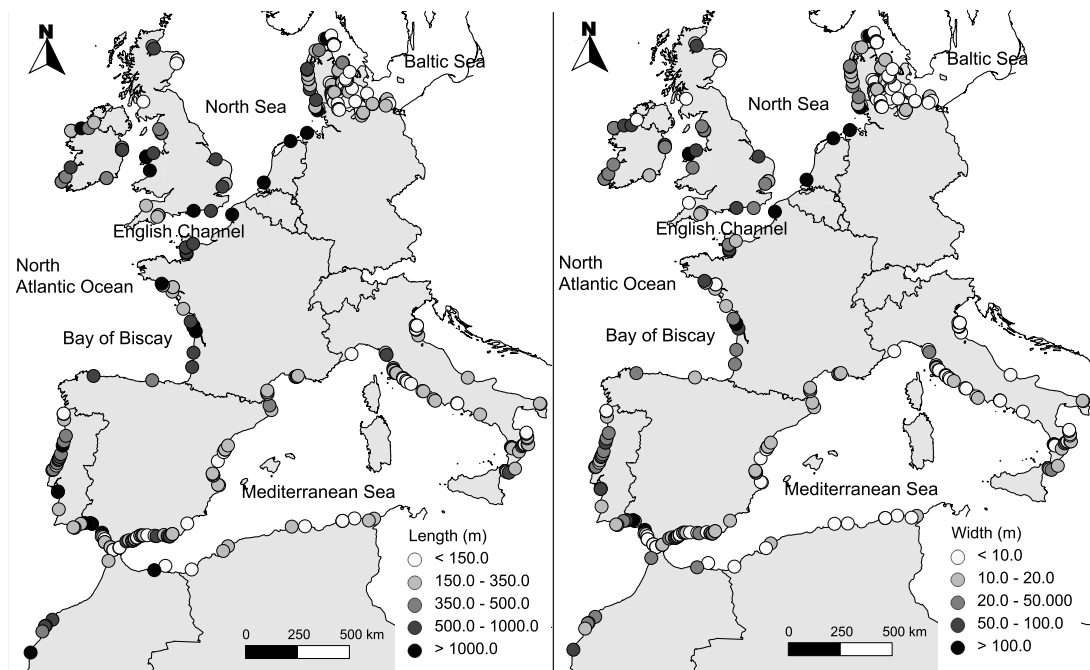


Figure 2.11: SU classified according to the range of wavelengths (a) and amplitudes (b).

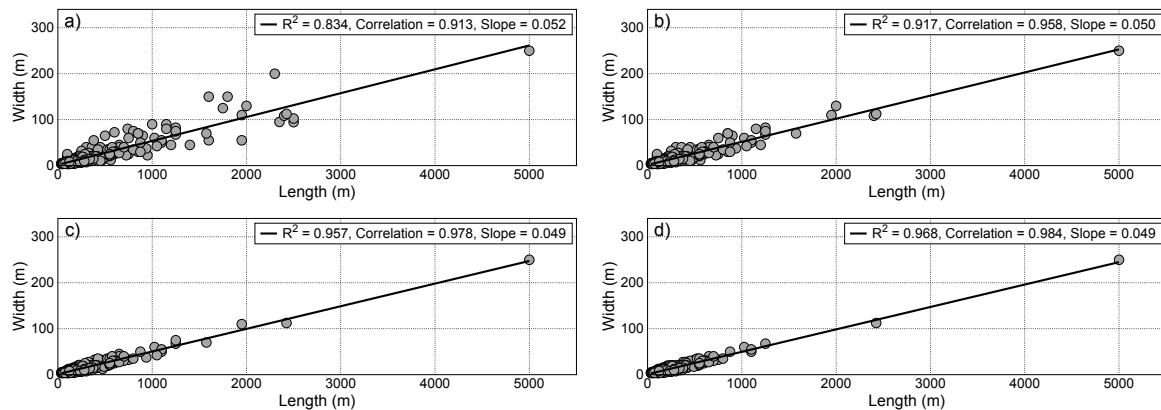


Figure 2.12: Fitting of average wavelength and amplitude.  $\sigma$  - standard deviation.

Regarding the shape of the SU, it varies from site to site and depends on the number of undulations at a given site. Similar to other typical shoreline morphological features, SU can be symmetric or asymmetric, although some of the sites are difficult to classify according to only one of the two groups. According to the variables defined in Fig. (2.4), if the difference between the wavelengths (amplitude) of the different individual SU in a series of undulations was  $\leq 20$  m ( $\leq 5$  m), the SU was considered symmetric with respect to its wavelength (amplitude). The same values were applied when comparing the wavelength and amplitude of the crest and sine of an individual SU. Therefore, two different types of studies were carried out regarding the symmetry of the SU: symmetry between the wavelength and amplitude of different individual SU and symmetry between the crest and sine of the different individual SU.

When studying the symmetry between the different individual undulations that are part of a series of SU, only sites that exhibited more than one undulation (195 sites) should be analyzed. Asymmetry with respect to wavelength was found for 83% of sites (161 sites) that exhibited more than one SU, whereas 62% (121 sites) showed asymmetry with respect to amplitude and 61% (119 sites) showed asymmetry with respect to both wavelength and amplitude.

When studying the symmetry with respect to the crest and sine of the sites showing two or more undulations, 64% of the sites (125 sites) showed asymmetry with respect to wavelength (crest wavelength and sine wavelength) whereas 73% (142 sites) showed symmetry with respect to amplitude.

In sites where only one shoreline undulation was present (99 sites), 54.5% (54 sites) were symmetric with respect to wavelength and 73% (72 sites) were symmetric with respect to amplitude. Symmetry with respect to both wavelength and amplitude was found for 46.5% of the sites (46 sites). When studying the symmetry with respect to crest and sine for the entire set of identified SU (294 sites), 58% of the sites (170 sites) showed asymmetry with respect to wavelength (crest length and sine wavelength), whereas 73% (214 sites) showed symmetry with respect to amplitude (Fig. 2.13).

### 2.3.3 Spain: a country-scale example of the database

Spain has a complete dataset of maritime information managed by Puertos del Estado (Ministerio de Fomento, Spain) that is available for research and management purposes. In the framework of different research projects, a complete recompilation of maritime climate along the Spanish coastline was gathered and has been published on the web <http://www.c3e.ihcantabria.com>. Fig. (2.14) depicts the main climate variables along the Spanish coastline in combination with the location and main characteristics of the SU.

Sites exhibiting SU are predominant along the Mediterranean and south Atlantic Spanish coasts, whereas they are very scarce along the northern coast (Fig. 2.14). As previously described, the density decreases from  $d=1/23$  at the southern coast of Spain to  $d=1/319$  at the northern coast. The length and width of SU are similarly distributed along the Spanish coast, with exceptions for the longest SU found along the south Atlantic coast (Figs. 2.14a-b).

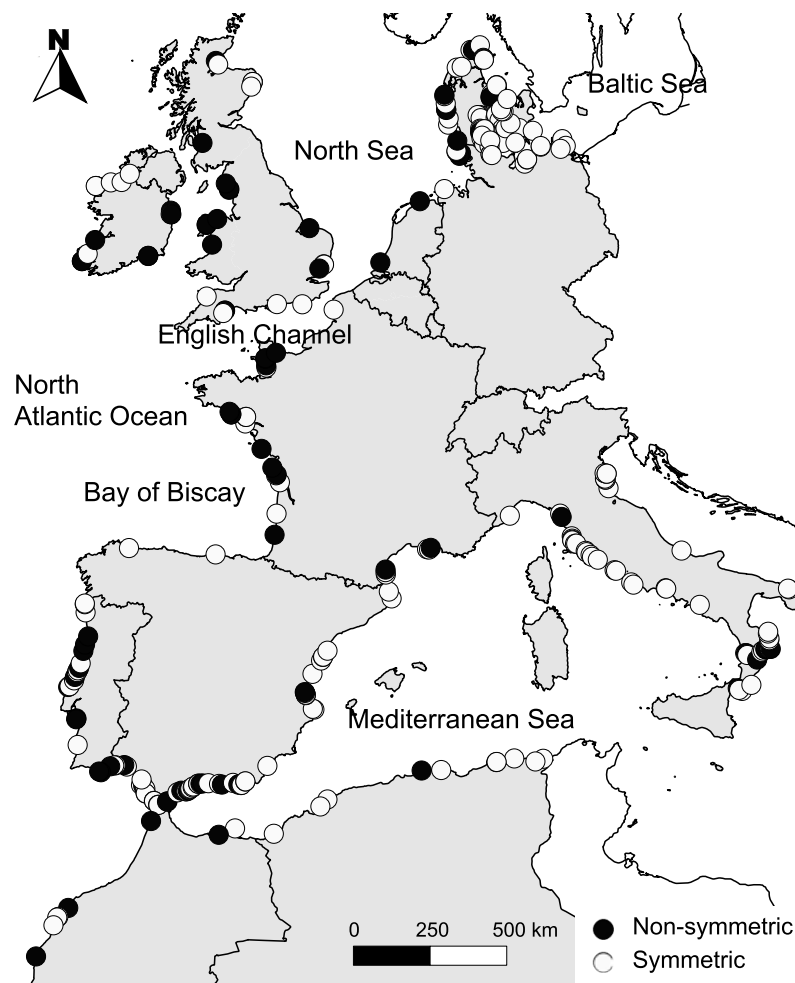


Figure 2.13: Symmetry with respect to the amplitude of the crest and sine of the SU.

The distribution of sites along the Spanish coast appears to be related to the values of the main maritime variables (Figs. 2.14c-f). The average values of significant wave heights are higher for the northern coast, whereas they are significantly reduced for the Mediterranean coast (Fig. 2.14c). This behavior appears to correlate with the number of identified sites, with a minimum (maximum) number of sites with higher (lower) wave energy. Waves with the largest peak periods arrive along the northern coast, whereas the shortest waves arrive along the south Mediterranean coast (Fig. 2.14d). These characteristics are directly related to the number of sites with SU, with more sites found where the peak period is shorter.

A similar trend is observed for the two remaining variables analyzed: the wave angle of incidence (Fig. 2.14e) and the tidal range (Fig. 2.14f). The wave angle of incidence was calculated as the difference between the shore normal and the wave fronts. Thus, the greater the angle, the more obliquely the waves arrive at the coast. For coastlines where the waves impinge more obliquely, fewer SU are identified. Conversely, when waves approach more perpendicularly, the development of SU is favored. Regarding the tidal range, more sites with SU are found where the tidal range is lower. The previous results indicate that a relationship between the maritime wave climate and sites exhibiting SU can be established.

These results would be enriched the incorporation of topographic and bathymetric data into the analysis; however, this is out of the scope of the present Thesis.

### 2.3.4 Discussion

A database of sites exhibiting shoreline undulations along the coast of 15 European countries identified by visual interpretation of Google Earth images is presented. Many uncertainties are inherent in the analysis, with the primary uncertainty being the temporal and spatial scales of the problem. Regarding the spatial scale, the analysis of 50.000 km of coast is a highly time-consuming and error-prone task; thus, certain sites could have been disregarded unintentionally. For the temporal scale, the only analyzed images correspond to the present configuration of the coast. If this work could have been performed in the past, the results would have been different because of natural and/or human interventions. However, this database has shown the potential for this type of analysis and provided the scientific community with access to an open, free database of SU.

#### 2.3.4.1 Geometry and shape of the shoreline undulations

Statistical and geometrical analysis of the results can be carried out with the information included in the database, and significant results have been obtained. We identified the country and location with the highest (Denmark and Spain) and lowest (Northern Ireland) frequency of SU. Our results indicate that a dominant order of magnitude of the relationship between amplitude and wavelength for SU is  $a/\lambda \simeq 0.05$ . This order of magnitude is similar to that of additional smaller spatial-scale shoreline features, such as beach cusps (Coco, 2004; Todd Holland, 1998). We found that tides discourage the formation of SU but do not similarly affect smaller-scale features. One possible explanation is that alongshore processes on the coast dominate how SU are formed, with cross-shore processes being of minor importance. When the tidal range is important, breaking zone moves cross-shore, changing the wave dissipation and sediment transport patterns.

To analyse the statistical importance of the relationship between the presence of SU and constraints along the coast, the existence of these constraints was also identified in the database. The results show that approximately 56% of identified SU could be influenced by constraints because 60% were located at a distance of  $2\lambda$  from a constraint.

Our data show that SU can be either symmetrical or asymmetrical with respect to width and length, although asymmetrical shoreline undulations are more likely to occur, with more than 50% of SU presenting some type of asymmetry (for sites with one or more undulations). Some authors proposed mechanisms for the formation of SU that generate symmetrical features (Ashton and Murray, 2006a) but are not capable of reproducing asymmetrical features (Ortega-Sánchez et al., 2008c). One of the main aims of this Thesis is consider some characteristics of the curvilinear coasts, that are not accounted by these authors, to generate these asymmetries.

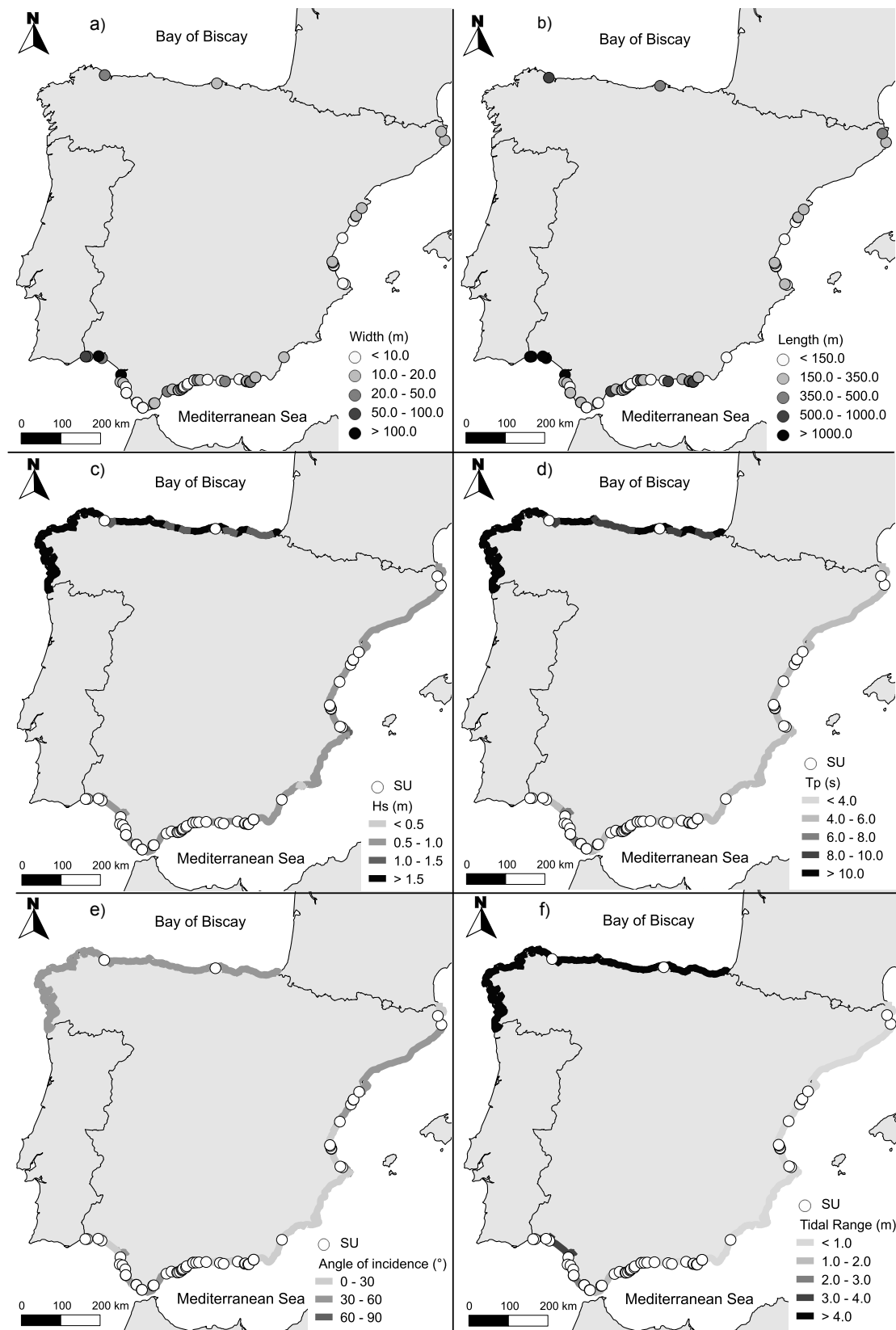


Figure 2.14: Maps showing different geometric (a, b) and maritime (c-f) information for the Spanish coast.

#### 2.3.4.2 Influence of the tides and waves

Because of the length scale of the area of study, collecting and analyzing wave and climate information and finding correlations with the shoreline undulations is not an easy task. For some areas, information is scarce, and for other areas, information collection is difficult. Regarding the influence of wave height on the development of the SU, our results indicate that undulations develop easily under low wave heights (protected coasts), which could explain the high number of undulations along the coast of Denmark, the southern Mediterranean coast of Spain or the western coast of Italy. However, this hypothesis is not verified for sites along the English Channel or the Adriatic Sea where the wave energy is generally low but SU appear at very low frequencies. Areas where the fetch is lower may develop more undulations; accordingly, the greater the fetch, the lower the number of undulations, which could be the case for Spain and Portugal, where a number of SU follow this trend (Fig. 2.5). However, this is not verified at the Adriatic site. While wave energy plays a significant role in the development of SU, other factors are also important. The combined effect of waves and tides appears to be a determinant for the development of the SU.

Tidal range is also relevant in the development of SU. Fig. (2.15) depicts the location of the sites as a function of the tidal range. In general terms, SU are predominant in areas where the tidal range is lower (Mediterranean Sea and along the Denmark coast); conversely, SU are infrequent along the northern Spanish coast, the English Channel and in some tracks of the French and English coast where the tidal range is higher. SU are not found at Bretagne where tidal ranges surpass 7 m, and the same pattern is observed along the English Channel, where tidal ranges easily exceed 5 m. This hypothesis is generally verified, except for sites along Portugal's coast, where other factors most likely play a significant role in the distribution of the features. The results are summarized in Fig. (2.16) and show that the highest number of undulations is found at sites with tidal ranges lower than 1 m and the number of SU decreases as tidal range increases. The results are significant considering that the length of coast with tidal ranges lower than 1 m and between 3.5 and 5.5 m are  $\approx 15000$  km and  $\approx 18000$  km, respectively.

The influence of tidal range in the dimensions of the undulations is also clearly observed when analyzing their wavelengths (Figs. 2.11 and 2.15). In the Mediterranean Sea, only two undulations are over 1.000 m (1.9%), whereas this ratio increases to 14.5 and 20% for the Atlantic Ocean and North Sea, respectively. The highest proportion of long undulations is found along the English Channel, where a total of 36% are over 1.000 m and the tidal ranges vary more intensively. For the Baltic Sea and Straits of Skagerrak and Kattegat, the undulations are predominantly short.

The influence of tides on coastal rhythmic features such as beach cusps was previously studied (Coco, 2004); it was concluded that height and cross-shore extent of beach cusps are tidally modulated. However, this refers to the short-term scale and small spatial-scale features, which are out of the range of SU. During recent years, different works have established the relationship between the formation and characteristics of large-scale shoreline features such as SU and wave climate characteristics (Ashton et al., 2001; Ortega-Sánchez et al., 2003b); however, the influence of tides in their formation has not been explored, which was most likely because short-term variables were not significant for the gener-

ation of medium- to long-term shoreline features. However, our results show that this variable should be included in the analysis.

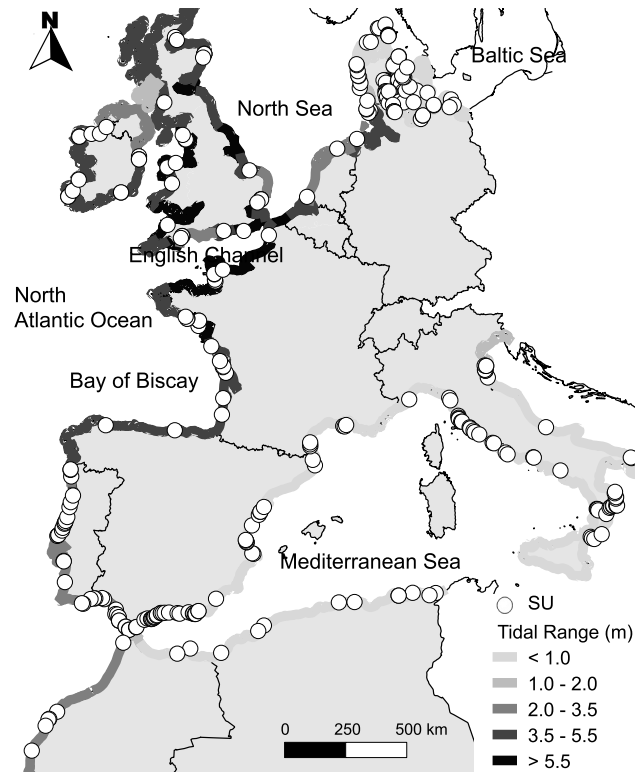


Figure 2.15: Distribution of the shoreline undulations superimposed over the tidal range.

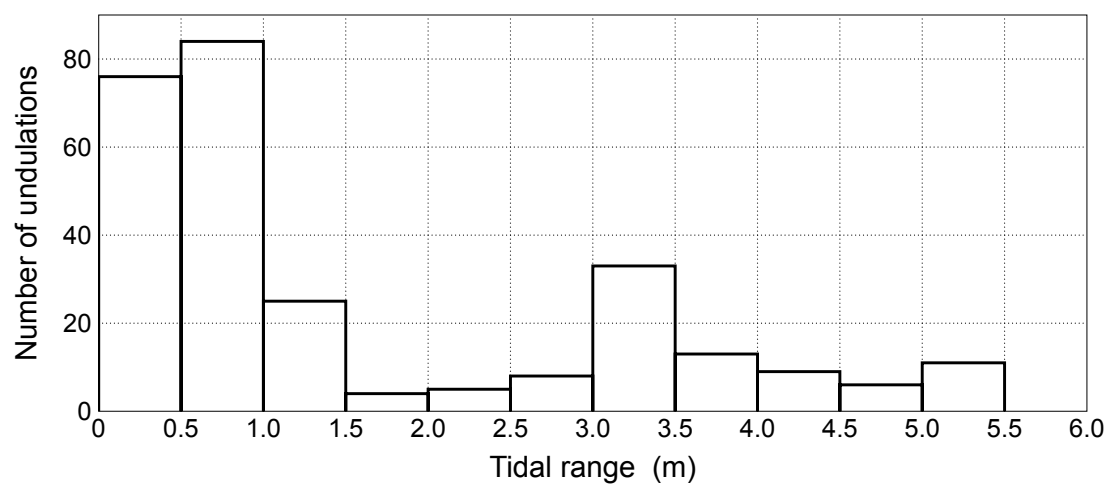


Figure 2.16: Number of undulations as a function of the tidal range. A total of 20 sites are located at areas with tidal ranges exceeding 5.5 m.



#### 2.3.4.3 Forming materials

Forming materials, characteristics of the topography-bathymetry and tidal range may contribute to a high percentage of the sites exhibiting SU. Different fractions of sand and gravel coexist at Mediterranean Spanish beaches (Bramato et al., 2012). It has been intensively reported in the bibliography that beach cusps are best formed when two different grain sizes are present at the beach (Nolan et al., 1999). In a similar manner, it seems that the redistribution of sediment of different sizes alongshore would facilitate the formation and development of undulations. However, the low number of identified sites where the coast is dominated by cliff or embayed beaches (i.e., coasts of England or the north of Spain) does not favour the genesis of SU. Our results would be significantly enriched by the incorporation of a detailed bathymetry-topography of the study area into the analysis.

#### 2.3.5 Conclusions derived from the European database

The following conclusions can be drawn from the analysis presented in the previous sections:

- More than 35% of the SU identified are in the Mediterranean Sea, although the country with more SU is Denmark. The coast with a greater density of SU per km of coast is the Southern coast of the Iberian Peninsula (both the Mediterranean and Atlantic coasts).
- The majority of the sites with SU exhibit less than 4 undulations (Fig. 2.7). In these places, the mouth/outlet and curvilinear coasts dominate (Fig. 2.9), whereas in the locations with 5 or more undulations, rectilinear beaches are more likely to occur.
- Almost 50% of the sites have a constraint located at a distance  $< 5\lambda$  of the undulations. In fact, 60% of these constraints are located within a distance  $< 2\lambda$ , which indicated the important role that the constraints are playing on the formation of SU.
- 58% of the sites (170 sites) showed asymmetry with respect to wavelength (lengths of the crest and sine), whereas 73% (214 sites) showed symmetry with respect to amplitude.
- The analysis of the presence of SU in combination with the wave forcing agents for the Spanish coast reveals that larger wave heights, wave periods, tidal ranges and wave obliquity inhibit the development of SU. Hence, their formation is favored under mild wave conditions and micro or mesotidal conditions.

Hence, it can be concluded that the presence of a curvilinear or at least discontinuous bathymetry is a very common characteristic of the locations where SU are identified. The wave propagation over these bathymetries may provoke alongshore gradients in the nearshore wave conditions and therefore, in the alongshore sediment transport. In Chapter 3, the main effects of curvilinear or irregular bathymetries on wave propagation are analyzed.

# **Curvilinear coasts (I): effects on wave propagation**

---

In this chapter, the effects of the presence of curvilinear bathymetries on wave propagation are examined. Two main variables were analyzed: (1) the surf zone width (distance between the shoreline and the breaking line), and (2) the nearshore wave angle. Visual evidences through the analysis of video-imagery, and numerical results obtained with the SWAN wave propagation model were used to characterize those effects. The results show that the presence of curvilinear bathymetries induce important alongshore gradients in both variables. These gradients may play a key role in the morphodynamic evolution of curvilinear coasts.

## **3.1 Introduction**

This Thesis focus on the alongshore sediment transport on curvilinear coasts and the related morphodynamic evolution. Therefore, to analyze the effects of curvilinear bathymetries on nearshore waves, we considered the two main wave characteristics that are related to these topics: the wave energy and the wave angle. The first was characterized by the surf zone width defined as the distance between the shore and the breaking lines measured in the cross-shore direction. The latter, is measured with respect to the same direction at a depth close to the breaking point.

These two variables are of major importance in many classical formulations for the alongshore sediment transport, as the CERC expression (USACE, 1984) obtained through an energetic approach, or the experimental expression of Kamphuis (1991). Other important wave parameter for the sediment transport is the wave period, which was already included in the (Kamphuis, 1991) formula, although its value does not vary significantly during the wave propagation.

The analysis of the surf zone width and the nearshore wave angle was done in two phases. First, images obtained with video-imagery techniques in Carchuna Beach, Southern Spain, were analyzed to preliminarily analyze the wave behavior over curved bathymetries. This beach is a horn-embayment system characterized by the presence of a submarine canyon. Once the alongshore wave variations were observed on those images, a numerical wave propagation model was used to quantify this variations. Several cases

were performed for an undulating coast and for a prograding front of a sandy spit, where there is a transition between a straight and a curved coastline. The results are examined in the following sections.

### 3.2 Evidences on nature

Carchuna Beach is located on the southeastern coast of Spain and faces the Alborán Sea. The beach exhibits a series of large-scale cusped features with an alongshore spacing of hundreds of meters. These features are bounded by a series of seaward-extending horns (H1–H6, Fig. 3.1), forming a curvilinear coast. The beach is bounded to the west by Cape Sacratif (H1) and to the east by the Punta del Llano Promontory (H6), which corresponds to the west side of the Calahonda Spit. Moreover, as will be detailed in Chapter 7, the bathymetry of the beach is also characterized by the presence of a submarine canyon that will affect the wave propagation (Fig. 7.11). The wave climate is characterized by two m  
th  
a :

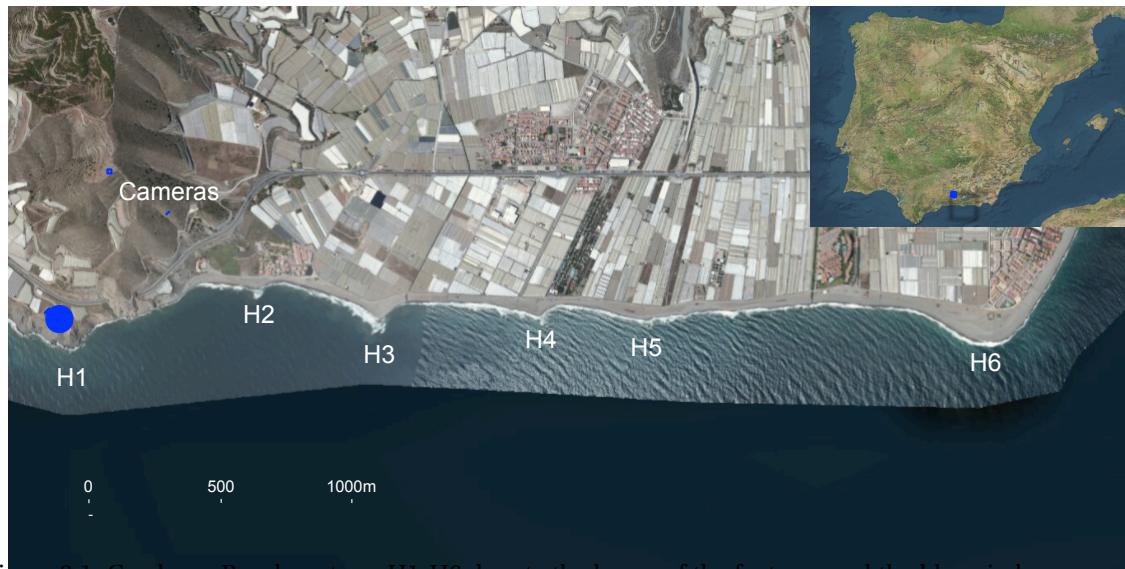


Figure 3.1: Carchuna Beach system. H1–H6 denote the horns of the features and the blue circle represents the location of the cameras [courtesy of Apple Inc.]

The Environmental Fluid Dynamics Research Group (University of Granada) installed in October 2003 a video-monitoring station based on the ARGUS technique (Aarninkhof and Holman, 1999) at the Sacratif lighthouse (located at H1), 50 m above mean sea level. The station includes 3 video cameras that collect images during the first 10 min of each daylight hour at a frequency of 2 Hz. Video-images consist of an instantaneous image (snapshot), a 10-minute time-averaged image (timex) and a variance image over the same period.

After installation, the location of the cameras and a number of clearly visible ground control points (GCPs) were surveyed relative to a known benchmark. When no fixed GCPs

were available, virtual GCPs were used (i.e. camera 2). From comparison of the image and world location of the GCPs, the photogrammetric transformation from image to world space was computed using the technique presented by Holland et al. (1997) to allow geo-referenced digitization of morphological features. Accuracy of this process is typically one pixel. At midbeach, one pixel corresponds to a ground accuracy of 0.25 and 1.4 m in the cross-shore and alongshore directions, respectively, worsening to 0.49 and 5.59 m at the far end of the beach.

Given the curvilinear character of the bathymetry due to the shoreline features and the submerged canyon, the images taken by the video-monitoring station were analyzed to check the presence of alongshore variations both on surf zone width and nearshore angle. The effort was centered in the storm events, since under these conditions the variations in wave propagation are more perceptible.

After the analysis, the presence of alongshore gradients in surf zone width were evident. The wave energy concentrates and diverges in some locations of the beach, with differences on the surf zone width of approximately 50% in some cases. The places where the wave energy concentrates are not only the horns, as might be expected. There are also energy concentrations in the embayments, presumably due to the effect of refraction over the curvilinear bathymetry. Moreover, the surf zone width tends to be larger in the side of the horn oriented to the direction where the waves come from.

An example of these effects is shown in Fig. (3.2), where a snapshot of the beach during a Westerly storm on March 14th, 2012 at 13h (Fig. 3.2a), and a filtered image of the same image Fig. (3.2b) are shown. The filter was used to contrast the surf zone (yellow to red colors) over the rest of the pic (green colors). It is shown that the wave energy concentrates around the horn H2 and the embayments between H2-H3 and H3-H4.

To check if similar effects can be observed for the wave angle, rectified snapshots of the nearshore were analyzed for storm conditions. These type of images are the only ones that allow to identify the relative orientation between the wave crests and the shoreline. Fig. (3.3) shows rectified view of the beach area located between H3 and H4 on the February 2nd, 2004 at 8h, during a Easterly storm. It is shown that the wave fronts are parallel to the shoreline in the left side of the horns, which are the sides of the horns oriented to the direction where the waves come from. However, for the embayments, and specially for the right side of the horns, the wave fronts and the shoreline form a significant angle (approximately 45°).

After the analysis of the video-images, it can be concluded that the presence of a curvilinear coast induce alongshore gradients both of surf zone width (an also on wave energy) and nearshore wave angle. Although these qualitative results are not enough to characterized these gradients, they justify a detailed and quantitative study of the wave propagation over this type of bathymetry. In the next section, this study is done using a numerical model and synthetic bathymetries.

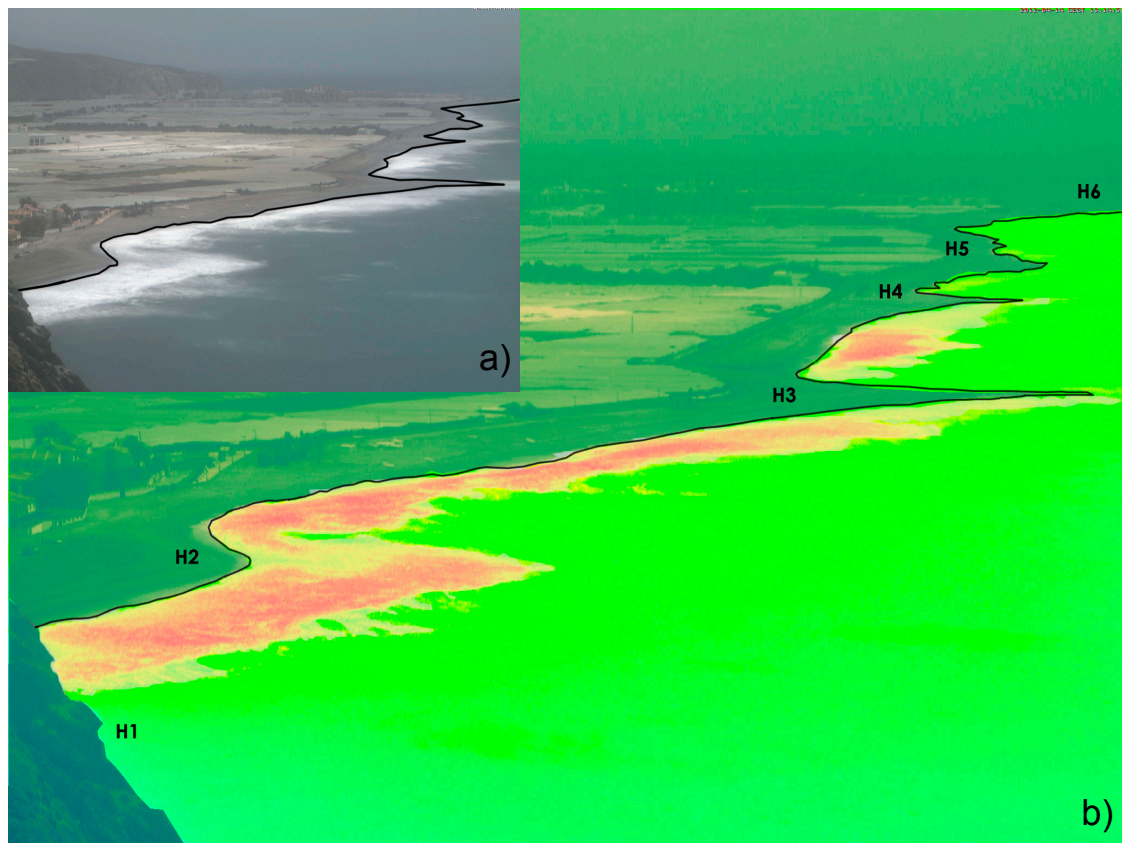


Figure 3.2: Snapshot of Carchuna Beach on March 14th, 2012 at 13h: a) Non-filtered image; b) Filtered image, where yellow and red colors identify the surf zone.

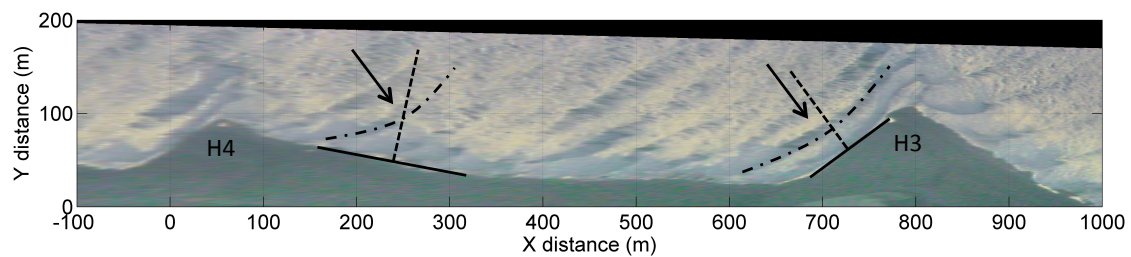


Figure 3.3: Rectified snapshot of the H3-H4 embayment (Carchuna Beach) for February 2nd, 2004 at 8h. Solid line: local beach alignment; dashed lines: normal to shore direction; dash-dotted lines: wave front; arrows: wave direction.

### 3.3 Numerical results

#### 3.3.1 Surf zone width variations

Along curved stretches of coast, the breaking wave height cannot be considered constant. Pocinki (1950) studied wave refraction on a circular island, and showed that in these

circumstances, propagation produces a convergence of the rays on the coastal zone nearest to the direction of the incident wave train and a divergence in the opposite direction. Fig. (3.4) shows the evolution of the ratio of deep-water wave height and breaking wave height on Pocinki's circular island for waves approaching from the left to the right.

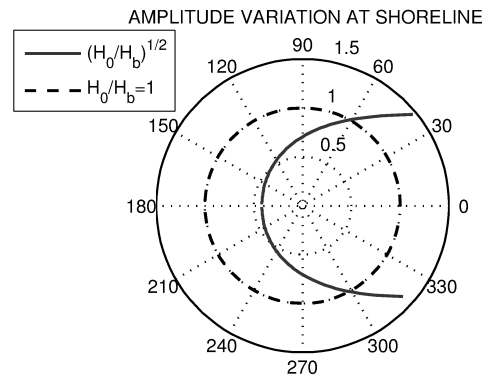


Figure 3.4: Wave propagation on Pocinki's circular island: evolution of the ratio of deep-water wave height and breaking wave height for waves approaching from the left of the figure (Pocinki, 1950).

This effect is not only characteristic of circular shorelines. Any curvilinear coast may produce zones where the wave rays converge (diverge) thus increasing (decreasing) the wave energy. In what follows, these alongshore wave energy variations are obtained for a prograding spit front and for a undulating shoreline.

### 3.3.1.1 Prograding spit front

To properly characterize the wave energy variation along a schematic spit, the SWAN model was used to generate different cases of wave propagation over an idealized conical bathymetry. This model can perform numerical computations on curvilinear grids. The SWAN model (Booij et al., 1999) is capable of simulating many complicated interactions and transformations experienced by waves propagating through space: refraction due to bottom and current variations, shoaling, blocking and reflections due to opposing currents, transmission/blockage through/by obstacles, effects of wind, whitecapping, depth induced wave breaking, bottom friction and non-linear wave-wave interactions. However, SWAN also has some limitations such as wave reflection (Wood et al., 2001). For the cases discussed in this paper waves experience little or no reflection, so this restriction is not important for our study. Hence, SWAN model is therefore capable of accurately reproducing the dominant phenomena under consideration, namely, shoaling and refraction (Ashton and Murray, 2006a).

The shoreline was defined as a straight stretch of coast followed by a elliptical one with a semi-major axis of 500 m parallel to the straight stretch of the coast, and a semi-minor axis of 200 m. The bathymetry was built using a constant beach slope value  $\tan \beta = 0.01$ . The alongshore variations of the surf zone width were obtained for different combinations of significant wave height, peak wave period and deep-water wave angle. Figs. (3.5a-e) show the significant wave height obtained for different wave incoming directions

(deep-water wave angle  $\alpha_0$  ranging between  $-60^\circ$  and  $60^\circ$ ) for a deep-water significant wave height of  $H_{s0} = 2$  m and peak period of  $T_p = 12$  s. These wave and beach data are representative of the values obtained in the SU analysis of Chapter 2. Wave angles are measured with respect to the Y axis, with positive values for waves incoming from the left to the right of the figure. The value of the non-dimensional surf zone width (the ratio between the obtained value and the value in the straight part of the coast) against the alongshore distance for different deep-water wave angles is showed in Fig. (3.5f). The results show that the main variable that characterizes the behavior of the surf zone width (and hence the alongshore variations of the wave energy) is the deep-water wave angle.

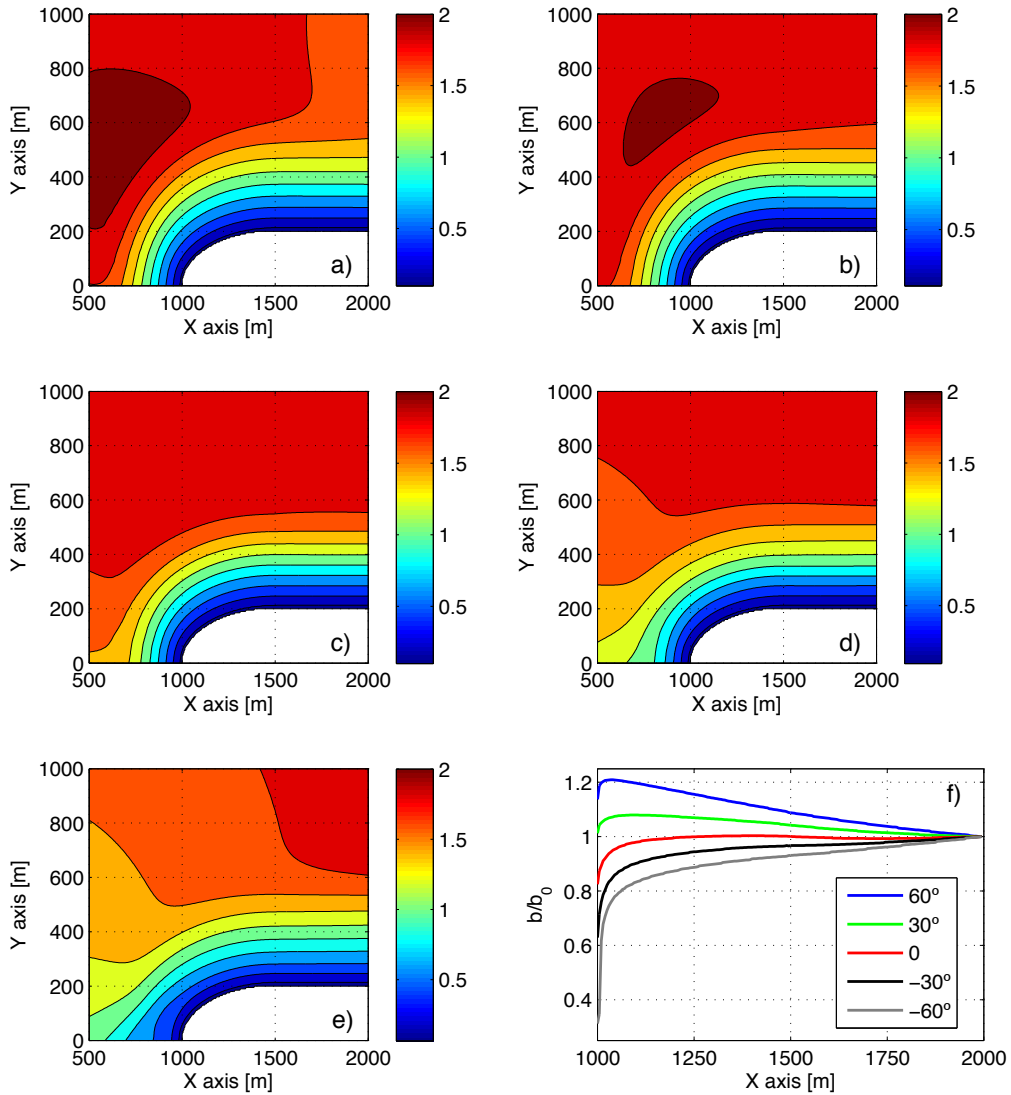


Figure 3.5: Results of the SWAN model for the elliptical spit front: a)  $H_s$  for  $\alpha_0 = 60^\circ$ ; b)  $H_s$  for  $\alpha_0 = 30^\circ$ ; c)  $H_s$  for  $\alpha_0 = 0^\circ$ ; d)  $H_s$  for  $\alpha_0 = -30^\circ$ ; e)  $H_s$  for  $\alpha_0 = -60^\circ$ ; f) Variation of the nondimensional surf zone width for different deep-water wave angles:  $\alpha_0 = 60^\circ$  (blue line),  $\alpha_0 = 30^\circ$  (green line),  $\alpha_0 = 0^\circ$  (red line),  $\alpha_0 = -30^\circ$  (black line), and  $\alpha_0 = -60^\circ$  (grey line).

For waves approaching at negative angles (black and grey lines in Fig. 3.5f), a pro-



gressive decay in the surf zone width towards the tip of the spit (up to 60%) is observed. However, when waves arrive approximately normal to the rectilinear stretch (red line) or with negative values (blue and green lines) there is an increase in the surf zone width (up to 20%), and hence on the wave energy since the beach slope is constant. This concentration of energy was already observed by Petersen et al. (2008) and it produces a variation in the surf zone width with a maximum at the transition zone. The exact location where this maximum is attained depends on the angle of incidence. The same pattern was observed for the rest of the wave climate combinations propagated with SWAN model. This behavior of the surf zone width is schematized in Fig. (3.6).

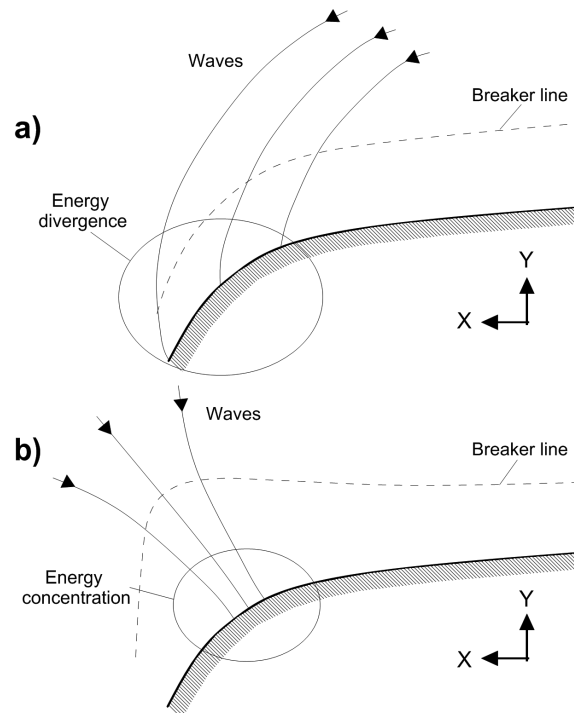


Figure 3.6: Wave energy pattern at the prograding front of a spit: a) energy divergence associated with low-angle wave approach; b) energy concentration associated with normal to positive wave angle values. The angles of incidence are measured counterclockwise from the positive Y-axis.

### 3.3.1.2 Undulating coast

The SWAN model also was used to analyze the alongshore wave energy gradients for an undulating coast. In this case, the shoreline was defined using a sine function. The wavelength of the undulations is 2000 m and the relationship between the amplitude and the wavelength is  $a/\lambda = 0.05$ . This value corresponds with the mean value obtained after the analysis of the SU described in Chapter 2. The beach slope was defined constant along the beach with a value of  $\tan \beta = 0.01$ , and the wave characteristics were the same as in the spit front cases. However, given that the beach is symmetric respect to the cross-shore direction, only positive values for the deep-water wave angle were used.

Fig. (3.7) shows the results for  $H_{s0} = 2$  m and  $T_p = 12$  s for the different waves angles. The significant wave height (Figs. 3.7a to c) is higher close to the horns of the undulations,



whereas it decays in the embayments. This behavior is also observed for the surf zone width in (Fig. 3.7d), where variations in 10% between the crests and the embayments of the undulations are observed. In this case, this variable was non-dimensionalized using the mean value along the coast. Regarding the effects of the variations in the deep-water wave angle, the locations of the maximums and minimums in the surf zone width are moved in the downdrift direction as this angle increases.

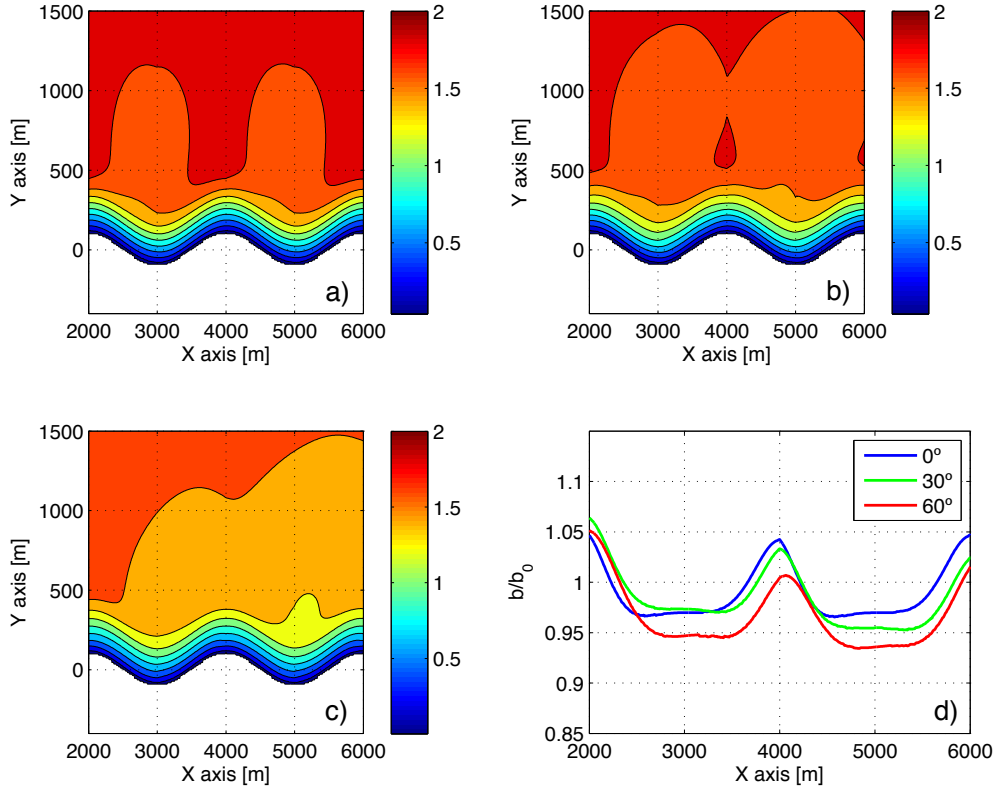


Figure 3.7: Results of the SWAN model for an undulation coast: a)  $H_s$  for  $\alpha_0 = 0^\circ$ ; b)  $H_s$  for  $\alpha_0 = 30^\circ$ ; c)  $H_s$  for  $\alpha_0 = 60^\circ$ ; d) Variation of the nondimensional surf zone width for different deep-water wave angles:  $\alpha_0 = 0^\circ$  (blue line),  $\alpha_0 = 30^\circ$  (green line),  $\alpha_0 = 60^\circ$  (red line).

Those results indicate that curvilinear bathymetries may induce important along-shore variations in the surf zone width (proportional to the wave height). The magnitude and location of the gradients of the surf zone width mainly depends on the deep-water wave angle, since tests with different wave periods show little variations.

### 3.3.2 Wave angle variations

Previous wave cases analyzed with SWAN were also used to study the nearshore wave angle  $\theta$ . The wave conditions were defined in the previous section ( $H_{s0} = 2$  m and variable wave period and deep-water wave angle). Wave angles were obtained at a depth of approximately 3 m to avoid physical effects induced by wave breaking.

### 3.3.2.1 Prograding spit front

Fig. (3.8) depicts the results for the prograding spit front forced by  $T_p = 12$  s waves. Tests with different wave periods provide similar results. Fig. (3.8a-e) shows the nearshore wave angle respect to the global coordinates  $X$  and  $Y$  for all the numerical domain, where angles are measured counter clockwise respect to the  $Y$  axis. Waves tend to arrive perpendicular to the shore due to refraction. However, they do not have enough time and distance to entirely refract and there are significant gradients in the wave angle, specially in the curvilinear stretch of the coast. This effect is clearly appreciable in Fig. (3.8f), where the wave angle is obtained at a depth of 3 m and measured respect to the cross-shore direction. It is shown that for every deep-water wave angle there are alongshore gradients of  $30^\circ$  between the straight stretch of the coasts and the tip of the spit.

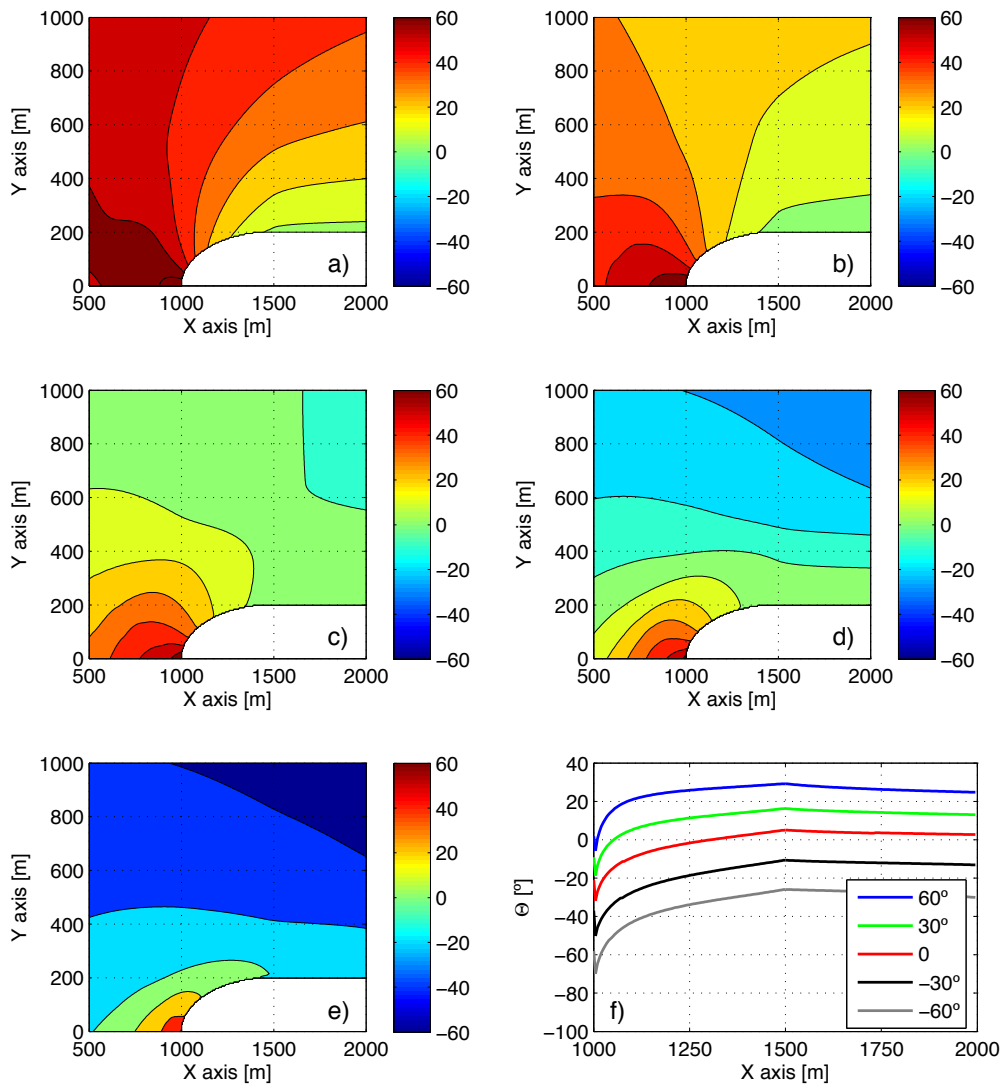


Figure 3.8: Results of the SWAN model for the elliptical spit front: a)  $\theta$  for  $\alpha_0 = 60^\circ$ ; b)  $\theta$  for  $\alpha_0 = 30^\circ$ ; c)  $\theta$  for  $\alpha_0 = 0^\circ$ ; d)  $\theta$  for  $\alpha_0 = -30^\circ$ ; e)  $\theta$  for  $\alpha_0 = -60^\circ$ ; f) Variation of the nearshore wave angle respect to the cross-shore direction for different deep-water wave angles:  $\alpha_0 = 60^\circ$  (blue line),  $\alpha_0 = 30^\circ$  (green line),  $\alpha_0 = 0^\circ$  (red line),  $\alpha_0 = -30^\circ$  (black line), and  $\alpha_0 = -60^\circ$  (grey line).

### 3.3.2.2 Undulating coast

For the case of an undulating coast, the behavior of the wave angle is similar. Fig. (3.9a-c) shows the wave angle respect to the Y axis for the whole numerical domain defined. The effect of refraction is distinguished by observing the differences between the left and the right side of the shoreline horns. Fig. (3.9d) depicts the nearshore wave angle respect to the cross-shore direction. For the case of  $\alpha_{0p} = 0$ , the wave angle is null both in the crests and horns of the shoreline. For the case of  $\alpha_{0p} = 30^\circ$ , the wave angle is null only in the left side of the horns (where the beach is oriented to the direction where the waves come from). For  $\alpha_{0p} = 60^\circ$ , the refraction is not enough to make the wave rays be normal to the shoreline and the nearshore angle is not null in any location of the coast. What these three cases have in common (and also the others combinations of wave period and direction) is that there are important alongshore gradients in the nearshore wave angle, with approximately  $20^\circ$  between the maximums and the minimums. the locations of this maximums and minimums vary depending on the wave direction. moving downdrift as

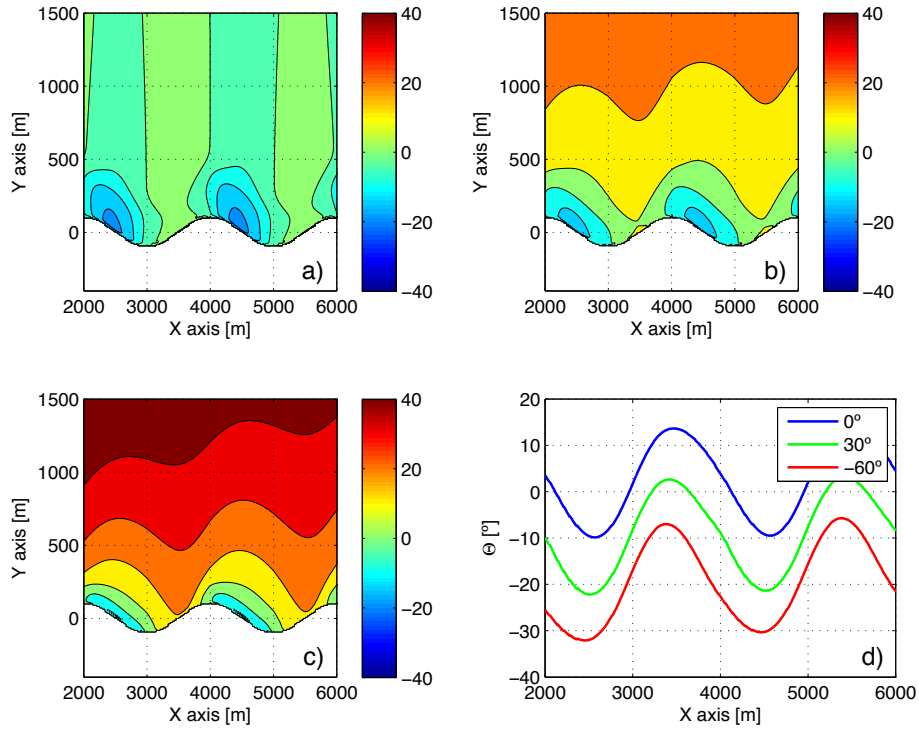


Figure 3.9: Results of the SWAN model for an undulation coast: a)  $\theta$  for  $\alpha_0 = 0^\circ$ ; b)  $\theta$  for  $\alpha_0 = 30^\circ$ ; c)  $\theta$  for  $\alpha_0 = 60^\circ$ ; d) Variation of the nearshore wave angle respect to the cross-shore direction for different deep-water wave angles:  $\alpha_0 = 0^\circ$  (blue line),  $\alpha_0 = 30^\circ$  (green line),  $\alpha_0 = 60^\circ$  (red line).

## 3.4 Conclusions

After the analysis of how wave propagate under the presence of: (1) a prograding spit front with an elliptical shape; and (2) an undulating coast, some conclusions were obtained:

- The presence of curvilinear bathymetries generates important alongshore wave variations in the breaking wave height, and hence, in the wave energy. For the case of a spit (undulating coast), typical wave conditions generate variations of approximately 20% (10%) in the surf zone width, which is proportional to the wave height. These variations may induce gradients of 45% (21%) in the wave energy, which is proportional to the square of the wave height.
- These curvilinear bathymetries also generates significant alongshore gradients of the nearshore wave angle. If it is measured respect to the cross-shore direction, differences of 30° and 20° are observed along the shoreline for the prograding spit and the undulating shoreline, respectively.
- Since the wave height (or equivalently the surf zone width) and the nearshore wave angle are the main variables usually considered to calculate the sediment transport rates, their gradients may induce important changes in the sediment transport pattern along the coast. Moreover, as this transport is the main responsible of the evolution of the shoreline, gradients of the sediment transport may trigger important morphological changes in the shoreline.



## **Curvilinear coasts (II): alongshore sediment transport**

---

In this Chapter, an alongshore sediment transport expression is updated to consider the effects of curvilinear bathymetries on wave propagation obtained in Chapter 2. Moreover, with our new framework we can consider other important factors in the analysis such as alongshore variations in beach slope, sediment size, shoreline orientation or type of wave breaking. Two different expressions are presented depending on the approximation to calculate the nearshore wave angle. Although the second approach, developed more recently, shows better agreement with numerical models for the wave angle, the first approach is retained because it was used in different applications which are described in the following chapters.

### **4.1 Framework and assumptions**

In wave-dominated sandy beaches, the alongshore sediment transport is the main responsible of the morphological evolution of the shoreline (Dean and Dalrymple, 2002b). The expressions for this sediment transport were traditionally obtained for straight coasts with shore-parallel contours, such as CERC (USACE, 1984) or Kamphuis (1991) formulas. However, if curvilinear bathymetries are considered the alongshore gradients in wave energy and wave angles at the nearshore must be accounted for, see Chapter 2. Hence, to study the implications of the wave propagation over curvilinear bathymetries on morphodynamics, an existing expression for alongshore sediment transport was adapted to curvilinear coasts.

We consider a sandy beach on a rectilinear or slightly curvilinear coast with periodic bathymetric changes along the coast defined by their amplitude  $a$  and wavelength  $\lambda$  (Fig. 2.4). The radius of curvature of the main alignment of the coast is large ( $R \gg \lambda$ , Fig. 2.1), whereas the local radius of curvature due to the bathymetric changes is  $R > 1000$  m. The

periodic bathymetric changes extend offshore according to the following equation:

$$h(X, Y) = \begin{cases} \tan\beta \left[ Y - \frac{a}{2} \cos\left(\frac{2\pi}{\lambda} X\right) \right] = \tan\beta [Y - \mu(X)] & 0 > h > h_1 \\ \tan\beta \left[ \frac{2Y - \left(\frac{a}{h_1 - h_2} h_2\right) \cos\left(\frac{2\pi}{\lambda} X\right)}{2 + \tan\beta \left(\frac{a}{h_1 - h_2}\right) \cos\left(\frac{2\pi}{\lambda} X\right)} \right] & h_1 > h > h_2 \\ \tan\beta Y & h_2 > h \end{cases} \quad (4.1)$$

where the global coordinates of the spatial domain are  $(X, Y)$ ;  $\mu(X)$  is the shoreline; and  $h(X, Y)$  is the depth (Fig. 4.1). The parameter  $h_2$  corresponds to the depth at which the beach bathymetry ends and intersects with the inner shelf of rectilinear shore-parallel contours. From the shoreline down to  $h_1$ , the beach slope  $\tan\beta$  is constant. From  $h_1$  to  $h_2$ , there is a smooth transition between the beach and the inner shelf. In the following, we assume that  $a \ll \lambda$ . Finally, the curvilinear local coordinates are  $(s, y)$ ,  $\alpha_{0p}$  is the deep-water wave angle with respect to the  $Y$  axis (Fig. 4.2),  $\phi(s)$  is the shoreline angle with respect to the  $X$  axis, and  $\theta(s, y)$  is the nearshore wave angle (angle between the wave ray and the cross-shore coordinate  $y$ ). The across-shore distance between the shoreline and the breaking line, defined as the surf zone width, is denoted by  $b$ .

The smooth alongshore variations in the coastline are expected to generate along-shore variations in the surf zone, and along- and cross-shore variations in the height and angle of the local nearshore waves, the radiation stress, the alongshore current, the setup, the wave energy dissipation per unit of coastline length, the sediment transport and the sediment size. One of the main objectives of this thesis is to analyze, to the order  $\mathcal{O}(a/\lambda)$  in a first approach, the morphodynamic response of this typology of sandy beaches when waves with different characteristics (in terms of their wave heights, angles and periods) impinge. To obtain a formulation as simple as possible that includes the main mechanisms that influence the morphodynamic response of the system, the following assumptions are adopted:

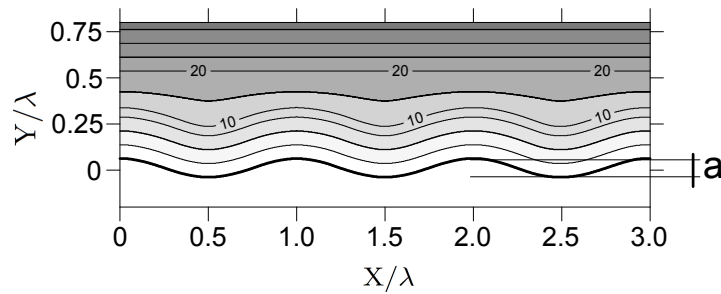


Figure 4.1: Scheme of the bathymetric framework showing the amplitude  $a$  of the SU in global coordinates  $X$  and  $Y$ . In the cases considered,  $h_1 = 10$  m and  $h_2 = 20$  m. The axis distances are non-dimensionalized by the wavelength of the SU  $\lambda$ .

1. The still water level is constant and only changes due to the wave setup. Hence, the effect of tides is neglected in this analysis (microtidal conditions).

2. In the surf zone, the wave height  $H(y)$ , the radiation stress representing the flux in the alongshore direction  $S_{sy}(y)$ , the wave energy flux  $E(y)C_g(y)$  and the wave energy dissipation decrease gradually towards the coast (i.e., spilling breakers).
3. The breaking index evolves smoothly within the surf zone and mainly depends on the local Iribarren number (Baquerizo and Losada, 1999). Wave reflection on the beach face and wave diffraction along the breaking crests are negligible.
4. The oscillatory vorticity field is transferred to the mean field leading to a steady alongshore current which follows the topography and so behaves the sediment transport (Holloway and Sou, 1996; Marinone, 1998).
5. The local along- and cross-shore sediment transports are proportional to the wave energy dissipation in the surf zone and are well represented by the Inman and Bagnold (1963) approach.
6. The shoreline evolution and the corresponding beach evolution are entirely driven by the gradients in alongshore sediment transport (Pelnard-Considère, 1956; Ashton and Murray, 2006a).
7. The local beach slope and the local sediment size are proportional; the greater the slope is, the coarser the sediment is (Short, 2001).

These assumptions have the following consequences:

1. The contribution to the transporting velocity by waves is negligible and only currents move the material (Nam et al., 2009).
2. The evolution of the undulating sandy beach is driven by the alongshore sediment transport gradients.
3. The local surf zone variables that exhibit variability in the  $y$  direction can be expressed in terms of the surf zone width along the coast  $b(s)$  (López-Ruiz et al., 2012b), which includes the effect of the undulating beach bathymetry up to  $\mathcal{O}(a/\lambda)$ .
4. Because wave reflection is neglected, all the wave energy flux that reaches the surf zone ( $E_b C_{gb}$ , where  $E$  is wave energy,  $C_g$  is group celerity and  $b$  denotes wave breaking) is dissipated between the breaking point and the shoreline, and the dissipation rate through the surf zone can be expressed as  $E_b C_{gb}$  (Inman and Bagnold, 1963).

Under such conditions, it is expected that a given initial beach morphology will evolve over time, depending on the alongshore variations in the alongshore sediment transport. This sediment transport may vary for different deep-water wave conditions and beach characteristics (beach slope and sediment size).



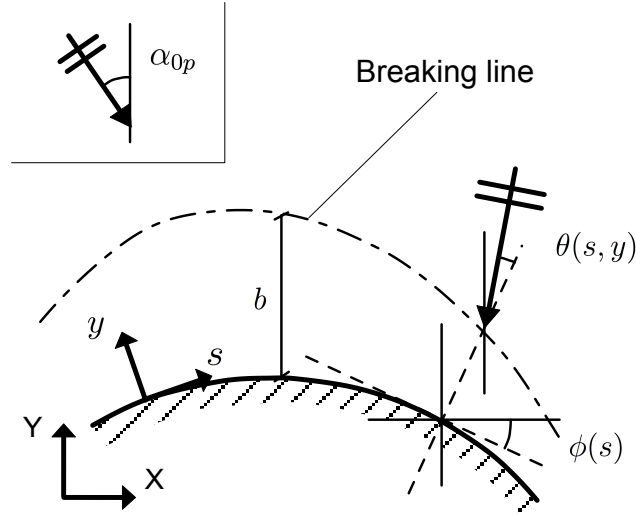


Figure 4.2: Definition of the main variables as a function of the local coordinates  $s$  and  $y$ , where  $\alpha_{0p}$  is the deep water wave angle respect to the global coordinates  $X, Y$ ,  $\theta(s, y)$  is the local nearshore wave angle,  $b(s)$  is the distance between the shoreline and the breaking line in the  $y$  direction (surf zone width), and  $\phi(s)$  is the local shoreline angle. Solid lines show the  $(X, Y)$  directions, whereas the dashed lines show the local  $(s, y)$  directions.

## 4.2 An updated expression for the AST

In this section, we present an updated version of the alongshore sediment transport formula of Inman and Bagnold (1963) for curvilinear coasts, using the framework defined previously. Under our assumptions, this formula is able to represent the local alongshore sediment transport in a bathymetry perturbed by shoreline undulations to the order  $\mathcal{O}(a/\lambda)$ .

The expression of Inman and Bagnold (1963) is a process model of sand transport on beaches, where the sand transport in the nearshore results from the combined effects of waves and currents, with the waves placing the sand in motion while the alongshore current produces the net sand advection. Their formula relates the volume of alongshore sediment transport including pores to the wave energy dissipation along the coast and can be written as follows:

$$S_{I\&B} = \frac{K}{(\rho_s - \rho)g(1 - p)} (EC_g)_b \cos \theta_b \frac{\bar{V}}{u_{mb}} \quad (4.2)$$

where  $\rho$  and  $\rho_s$ , are the water and sediment particle densities,  $p$  is the porosity of the material,  $K$  is a dimensionless coefficient which depends on the grain size (del Valle et al., 1993),  $g$  is the gravity acceleration,  $u_{mb}$  is the maximum horizontal bottom orbital velocity of the waves evaluated at the breaking, and  $\bar{V}$  is the averaged alongshore current caused by the oblique incidence of the waves in the surf zone (Longuet-Higgins, 1970). Note that  $E_b C_{gb}$  represents the wave energy flux per unit of wave crest that is dissipated in the whole cross-shore section of the surf zone.

The objective is to include the effects of spatial variations in the sediment size, beach slope, type of wave breaking, wave angle and wave energy. If hypothesis (1) to (3) are satisfied (Section 4.1) and the wave angle in the nearshore is known,  $EC_g$ ,  $V$  and  $u_m$  can be expressed in terms of the local variables  $s$  and  $y$ . In this case,  $E(s, y)C_g(s, y)\cos\theta(s, y)$  represents the wave energy flux per unit of wave crest in the direction of the waves. If nearshore values are retained, the local alongshore current becomes:

$$V(s, y) = \frac{5}{8}\pi g \frac{\tan^2 \beta \gamma}{f} \frac{\sin \theta(s, y)}{\sqrt{g \tan \beta y}} y \quad (4.3)$$

where  $f$  is a friction coefficient. The wave energy is:

$$E(y) = \frac{1}{8}\rho g H^2 = \frac{1}{8}\rho g (\gamma \tan \beta y)^2 \quad (4.4)$$

The group celerity is expressed as follows:

$$c_g(y) = \frac{c}{2} \left( 1 + \frac{2kh}{\sinh 2kh} \right) \simeq \sqrt{g \tan \beta y} \quad (4.5)$$

where  $c$  is the wave celerity. The orbital velocity of the particles at the sea bottom is:

$$u_m(y) = \frac{1}{2}\gamma \sqrt{g \tan \beta y} \quad (4.6)$$

Then, linear wave theory and depth-limited breaking can be used to obtain the local alongshore sediment transport per unit of cross-shore section:

$$S_{lst}(s, y) = K_T y^{5/2} \sin(2\theta(s, y)) dy \quad (4.7)$$

where:

$$K_T(s) = \frac{5 K \pi \rho \gamma^2 (\tan \beta(s))^{7/2} \sqrt{g}}{32(\rho_s - \rho)(1 - p)f} \quad (4.8)$$

The averaged sediment transport rate parallel to the coastline can then be obtained by integrating this local alongshore sediment transport per unit of shoreline along the surf zone (López-Ruiz et al., 2012a):

$$Q(s) = \frac{1}{b(s)} \int_0^{b(s)} S_{lst}(s, y) dy = K_T(s) \frac{1}{b(s)} \int_0^{b(s)} \sin(2\theta(s, y)) y^{5/2} dy \quad (4.9)$$

The integral in Eq. (4.9) has analytical solutions if an analytical expression is adopted for  $\theta(s, y)$ . Moreover, Eq. (4.9) was obtained without any restriction on the wave angle,

the sediment size or the beach slope. Thus, these parameters can be considered variables in both the  $s$  and  $y$  directions.

In the next sections, two different solutions are obtained for Eq. (4.9). The difference between these two approaches is the way in which the wave angle in the nearshore  $\theta(s, y)$  is obtained. The different solutions to account for wave refraction were chosen in order to obtain an analytical solution; however, any other solution for wave refraction could be used, solving Eq. (4.9) numerically.

### 4.3 First approach

In this first approach, the Snell law is applied using the deep-water wave angle  $\alpha_{0p}$ . Then, the result is corrected to account for the curvilinear bathymetry. Hence, the wave angle in the nearshore can be expressed as follows (Fig. 4.2):

$$\theta(s, y) = \alpha(y) + \phi'(s) \quad (4.10)$$

where  $\alpha(y)$  is the wave angle obtained with the Snell law and  $\phi'(s)$  is a parameter introduced to correct the Snell wave refraction for a curvilinear coast. As waves do not have sufficient time to adapt to the shoreline, it can be assumed that  $\phi'(s) \simeq \phi(s)$ , with  $\phi(s)$  being the shoreline angle defined in Fig. 4.5. After some analysis of SWAN results (see Section 4.4.1), the assumption can be considered acceptable for not very oblique waves. With the Snell law,  $\alpha(y)$  can be expressed in terms of deep-water waves:

$$k_0 \sin \alpha_{0p} = k \sin \alpha \quad (4.11)$$

where  $k_0$  and  $k$  are the wave numbers at deep water,  $k_0 = \frac{\sigma^2}{g}$ , and in shallow depths  $k = \frac{\sigma}{\sqrt{g \tan \beta y}}$ , with  $\sigma = 2\pi/T$ , which gives the following expression:

$$\alpha(y) = \arcsin(\Psi_1 \sqrt{y}) \quad (4.12)$$

where  $c_1$ :

$$\Psi_1 = \sigma \sin \alpha_{0p} \sqrt{\frac{\tan \beta}{g}} \quad (4.13)$$

Hence, the wave angle in the nearshore can be expressed as:

$$\theta(s, y) = \arcsin(\Psi_1 \sqrt{y}) + \phi(s) \quad (4.14)$$

In this first approach, two additional assumptions are considered: (1) the beach slope  $\tan \beta$  is assumed to be constant in the across-shore direction; and (2) sediment size

monotonically varies across-shore along the beach according to Dean and Dalrymple (2002b).

A relation between the mean sediment size ( $D_{50}$ ) and the  $K$  coefficient, which is proportional to the alongshore sediment transport (Eq. REF), was obtained by del Valle et al. (1993). According to their expression, and in order to obtain an analytical expression for the total sediment transport  $Q$ , a linear law with the distance to the shoreline  $y$  was adopted:

$$K(y) = A_1 y + A_2 \quad (4.15)$$

This choice is valid for small variations of  $D_{50}$ , for which the exponential law can be approximated with a linear function, after assuming a linear dependency of the sediment size on the distance to the shoreline.

The total sediment transport parallel to the coastline can now be calculated by solving Eq. (4.9) using the obtained expressions for the nearshore wave angle (Eq. 4.14) and the  $K$  coefficient (Eq. 4.15):

$$Q(s) = \frac{1}{b(s)} \int_0^{b(s)} \left[ \frac{1}{2} K_T (A_1 y + A_2) y^{5/2} \sin(2 \arcsin(\Psi_1 \sqrt{y}) + 2\phi(s)) \right] dy \quad (4.16)$$

This integral has the following explicit solution:

$$Q(s) = P_1(b(s)) \cdot \cos(2\phi(s)) + P_2(b(s)) \cdot \sin(2\phi(s)) \quad (4.17)$$

where  $P_1(b(s))$  and  $P_2(b(s))$  are two polynomial functions dependent on the surf zone width and the characteristics of deep-water waves. These polynomials are modulated by trigonometric functions of the angle of the coastline:

$$\begin{aligned} P_1(b) = & \frac{K_3}{b} \left[ -2(1 - \Psi_1^2 b)^{3/2} \left( 11A_2 \Psi_1^2 \left( 16 + \Psi_1^2 b (24 + 5\Psi_1^2 b (6 + 7\Psi_1^2 b)) \right) \right) - \right. \\ & - 2(1 - \Psi_1^2 b)^{3/2} 11A_2 \Psi_1^2 A_1 \left( 128 + \Psi_1^2 b \left( 192 + 5\Psi_1^2 b (48 + 7\Psi_1^2 b (8 + 9\Psi_1^2 b)) \right) \right) + \\ & \left. + 22A_2 \Psi_1^2 (16 + 128A_1) \right] \end{aligned} \quad (4.18)$$

and

$$P_2(b) = K_3 \Psi_1^9 \left[ 5b^{5/2} (A_2 (99 - 154\Psi_1^2 b) - 7A_1 (-11 + 18\Psi_1^2 b)) \right] \quad (4.19)$$

with  $K_2 = 2/3465$ ,  $K_3 = K'_1/(2K_2\Psi_1^9)$  and  $b = b(s)$  as the breaking zone width.

### 4.3.1 Surf zone width-dependent sediment transport

In this section, the obtained alongshore sediment transport expression for this first approach (Eq. 4.17) is compared with the one in Ozasa and Brampton (1980) and the CERC formulation. These expressions were applied to a syntetical shoreline where  $\phi(s) \in [0, \pi/2]$ . Different deep-water wave angles were used to establish different shapes of the surf zone width (See Chapter 3).

Fig. 4.3 shows the results for three different shapes of  $b$ . These shapes are represented in the lower left corner of each graph along with a schematic representation of the coastline. For cases a) and b), the maximum value of  $b(s)$  is the same and its position varies from  $\phi(s) = 0^\circ$  to  $30^\circ$ . The values of the corresponding deep-water wave angles are  $\alpha_{0p} = 40^\circ$  and  $\alpha_{0p} = -40^\circ$ , respectively. These values are representative of the situations described in Fig. (3.6). Case c) is a hypothetical situation (constant  $b$ ) defined to compare the behavior of the three formulations. For all of them, a slope  $\tan \beta = 0.01$ , a wave period  $T = 12$  s, and significant wave height in deep water  $H_0 = 2$  m were defined. These characteristic wave energy conditions ensure that the longshore transport is capable of causing changes in the coastal morphology. Similar results were obtained for other typical values for wave-dominated sandy beaches.

The relative alongshore sediment transport rate obtained with the three expressions shows a similar behavior with the maximum value reached at a similar shoreline position  $\phi(s)$ . Moreover, the maximum values of all the relationships move towards  $\phi = \pi/2$  as the position of the maximum breaker width shifts in the same direction. For constant  $b$ , the CERC and the Ozasa and Brampton (1980) expressions coincide since the Ozasa and Brampton (1980) formula is a modification of the CERC formula, which includes the breaking wave height gradient (see Falqués and Calvete, 2005). The modified Inman and Bagnold (1963) formula shows a similar trend, but the maximum transport is reached for a smaller shoreline angle of  $\phi(s) = 38^\circ$ .

For cases (a) and (b), there is an inversion in the sediment transport direction for those points of the coastline at which  $\alpha_b(s) + \phi(s) \geq 90^\circ$ . These points do not vary significantly in all of the three cases studied. This indicates that the sediment transport direction is mainly determined by the alignment of the coast and the deep-water wave angle. Finally, the results of the formulation for larger values of  $\phi(s)$  should be used with care since the wave refraction was calculated using the Snell law. However, for undulating coasts where  $a/\lambda \ll 1$  the shoreline angle is  $\phi \leq \pi/4$ .

## 4.4 Second approach

The approximation for the wave angle in the nearshore used through Section 4.3 shows accurate results for waves incoming with a deep-water wave angle  $\alpha_{0p} < 45^\circ$ . However, under more oblique waves, it may induce significant errors. Hence, an effort was made to increase the range in which the results for the refraction approximation were valid to study the nearshore hydrodynamics.

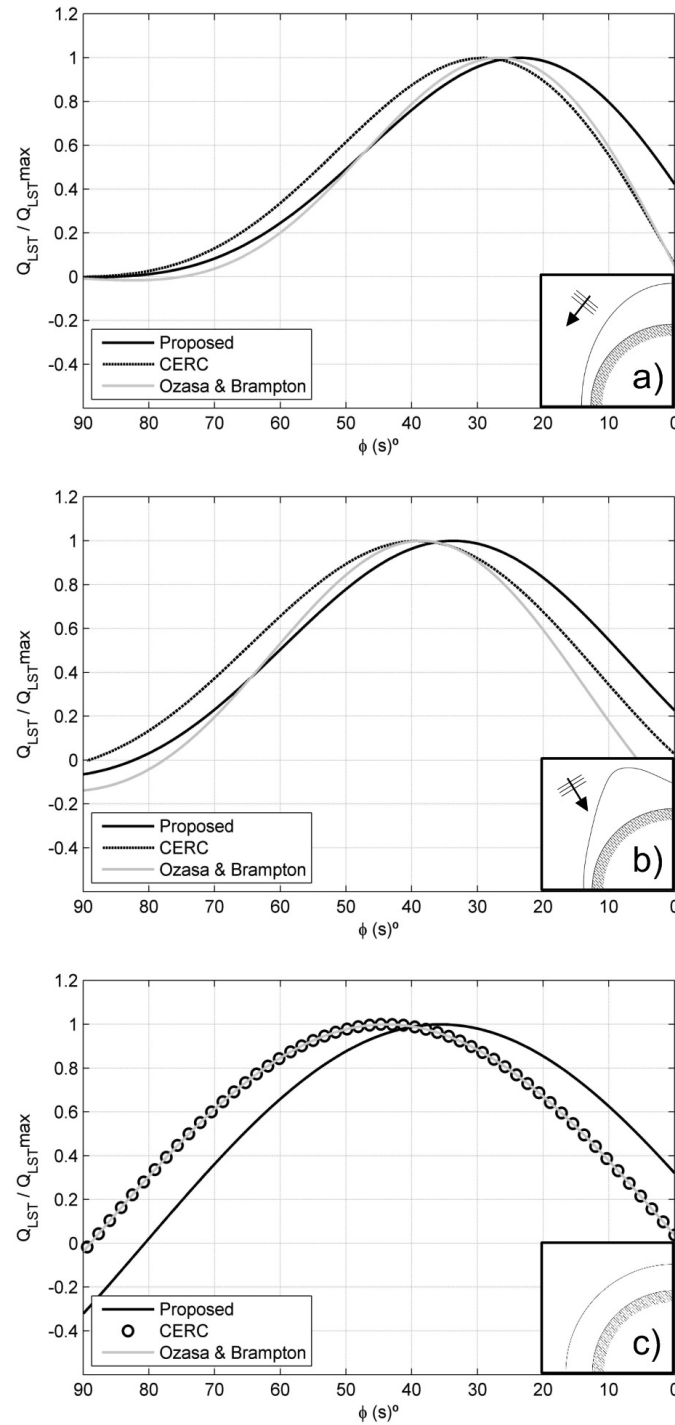


Figure 4.3: Relative alongshore sediment transport for the modified Inman and Bagnold (1963) formula, the CERC formula and the Ozasa and Bampton (1980) formula. Three cases were defined, depending on the shape of the surf zone: (a) surf zone width maximum on  $\phi(s) = 0^\circ$ ; (b) surf zone width maximum on  $\phi(s) = 30^\circ$ ; (c) constant surf zone width.

In this section, a second expression for the alongshore sediment transport is presented using a different approximation for the wave angle in the nearshore. In this case, the wave angle is corrected before the application of the Snell law (corrected before refraction).

The results show that this refraction approximation is accurate for waves incoming with, at least,  $\alpha_{0p} < 60^\circ$ . Moreover, a simple model to obtain the nearshore wave height (and hence the surf zone width) is also presented.

#### 4.4.1 Surf zone wave angle approximation

The second wave angle approximation assumes that if inverse shoaling is considered, the wave ray in deep water has the orientation of the approximation defined. For every shoreline position  $s$ , the modified deep-water wave angle is defined as follows:

$$\alpha_0(s) = \alpha_{0p} + \phi(s) \quad (4.20)$$

Hence, every section of the shoreline is considered locally as a rectilinear stretch of the coast with shore-parallel contours. An expression for  $\theta(s, y)$  can then be obtained using Snell law for shore-parallel contours:

$$k_0 \sin \alpha_0(s) = k \sin \theta(s, y) \quad (4.21)$$

where  $k$  is the wave number and the subscript 0 indicates deep-water values. Again, the wave number is obtained by means of linear theory, with  $k_0 = \sigma^2/g$  and  $k = \sigma/\sqrt{g \tan \beta(s) y}$ ,  $\sigma = 2\pi/T$  being the wave frequency and  $g$  being the acceleration of gravity. The wave angle in the nearshore yields the following expression:

$$\theta(s, y) = \arcsin \left[ \sigma \sqrt{\frac{\tan \beta}{g}} \sin \alpha_0(s) \sqrt{y} \right] = \arcsin \left( \Psi_2(s) \sqrt{y} \right) \quad (4.22)$$

where

$$\Psi_2(s) = \frac{2\pi}{T} \sqrt{\frac{\tan \beta}{g}} \sin (\alpha_{0p} + \phi(s)) \quad (4.23)$$

This parameter can be interpreted as a measure of the wave refraction for a given coast configuration ( $\phi(s)$  and  $\tan \beta$ ) or for a given deep-water wave conditions ( $\alpha_{0p}$  and  $T$ ).

To check the validity of this new refraction approximation, the results were compared with numerical propagations obtained using the SWAN model (Booij et al., 1999). The results for the first refraction approximation (Section 4.3) are also depicted to show the improvement achieved correcting the wave angle before using the Snell law. The bathymetry is defined by Eq. (batimetria) with  $\lambda/a = 5$  (Fig. 4.1). The beach slope in the surf zone was  $\tan \beta = 0.01$ . Offshore waves were characterized by a significant wave height of  $H_0 = 2$  m, periods of  $T = 6$  and  $12$  s and different directions of incoming waves, ranging between  $-60^\circ$  and  $60^\circ$  with respect to the mean shoreline alignment (X-axis in Fig. 4.2). Those values are close to real scenarios, but any others that fulfill the governing hypothesis described below can be used.

The wave angle was obtained along the 3-m bathymetric line, close to breaking for the conditions defined (Fig. 4.4). The coherences between the model and the approximations were analyzed by the root mean square error (RMSE), the correlation coefficient (R), and model performance (skill, S) (Olabarrieta et al., 2011). Considering that  $A_n$  and  $M_n$  are the approximation and the SWAN model results, respectively, at  $N$  discrete points along the coast, the RMSE is given by:

$$\text{RMSE} = \left[ \frac{1}{N} \sum_{n=1}^N (A_n - M_n)^2 \right]^{1/2} \quad (4.24)$$

The correlation coefficient (R) between  $A_n$  and  $M_n$  is defined by:

$$R = \frac{\frac{1}{N} \sum_{n=1}^N (A_n - \overline{A_n})(M_n - \overline{M_n})}{\sigma_A \sigma_M} \quad (4.25)$$

where  $\sigma_A$  and  $\sigma_M$  are the standard deviations of the analytical and numerical results, respectively. The overline represents the mean value. The correlation ranges from 0 (bad correlation) to 1 (good correlation). The model performance (skill, S) is a measure of the coherence between the two series of data in the local maximums and minimums (transition between the horns and the crests of the undulations), and its formulation is given by:

$$S = 1 - \frac{\frac{1}{N} \sum_{n=1}^N |A_n - M_n|^2}{\frac{1}{N} \sum_{n=1}^N (|A_n - \overline{A_n}|^2 + |M_n - \overline{M_n}|^2)} \quad (4.26)$$

This skill formulation ranges from 0 (bad skill) to 1 (good skill). The results for these three parameters are shown in Fig. (4.4).

With respect to the influence of the wave angle, as the value of  $\alpha_{0p}$  increases, the refraction approach differs more from the numerical model, especially in the transition between the crests and the horns of the shoreline (Fig. 4.4e and 4.4j). This is because in these locations the angle between the normal-to-shore and deep water wave directions is larger. The value of S decreases faster than R as the wave obliquity increases. However, the alongshore gradients of the wave angle are similar. For the same wave angle, the results for  $T = 6$  s fit better with the numerical model in the crests and troughs, with a higher skill. Nevertheless, the differences considering the full alongshore domain are smaller in the case of  $T = 12$  s, and the R value is better. This behavior is observed for both approximations, although the results for the second (correct before refract) show a much better fit, specially in the transition between horns and embayments.

Hence, this second approximation differs slightly from the model but is much simpler to implement. Only under highly oblique waves ( $\alpha_{0p} > 45^\circ$ ) are the correlations and skills lower than  $R < 0.94$  and  $S < 0.6$ , respectively. However, the alongshore patterns of wave



angle gradients are well reproduced. As will be discussed later, these gradients drive the alongshore changes in sediment transport, and hence, the coastline evolution.

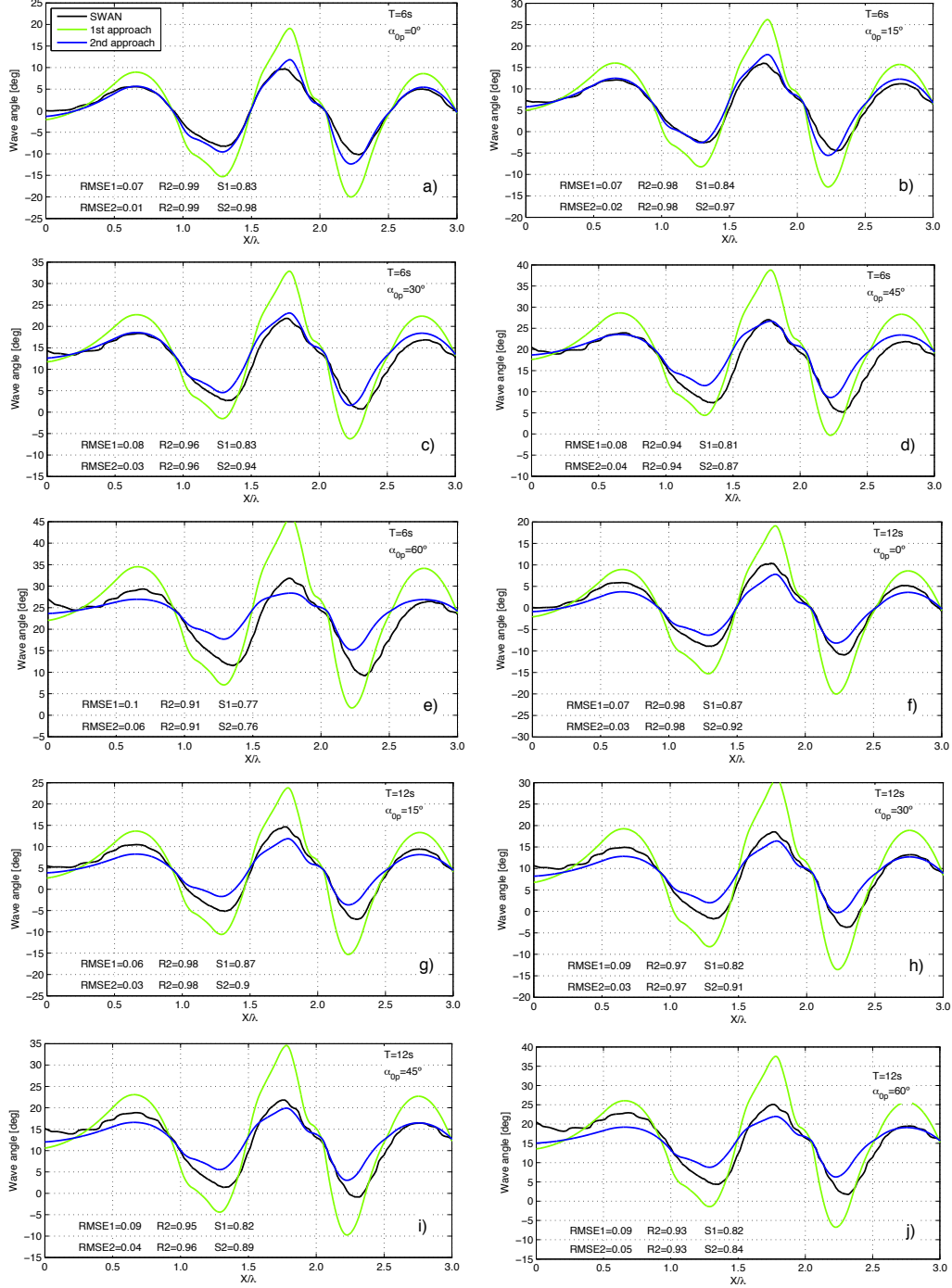


Figure 4.4: Wave angle of the SWAN model (black line), first angle approach (green line), second angle approach (blue line) and root-mean-square error (RMSE), correlation coefficient (R) and skill (S) between the approximations and the model results for different combinations of deep-water wave angle  $\alpha_{op}$  and wave period  $T$

### 4.4.2 Surf zone wave height

To obtain the surf zone width  $b$ , the wave height is obtained using the shoaling and refraction coefficients. The former is obtained using the relation between the group celerity in deep water and in the nearshore. The latter is obtained using the conservation equation of wave energy flux along the wave crests. The wave height in the nearshore can then be estimated as follows:

$$H = H_0 K_p = H_0 K_s K_r = H_0 \sqrt{\frac{C_{g0}}{C_g}} \sqrt{\frac{d_0}{d}} \quad (4.27)$$

where  $d$  is the distance between wave rays,  $C_g$  is the group celerity, the subscript 0 indicates deep water, and  $K_p$ ,  $K_s$  and  $K_r$  are the propagation, shoaling and refraction coefficients, respectively. The distance between wave rays can be assessed geometrically or can be calculated solving the ODE system defined by Noda (1974). The surf zone width  $b$  can then be determined using a variable breaking index (hypothesis 3, Section 4.1). This approximation was successfully applied to various wave and beach conditions, considering smooth SH ( $\alpha/\lambda \leq 0.1$ ) and waves that are not high breaking ( $\alpha \leq 60^\circ$ ).

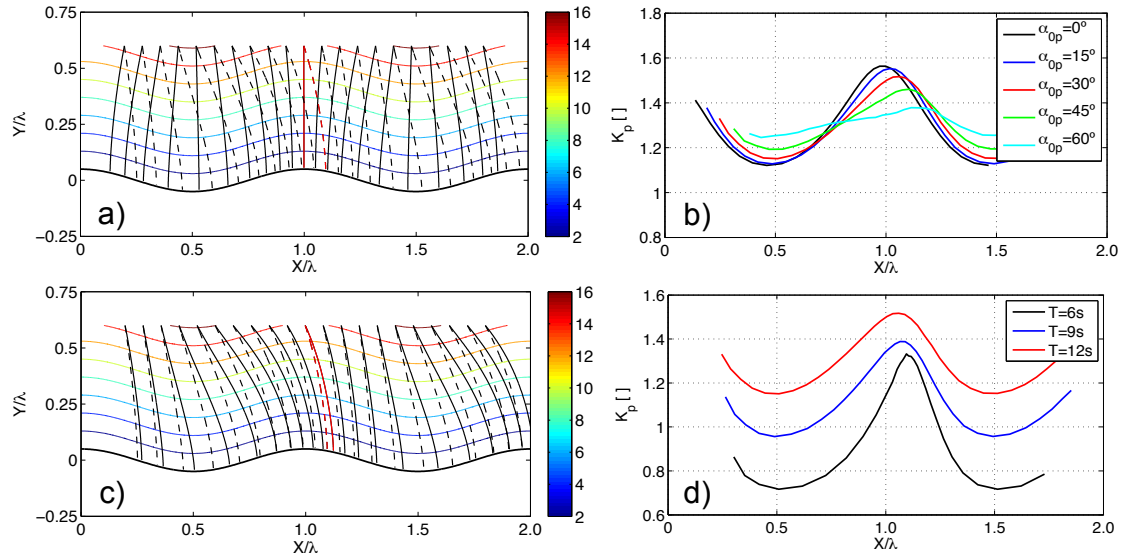


Figure 4.5: Wave ray paths and propagation coefficient ( $K_p$ ) for an undulating bathymetry: a) ray paths for  $T = 12$  s and  $\alpha_{0p} = 0^\circ$  (solid lines) and  $\alpha_{0p} = 30^\circ$  (dashed lines); b)  $K_p$  for  $T = 12$  s and  $\alpha_{0p} = 0, 15, 30, 45, 60^\circ$  (colored lines); c) ray paths for  $\alpha_{0p} = 30^\circ$  and  $T = 9$  s (solid lines) and  $T = 12$  s (dashed lines); d)  $K_p$  for  $\alpha_{0p} = 30^\circ$  and  $T = 6, 9, 12$  s (colored lines). The color scale shows the depth of the domain.

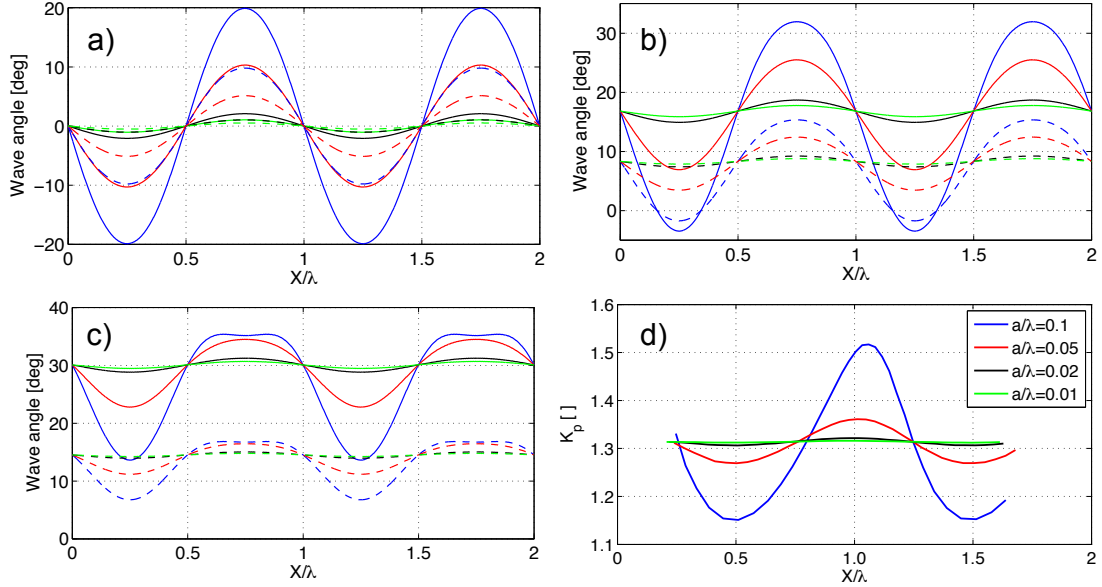


Figure 4.6: Alongshore wave angle variation for different  $\lambda/a$  values (colours), with  $T = 6$  s (solid lines) and  $T = 12$  s (dashed lines) for different deep-water wave angles: a)  $\alpha_{0p} = 0^\circ$ ; b)  $\alpha_{0p} = 30^\circ$ ; c)  $\alpha_{0p} = 60^\circ$ . Panel d) shows the results for  $K_p$  for  $\alpha_{0p}$  and  $a/\lambda = 0.1, 0.05, 0.02, 0.01$

The maximum and minimum values of the wave angle are obtained in the transition between the crests and troughs of the shoreline. Areas where the wave angle is negative correspond to the right-hand side of the crests for cases with a small value of  $a/\lambda$ , where the angle of the shoreline  $\phi$  is too large to be compensated by refraction. This refraction is more pronounced for  $T = 12$  s, with  $|\theta| < 12^\circ$ . As  $T$  increases, the alongshore gradients in the wave angle decrease. Moreover, as  $\alpha_{0p}$  increases, the  $\theta$  increases, and asymmetries between the updrift and the downdrift side of the crest become more evident. These asymmetries are due to the sign of  $\alpha_{0p}$ : for positive values, the shadow zones for the waves propagating toward the coast are in the updrift side.

Furthermore, as  $\alpha_{0p}$  increases, some perturbations are observed for the cases with greater  $a/\lambda$ . This effect is significant for the case of  $\alpha_{0p} = 60^\circ$  and  $a/\lambda = 0.1$ , where the pattern for maximums and minimums is different. This suggests that the wave propagation approach may not accurately reproduce the wave angle for coasts with steeper undulations and oblique waves, such as beach cusps. However, general beach cusp theories assume that beach cusps tend to disappear with oblique waves (Dodd et al., 2008). The results also indicate that  $\theta$  is almost constant in the alongshore direction for  $a/\lambda \leq 0.02$ . However, for the case of  $a/\lambda = 0.05$ , which corresponds to the typical geometry of SU, there are gradients in the wave angle of approximately  $10^\circ$  in half of the wavelength.

### 4.4.3 Specific solution for alongshore sediment transport

A simple analytical solution of Eq. (4.9) was obtained considering the second approximation for the nearshore wave angle. However, to find the solution for Eq. (4.9), two additional assumptions were adopted: (1) the beach slope is constant in the  $y$  direction; and (2) the sediment size is also constant in the across-shore direction.

Combining Eq. (4.22) and (4.9), it follows for the alongshore sediment transport:

$$Q(s) = K_T \frac{4}{315b\Psi_2^7} \left[ 16 - (1 - b^2\Psi_2)^{3/2} \left[ 16 + b\Psi_2^2 (24 + 5b\Psi_2^2(6 + 7b\Psi_2^2)) \right] \right] \quad (4.28)$$

where  $Q(s)$  is expressed as a function of the alongshore distribution of beach slope and sediment size (included in  $K_T$  and  $\Psi_2$ ), the surf zone width, the wave period, and the deep-water wave and shoreline angles (included in  $\Psi_2$ ).

Eq. (4.9) only has an analytical solution (Eq. 4.28) for combinations of  $b$  and  $\Psi_2$  that fulfill breaking depths  $h_b \leq gT^2/40$ , which is true for the majority of typical wind-generated waves (wave periods between 3 and 30 s). Although Eq. (4.28) is not mathematically defined for  $\Psi_2 = 0$  (shore-normal wave incidence) and  $b = 0$ , the limit of this function has a finite value:  $\lim_{\Psi_2(s) \rightarrow 0} Q(s) = \lim_{b(s) \rightarrow 0} Q(s) = 0$ . This implies vanishing alongshore sediment transport for both waves arriving normal to the shoreline and for no incident wave energy. To simplify the application of Eq. (4.28) in the vicinity of  $b = 0$  and  $\Psi_2 = 0$ , it can be expressed as a power series expansion around these values. The result for the series in the vicinity of  $b = 0$  and  $\Psi_2 = 0$  to the order  $\mathcal{O}[\Psi_2^7 b^6]$  is as follows:

$$Q(s) = K_T \left( \frac{\Psi_2 b^3}{2} - \frac{\Psi_2^3 b^4}{5} - \frac{\Psi_2^5 b^5}{24} + \mathcal{O}[\Psi_2^7 b^6] \right) \quad (4.29)$$

Considering typical values of  $\Psi_2 = \mathcal{O}[10^{-2}]$  (see Fig. 4.7 lower panel) and  $b = \mathcal{O}[10^2]$ , the terms on the right side of this expression decrease as their exponents increase, and the second and subsequent terms on the right side can be neglected with respect to the first term. Thus, for those cases:

$$Q(s) \simeq K_T \left( \frac{\Psi_2 b^3}{2} \right) \quad (4.30)$$

which is an expression that is simple to implement in practical applications and that avoids numerical problems in the vicinity of  $\Psi_2 = 0$  and  $b = 0$ . Fig. (4.7) shows the area in which the relative difference between Eqs. (4.29) and (4.30) is less than 5% (upper panel). Fig. (4.7) also depicts the values of  $\Psi_2(s)$  for  $\sin \alpha_0(s) = 1$  as a function of  $T$  and  $\tan \beta$  (lower panel). In the next Chapter, in which Eq. (4.28) is analyzed, Eq. (4.30) was used for the cases in which the relative difference was less than 5% (Fig. 4.7, upper panel) to check the applicability of this simplification and to avoid situations with  $\Psi_2 = 0$  where Eq. (4.28) is not defined.

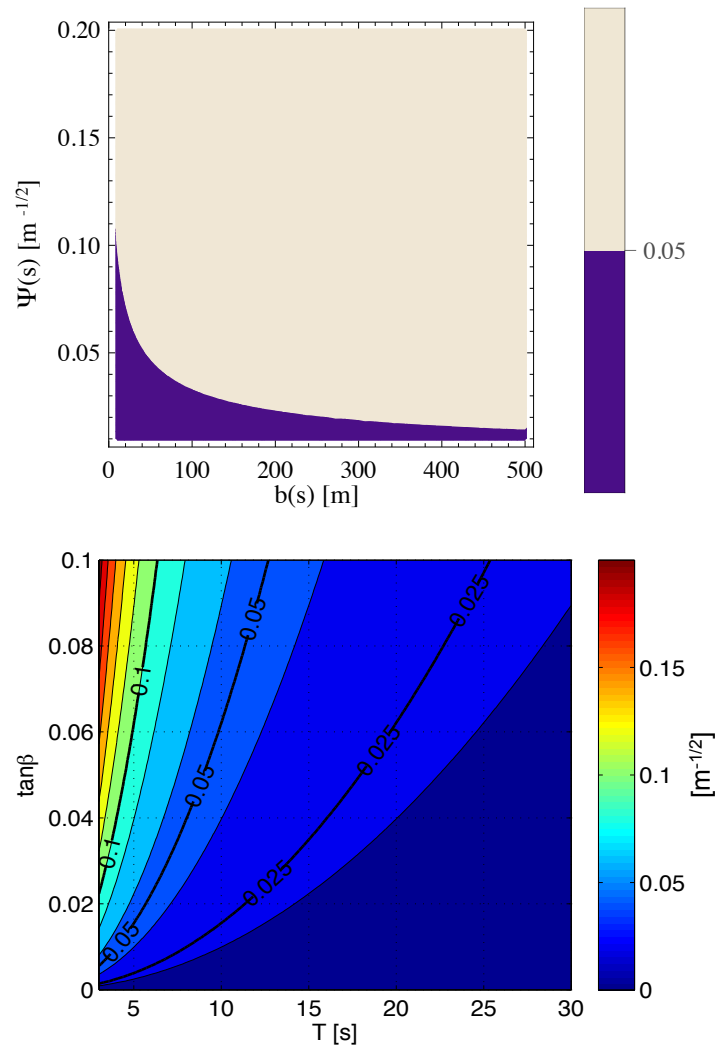


Figure 4.7: Upper panel: relative difference between  $Q(s)$  of Eq. (4.28) and of Eq. (4.30). Lower panel:  $\Psi_2(s)$  values depending on beach slope  $\tan \beta$  and wave period  $T$ .

# **Implications on coastal evolution (I): shoreline movements and hydrodynamics**

---

In Chapter 4, an updated framework to obtain an alongshore sediment transport expression was presented. It considers the effects of the presence of a curvilinear bathymetry, as well as the variation of some beach characteristics such as beach slope, sediment size or shoreline orientation. Two different expressions were obtained for this transport depending on the approximation for the nearshore wave angle. Now, the expression obtained with the second approach is used to analyze the potential changes in the shoreline geometry and the hydrodynamics due to the presence of curvilinear bathymetries.

## **5.1 Numerical experiments and overall procedure**

Some numerical experiments were carried out using the the procedure described in Section 4.4. The obtained expression for the alongshore sediment transport (Eq. 4.29 and Eq. 4.30 when possible) was applied to various syntetical scenarios of undulating sandy beaches to evaluate the influence of changes in deep-water wave conditions (wave height, period and angle) and also beach characteristics such as the beach slope and the shoreline geometry, on the sediment transport.

Five bathymetries were built using Eq. (4.1) with various alongshore distributions for beach slope and  $a/\lambda$  values. For each case, the sediment size varied according to the assumptions presented in Section (4.1). Variable deep-water wave conditions were used according to the cases defined in Table (5.1), but any other values of the parameters shown in this Table that fulfill the governing hypotheses can be used in practical applications. Case 03 is considered the *basic state*, with average values for the different variables.

After the wave height is obtained using Eq. (4.27), a variable breaking index (Komar, 1998), which depends on the Iribarren number,  $Ir_b$  (Iribarren and Nogales, 1949), is used to find wave breaking and to estimate the surf zone width  $b(s)$ :

$$\gamma = 1.2Ir_b^{0.27} \tag{5.1}$$

Case	$\alpha_{0p}$ [°]	$T$ [s]	$H_0$ [m]	$a/\lambda$	$K_\beta$
01	0	6	2	0.05	0
02	0	12	1	0.05	0
03	0	12	2	0.05	0
04	0	12	4	0.05	0
05	0	12	2	0.1	0
06	0	12	2	0.02	0
07	0	12	2	0.05	-0.005
08	0	12	2	0.05	0.005
09	0	18	2	0.05	0
10	30	12	2	0.05	0
11	60	12	2	0.05	0

Table 5.1: Cases defined. For the beach slope:  $\tan \beta = 0.01 + K_\beta \cos\left(\frac{2\pi}{\lambda} s\right)$ .

The value of  $Ir_b$  was also obtained to check whether there were changes in the type of wave breaking (Losada, 2009):

$$Ir_b = 1.25T \frac{\tan \beta}{\sqrt{H_b}} = 1.25T \sqrt{\frac{\tan \beta}{\gamma b}} \quad (5.2)$$

Alongshore variations in the sediment size ( $D_{50}$ ) were included because the sediment is coarser (finer) where the beach slope is steeper (lower) on those coastlines where the beach slope varies alongshore. The relationship between  $D_{50}$  and  $\tan \beta$  was adapted from the results for spilling breakers obtained by Reis and Gama (2010), based on multiple observations of different coasts in many parts of the world. The experimental relationship reads:

$$D_{50} = \frac{20}{3} \tan \beta + \frac{7}{30} \quad (5.3)$$

## 5.2 Results

In this section, the results of the numerical experiments are presented and used to analyze the potential erosion and depositional zones and to estimate how the beach would respond to variations in the main variables governing the problem. The erosion (accretion) zones correspond to those areas where the sediment transport rate increases (decreases) in the downdrift direction along the coast. This morphological analysis assumes assumption (6) in Section 4.1.

After all the calculations, Eq. (4.30) could be used in the majority of the cases defined, except for case with small wave period (case 01) and those with variable beach slope (cases 07 and 08), where the relative difference between Eqs. (4.30) and (4.29) was more than 5%. It seems to confirm that the simple expression given in Eq. (4.30) can be used in a wide range of shoreline configuration and waves conditions.

### 5.2.1 Deep-water wave angle

Cases 03, 10 and 11 (Table 5.1) were used to study the influence of  $\alpha_{0p}$  (Fig. 5.1); for cases 10 and 11, waves propagate from the left- to the right-hand side of the figure.

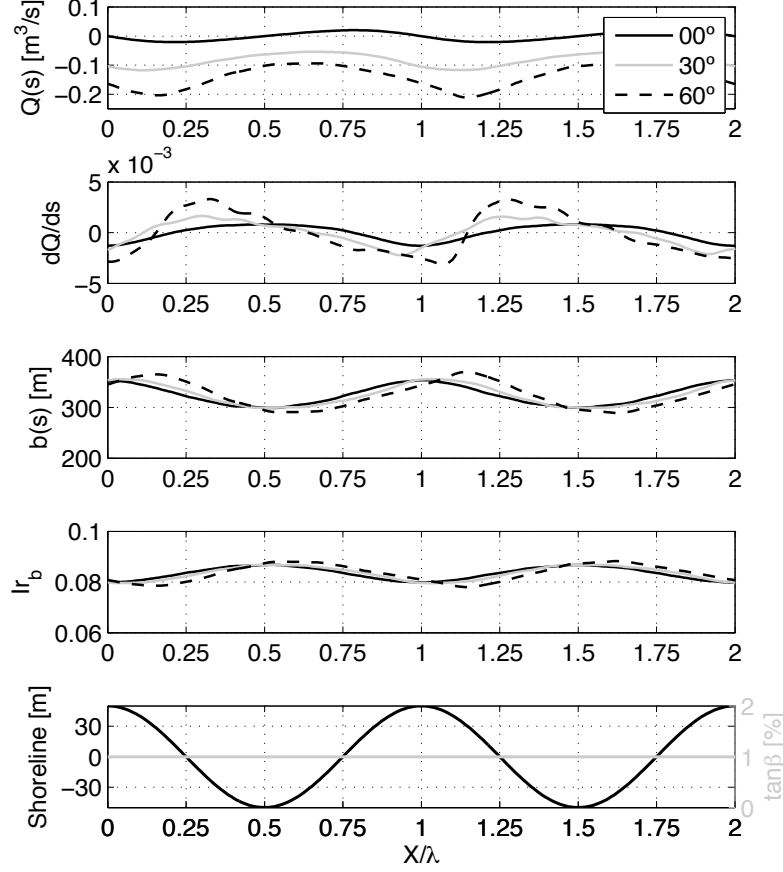


Figure 5.1: Alongshore sediment transport  $Q(s)$ , alongshore gradient of  $Q(s)$ , surf zone width  $b(s)$ , Iribarren number  $Ir_b$ , and shoreline and beach slope for cases 03 (solid black lines), 10 (solid grey lines) and 11 (dashed black lines) in which  $\alpha_{0p}$  varies.

One important difference between these cases is the locations at which the sediment transport reaches its alongshore local maxima and hence the locations at which the transitions from erosion to deposition occur. As  $\alpha_{0p}$  increases, these transitions migrate up-drift. It is expected that an increase in  $\alpha_{0p}$  will cause the updrift migration of the undulations. In the three cases, the stretch of coast where the erosion is more likely to occur (where the sediment transport gradient is positive) corresponds to the troughs of the shoreline undulations.

The mean and maximum absolute values of the sediment transport also increase with  $\alpha_{0p}$  even more than expected, considering the results for  $b$ . This is due to the effect of the coastline curvature on nearshore hydrodynamics considered in  $\Psi_2$  in Eqs. (4.28) and (4.29) (López-Ruiz et al., 2012a). The alongshore sediment transport  $Q(s)$  is also more asymmetric with respect to the crests of the shoreline as  $\alpha_{0p}$  increases, and  $dQ/ds$  decreases more smoothly than it increases, which may be due to the wave energy concentration produced in the downdrift part of the undulation crests. Large differences are not



observed in  $Ir_b$ , so  $\alpha_{0p}$  does not seem to play an important role in the type of breaking waves.

### 5.2.2 Wave period

Cases 01, 03 and 09 were used to analyze the influence of the wave period. Cases 01 and 03 correspond to short and long periods, respectively, and case 09 was defined to analyze the mathematical behavior of Eq. (4.28). As  $T$  increases,  $b$  increases due to wave shoaling (Fig. 5.2). However, this growth does not translate into a proportional increase in  $Q$  because of the opposite effect of  $T$  on  $b$  and  $\Psi_2$ : as  $T$  increases,  $b$  increases, but  $\Psi_2$  decreases (Eq. 4.23), and they counteract each other. As in section 5.2.1,  $\Psi_2$  modifies the hydrodynamics of curvilinear coasts and modulates the effect of  $b$  on sediment transport. The analysis of these effects is not straightforward with other models that are not conceived for curvilinear coasts.

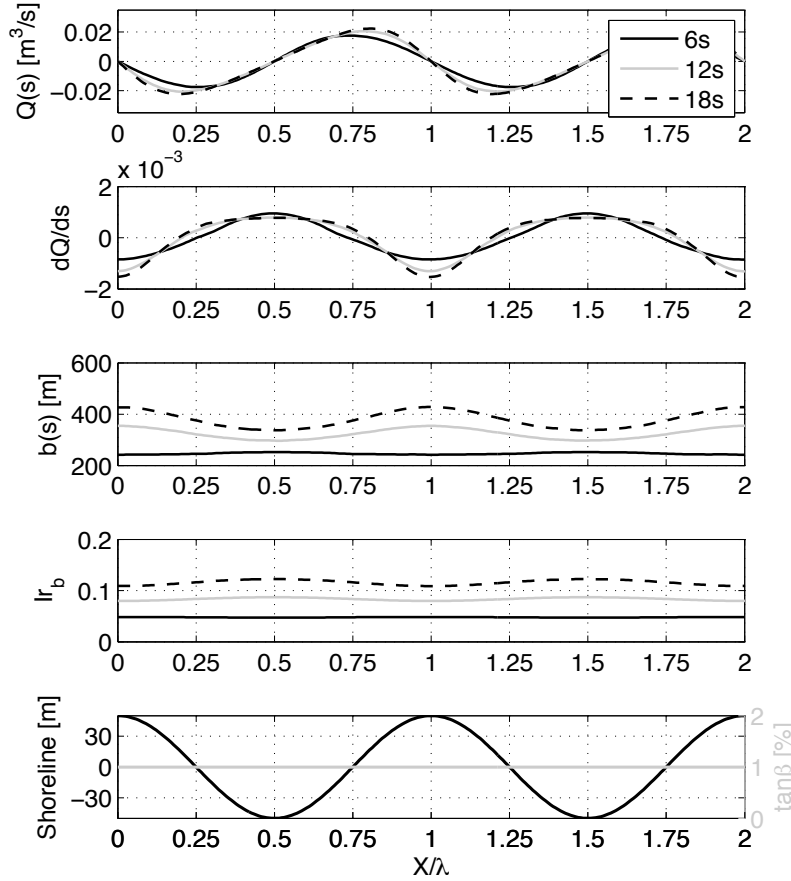


Figure 5.2: Alongshore sediment transport  $Q(s)$ , alongshore gradient of  $Q(s)$ , surf zone width  $b(s)$ , Iribarren number  $Ir_b$ , and shoreline and beach slope for cases 01 (solid black lines), 03 (solid grey lines) and 09 (dashed black lines) in which  $T$  varies.

No significant differences were found for the transition from erosion to deposition. For the smallest value of  $T$ , the length of the erosional zones in the undulation troughs decreases. Thus,  $T$  seems to control how fast  $a$  changes without significant variations in

$\lambda$ . The wave period  $T$  also plays an important role in the type of breaking, as its variations produce great changes in  $Ir_b$  and then in  $\gamma$  and  $b$ . In any case,  $T$  seems to be less important than  $\alpha_{0p}$  in the evolution of the coast, as the variability of the alongshore gradients of  $Q(s)$  is smaller between cases 01, 03 and 09 than between the cases analyzed in the previous section.

### 5.2.3 Deep-water wave height

Cases 02, 03 and 04 were used to study the influence of  $H_0$  (Fig. 5.3). The results show that as  $H_0$  increases,  $b$  and the maximum values of  $Q(s)$  and  $dQ/ds$  also increase. However, no variations in the location of the erosion and deposition zones are observed. If  $H_0$  increases, the shoreline tends to increase the amplitude of the undulations without changing the wavelength, as there is symmetric erosion and deposition in troughs and crests, respectively.

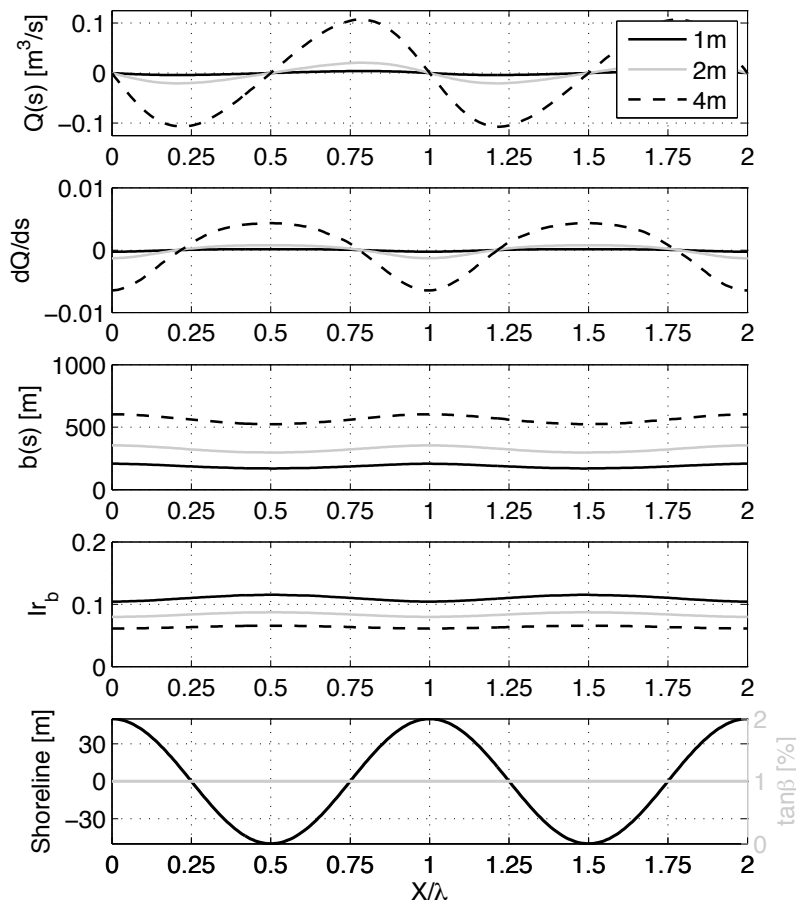


Figure 5.3: Alongshore sediment transport  $Q(s)$ , alongshore gradient of  $Q(s)$ , surf zone width  $b(s)$ , Iribarren number  $Ir_b$ , and shoreline and beach slope for cases 02 (solid black lines), 03 (solid grey lines) and 04 (dashed black lines) in which  $H_0$  varies.

The differences in  $Q$  and  $dQ/ds$  between 03 and 04 are greater than between 02 and 03. This is mainly because of the nonlinearity of the wave height in the energy approach

of Inman and Bagnold (1963), Eq. (4.2). These differences are also observed in  $b$ , although they are less pronounced in this case. With respect to wave breaking, variations in wave height cause uniform changes in  $Ir_b$  along the shoreline. Hence, if other wave conditions that enhance the growth of  $Ir_b$  are considered, the change in the type of breaking would be uniform throughout the domain.

### 5.2.4 Shoreline geometry

To analyze the influence of variations in the shoreline geometry, cases 03, 05 and 06 were used. These cases were defined using three different values of  $a/\lambda$ , ranging from 0.04 to 0.01. The first value is representative of an average shoreline undulation, whereas the later corresponds to a quasi-curvilinear shoreline. When  $a/\lambda$  decreases, the surf zone width and the intensity of the sediment transport increase, and consequently,  $dQ/ds$  (Fig. 5.4) also increases. However, no significant changes in the location of the null sediment transport gradient points are observed. The smaller  $a/\lambda$  is, the more erosion occurs in the troughs and the more deposition occurs in the crests of the undulations. Therefore, when  $a/\lambda$  decreases, the growth rate of the undulation amplitude increases. With respect to wave breaking, as  $a/\lambda$  decreases,  $Ir_b$  increases at the troughs of the shoreline, where a change in the type of breaking is more likely to occur if other wave conditions that enhance the growth of  $Ir_b$  are considered.

### 5.2.5 Beach slope and sediment size

One of the important effects introduced by the sediment transport formulation (Eqs. 4.2 to 4.28) is the alongshore variations in both the beach slope ( $< 1/30$ ) and the sediment size [ $0.15 < D_{50}(\text{mm}) < 0.40$ ]. Cases 03, 07 and 08 were used to investigate these aspects. Case 03 has a constant slope and sediment size, whereas case 07 (08) considers higher values of  $\tan\beta$  and  $D_{50}$  on the troughs (crests) of the shoreline undulations (Nolan et al., 1999). Fig. (5.5) depicts the results for these three cases, with  $b$  exhibiting behavior opposite that observed for cases 07 and 08. These differences are largely counteracted by the variations in  $\tan\beta$ , as the gradients in  $Q$  are similar. However, the locations of the maximum and minimum of sediment transport are different for each case. For case 07, for which the slope is greater in the troughs, the zone of the coast where  $dQ/ds > 0$  (erosion) is smaller than for case 03. The opposite effect occurs for case 08. Hence, alongshore variations in the beach slope may change the length of the erosional and depositional zones, generating alongshore asymmetries in the shoreline geometry and changing their  $\lambda$ .

Fig. (5.5) also shows that  $Ir_b$  reaches its maximum and minimum at different locations for cases 07 and 08. If other wave conditions that enhance the growth of  $Ir_b$  are considered, plunging breaking is more likely to occur in the undulation troughs (crests) for case 07 (08).

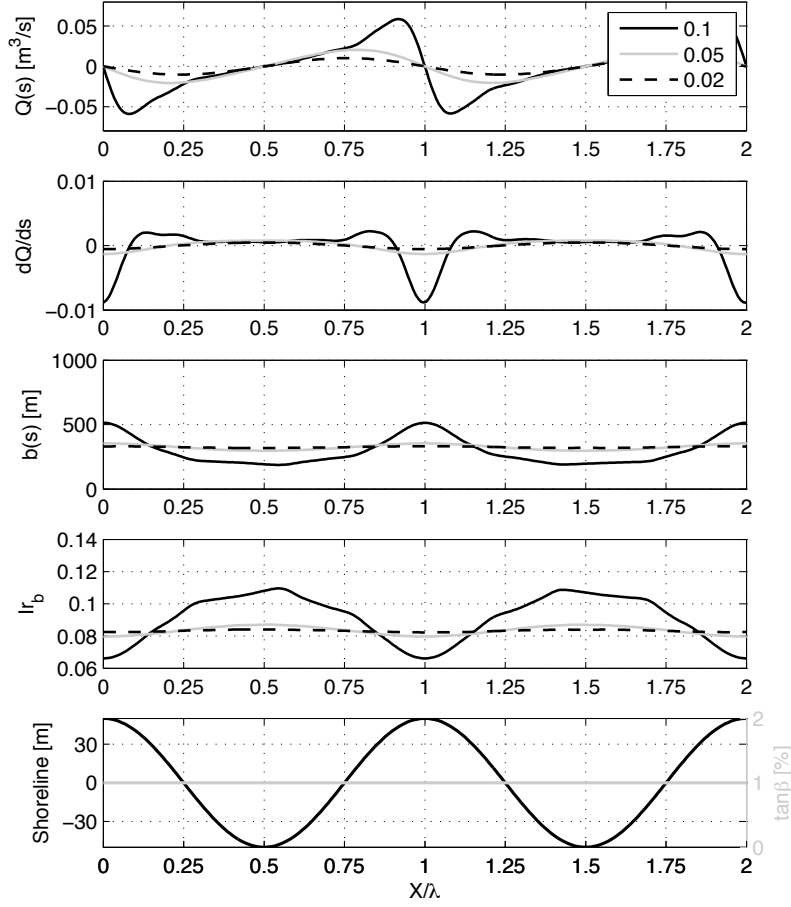


Figure 5.4: Alongshore sediment transport  $Q(s)$ , alongshore gradient of  $Q(s)$ , surf zone width  $b(s)$ , Iribarren number  $Ir_b$ , and shoreline and beach slope for cases 05 (solid black lines), 03 (solid grey lines) and 06 (dashed black lines) in which  $a/\lambda$  varies.

### 5.3 Discussion

Shorelines change according to the interaction between the forcing conditions (i.e., wave conditions, mean sea level) and the morphological setting (i.e., grain size, beach slope). In this study, an approach to analyze the possible response of the shoreline based on basic physical processes is proposed. A similar procedure for curvilinear coasts can be found in Falqués and Calvete (2005), in which the CERC formula for alongshore sediment transport is used to analyze the diffusivity of small-amplitude shoreline features. In our work, an updated formulation for sediment transport is supported by a simple wave propagation model that does not require the use of advanced numerical models. Our approach includes variation in some important hydrodynamics variables such as sediment size and beach slope. Although we could not find in the bibliography enough field or laboratory data to compare with our results, the Inman and Bagnold (1963) approach is widely accepted and the simple model for wave propagation has been tested with good results.

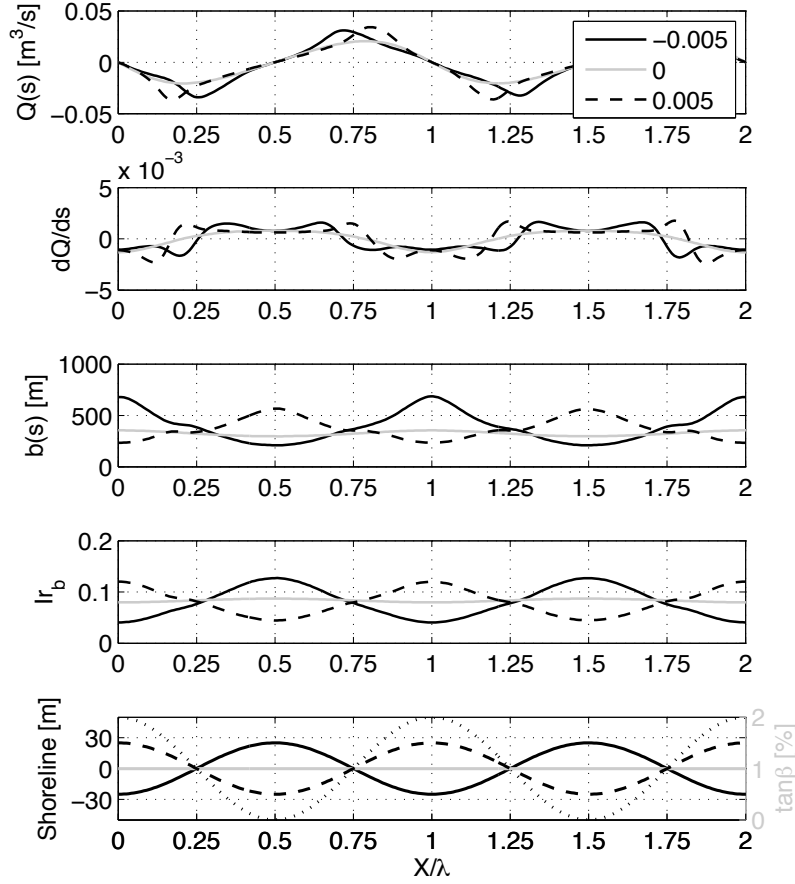


Figure 5.5: Alongshore sediment transport  $Q(s)$ , alongshore gradient of  $Q(s)$ , surf zone width  $b(s)$ , Iribarren number  $Ir_b$ , and shoreline (dotted line) and beach slope for cases 07 (solid black lines), 03 (solid grey lines) and 08 (dashed black lines) in which  $K_\beta$  varies.

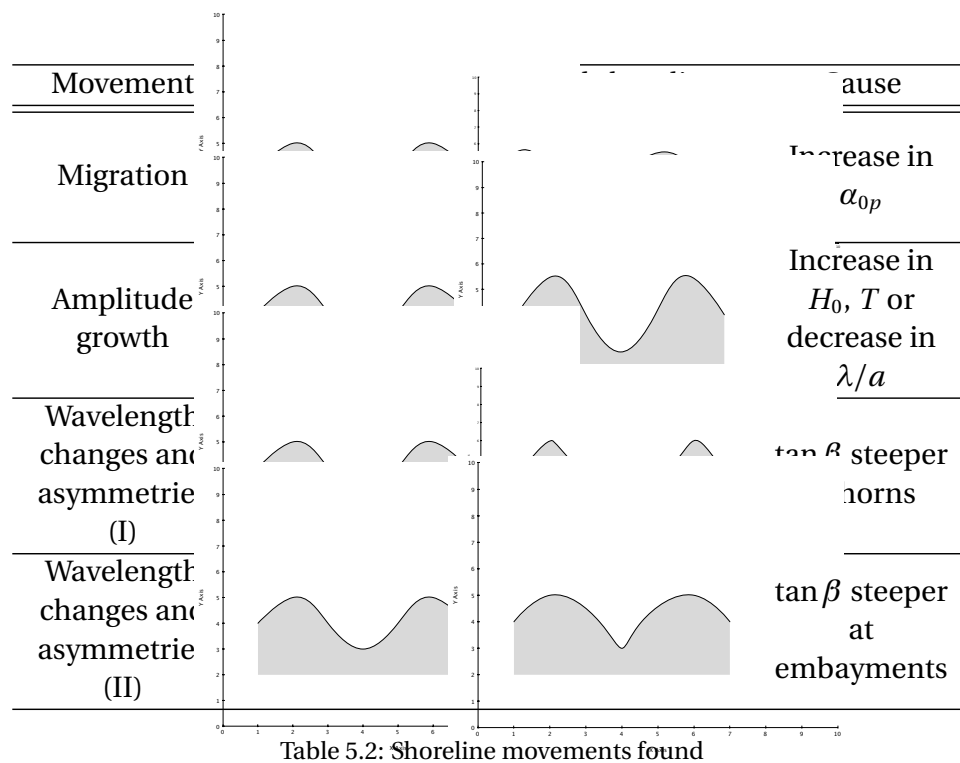
As noted throughout the paper, some hypotheses and simplifications have been considered, and it can be argued that such simple analytical approaches provide results that may be far from reality, even more with the advanced models that currently exist. However, given that the influences of many variables are still not well described (i.e., how the curvature of the shoreline affects the sediment transport), simple approaches are valid and important tools for these analyses (Ashton and Murray, 2006a). The basic knowledge gained using such tools can be used to improve numerical models.

### 5.3.1 Erosion-deposition patterns

Eq. (4.28) consistently predicts erosion in the troughs and deposition in the crests of the undulations for all the cases defined. However, as the length and location of the erosion zones differs for the different waves and geometric conditions, three different basic movements of the shoreline can be identified (see Table 5.2):

- Migration: erosional and depositional zones migrate updrift with only small changes in their lengths as  $\alpha_{0p}$  increases.

- Amplitude changes: when  $\alpha_{0p} = 0^\circ$ , the beach slope remains constant and only  $H_0$  and  $T$  vary. The erosional and depositional zones are symmetric with respect to the horns of the undulations, and the transition between them is at the middle point between horns and embayments. The amplitudes of the undulations change without their wavelengths and shapes changing.
- Wavelength changes and asymmetries: alongshore changes in the beach slope cause the length of the erosional and depositional zones to change. When the beach is steeper in the embayments, the erosional zones becomes smaller, and the embayments tend to be shorter and more pronounced, whereas the crests tend to be wider and smoother (due to the mass conservation principle). The opposite effects are observed when the beach is steeper in the horns.



In this study, we only analyzed the behavior of the system when one variable at a time was modified. With this information, we can improve our understanding of how each variable influences the basic physical processes of wave propagation and sediment transport on undulating coasts and their possible implications on morphological evolution. However, real scenarios involve combinations of those simple cases. For example, some combinations of  $\alpha_{0p}$ ,  $H_0$  and  $T$  may lead to the extinction of the undulations.

Changes in the beach slope and wave conditions modify the Iribarren number and may alter the type of wave breaking (spilling to plunging). As the broken wave height was defined as a linear function of the water depth, this change may lead to some errors in the dissipation of wave energy by breaking and hence in the alongshore sediment transport. However, if steeper beaches and more severe wave conditions that ensure plunging breaking are considered, wave reflection becomes important, and its influence on

the alongshore sediment transport cannot be neglected. The change in the type of wave breaking can be corrected by the inclusion of a coefficient in Eqs. (4.9) to (4.28) to model the wave height decay inside the breaking zone. For all of the cases described in this study, for a mean beach slope of  $\tan \beta = 0.01$ , the Iribarren number obtained was between 0.07 and 0.12. Hence, no changes in the type of breaking are expected, and reflections can be neglected, ensuring that this assumption is satisfied.

## 5.4 Consequences on nearshore coastal morphodynamics

### 5.4.1 Wave energy dissipation and setup

In this section, the alongshore component of the wave energy dissipation per unit of wave crest and surf zone surface is analyzed. This dissipation rate is closely related to the alongshore sediment transport presented in Eq. (4.28), since the formulation of Inman and Bagnold (1963) is based on an energy approach.

According to hypothesis (2) in Section 4.1, the wave energy flux per unit wave crest in the direction of the waves that reaches the surf zone is as follows:

$$F_{wb}(s) = E_b(s)C_{gb}(s)\cos\theta_b(s) \quad (5.4)$$

where the subscript  $b$  indicates conditions at breaking. The projection in the alongshore direction of this wave energy flux per unit of surf zone width surface  $b ds$ , yields the following expression:

$$\frac{F_{lb}(s)}{b(s)ds} = \frac{F_{wb}(s)}{b(s)ds} \sin\theta_b = E_b(s)C_{gb}(s)\cos\theta_b(s)\sin\theta_b(s)\frac{1}{b(s)ds} \quad (5.5)$$

Considering the assumptions previously presented (Section 4.1),  $H_b = \gamma h_b = \gamma \tan\beta b$ ,  $C_{gb} \simeq \sqrt{gh_b}$  in shallow waters,  $ds = dX\sqrt{1+\phi(s)^2}$ , and applying simple trigonometric transformations, the alongshore energy dissipation per unit of wave crest and surf zone surface  $D_{sz}/ds$  yields the following expression:

$$\frac{D_{sz}(s)}{ds} = \frac{F_{lb}(s)}{b(s)ds} = \frac{1}{16}\rho g^{3/2}\gamma^2 \tan\beta(s)^{5/2}b(s)^{3/2}\sin 2\theta_b(s)\frac{1}{dX\sqrt{1+\phi(s)^2}} \quad (5.6)$$

In this expression,  $\tan\beta$ ,  $b$ ,  $\theta_b$  and  $\phi$  are local variables that may vary along the coast. The alongshore variations in wave setup  $\eta_s$  were also obtained using the expression of Corniero and Giménez-Curto (2012) for obliquely incident waves:

$$\eta_s = \frac{1}{16}\gamma H_b (5 - 3\sin^2\theta_b) \quad (5.7)$$

Both  $D_{sz}$  and  $\eta_s$  were obtained for cases 03, 07 and 08 to analyze the influence of alongshore beach slope variations (Fig. 5.6). The variations of  $D_{sz}$  along the coast follow

the same pattern as the alongshore sediment transport for the same cases (Fig. 5.5), being null at the horn and embayment extremes due to the normal wave incidence. Both  $Q$  and  $D_{sz}$  are smoother for a constant beach slope. The integral of the wave energy dissipation along a shoreline wavelength is null for all the cases shown. Moreover, for oblique incidence, the average wave energy is the same for a sinusoidal shoreline as for a rectilinear one.

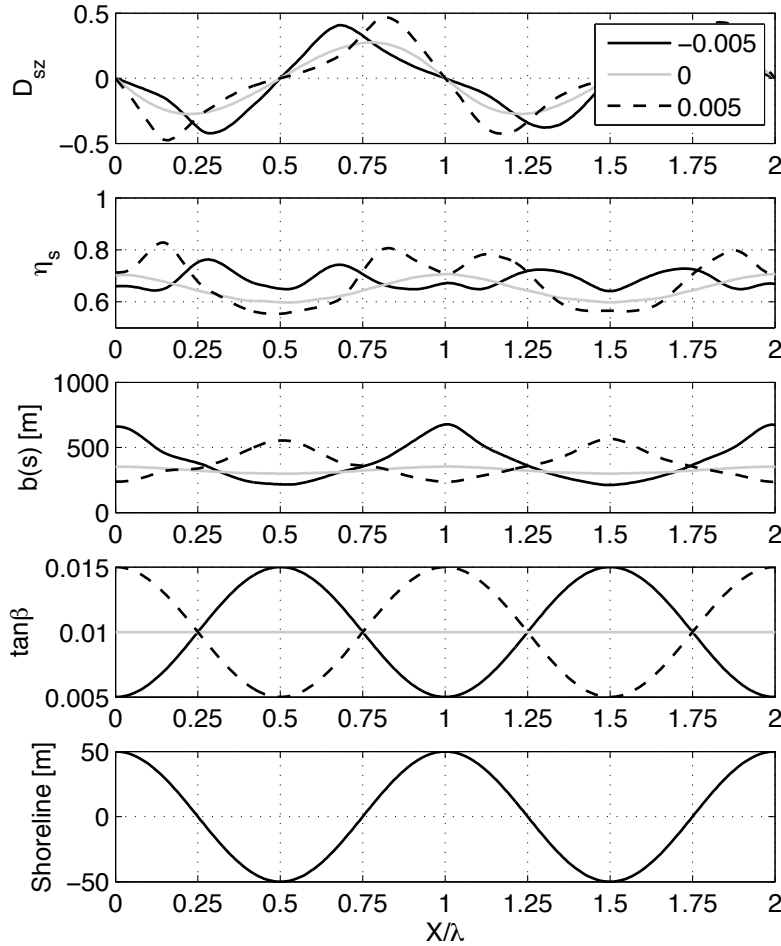


Figure 5.6: Alongshore energy dissipation per unit of wave crest and surf zone surface  $D_{sz}$ , wave setup  $\eta_s$ , surf zone width  $b(s)$  (including setup), beach slope  $\tan\beta$ , and shoreline for cases 07 (solid black lines), 03 (solid grey lines) and 08 (dashed black lines).

Fig. (5.6) also shows the alongshore variations in  $\eta_s$ . For the case of constant beach slope,  $\eta_s$  is higher at the horns, where the wave energy is concentrated. Hence, an alongshore current is expected to form from the horns toward the embayments. This current may enhance the formation of a nearshore circulation pattern characterized by closed cells. For case 08, in which the beach slope is greater at the horns, this effect is more pronounced, as the gradients in  $\eta_s$  are higher. However, for case 07, these gradients are lower, the setup alongshore evolution is more irregular, and the alongshore currents that are expected to develop are less organized. Hence, the formation of these closed cells of circulation is not enhanced for this case.



### 5.4.2 Edge waves

Rhythmic beaches have been related in the past with edge waves and the development of circulation systems (Dean and Dalrymple, 2002a; Masselink, 2004). The results in section 5.4.1 show how the alongshore gradients in setup cause alongshore currents that enhance the formation of circulatory systems with onshore (offshore) currents in the horns (embayments), especially for sinusoidal shorelines with steeper slopes in the beach horns. According to the edge wave theory, their nodes (antinodes) coincide with the horns (embayments) of rhythmic beaches. This effect has been reported to occur for beach cusps (see Dean and Dalrymple, 2002a; Chapter 9). To check whether this can also happen along curvilinear coastlines with shoreline undulations, the edge wave dispersion relationship was applied:

$$\left( \frac{2\pi}{T_{ew}} \right)^2 = g \frac{2\pi}{\lambda} (2n + 1) \tan \beta \quad (5.8)$$

with  $n$  being the edge wave mode and  $T_{ew}$  being the edge wave period. For characteristics similar to those used through this paper and for values of  $a/\lambda = 20$ ,  $\lambda = 100$  m, and  $\tan \beta = 0.07$ , the resulting edge wave period is  $T_{ew} = (30.2, 17.5, 13.5, 11.4, 10.1)$  s for  $n = (0, 1, 2, 3, 4)$ , respectively. Thus, the mode-zero could be the sub-harmonic edge wave for incident waves of  $T \simeq 20$  s. This mode is the most easily excited and is usually implicated in the formation of rhythmic shoreline features such as beach cusps (Masselink, 2004). Hence, they can also enhance the growth of shoreline undulations.

# **Implications on coastal evolution (II): shoreline modeling**

---

In this chapter, a morphological evolution model which predicts the time evolution of the shoreline is presented. This so-called oneline model is based on the principle of mass conservation and uses the gradients in the alongshore sediment transport to compute the position of the shoreline. The effects of including the two approaches defined for the alongshore sediment transport in the oneline model are analyzed in terms of diffusivity. Results show that including gradients in shoreline angle, surf zone width and wave angle causes the appearance of new terms that may play a key role in the morphological evolution of the shoreline.

## **6.1 Oneline modeling**

The oneline model predicts the time evolution of the shoreline in a given stretch of the coast considering wave conditions previously defined. The time scale in which this model is accurate is the short to medium term, ranging between hours to tens of years. The model was first developed by Pelnard-Considère (1956), who obtained analytical solutions considering equilibrium beach profiles. These profiles advance (step back) as the beach accrete (erode) without changing their shape.

After the work of Pelnard-Considère (1956), many analytical solutions for different conditions were obtained. Bakker and Edelman (1965) applied the oneline model to obtain solution for deltas and estuaries. LeMehaute and Soldate (1977) included the effects of changes in the mean water level and considered diffraction, refraction and reflection due to the presence of coastal structures. A general solution using Laplace transformation was performed Larson et al. (1997). Their solution can consider beach nourishments, sand removals and the presence of jetties and dikes. More recently, Dean (2002) studied beach nourishment projects analyzing the alongshore variations of the diffusivity that arises from the analytical solutions.

In addition to the analytical studies, the numerical solutions of the oneline model have been developed at the same time as the computational techniques and calculation capacity improved. The first numerical solution was proposed by Price et al. (1972), who used an explicit finite differences scheme. Using their work, several solutions considering

different boundary conditions and geometries were obtained. Some examples of these models are: GENESIS (GENeralized model for SIMulating Shoreline change, Gravens et al., 1991), UNIBEST (UNiform BEach Sediment Transport, Bosboom et al., 1997), LIT-PACK (LIToral Processes And Coastline Kinematics, Foster and Skou, 1992) and the ONE-LINE (Dabees and Kamphuis, 1998).

The oneline model has been further developed in the last years. Payo et al. (2002) obtained a quasi-analytic solution with time dependent boundary conditions. Their model also considers alongshore variations in wave height and wave angle, changes in the mean sea level and the presence of sources/sinks of sediments. Ashton and Murray (2006a) obtained a solution for the model using an expression of the alongshore sediment transport in terms of deep-water quantities. The resulting diffusivity, which depends on the shoreline angle, the wave period and the deep-water wave height and angle, induces the growth of undulating features when waves approach with a obliquity greater than  $\simeq 45^\circ$ . A detailed study of the diffusivity is done in Section 6.2. Finally, Losada et al. (2011) presented a numerical solution with an explicit scheme in which the effect a river discharges was included. They apply the model to the Guadalfeo river mouth (Southern Spain), performing a study of the uncertainty of the simulations.

### 6.1.1 Hypothesis and governing equation

The oneline model uses the mass conservation equation to evaluate the gain or loss of sediment in a beach profile trough the time. It is based on the following hypothesis:

- The sediment transport responsible of the evolution of the plain view of the shoreline is mainly alongshore, so the cross-shore sediment transport is neglected.
- It is assumed that the beach has a fixed profile shape that only moves onshore or offshore without deformation. Hence, the nearshore bathymetry can be defined just with the shoreline position and the shape of the beach profile.
- The changes in the bathymetry only extend until a given depth called active depth. Offshore this depth, the bathymetry is assumed constant.

The beach profile defined as the control volume to perform the mass balance is defined in Fig. (6.1), where  $(s, y)$  is the local system of coordinates,  $t$  is time,  $\mu(s, t)$  is the shoreline position,  $D_a$  is the active depth,  $D_b$  is the berm height,  $\Delta s$  is the width of the profile,  $\Delta \mu$  is the shoreline movement between the instants  $t_0$  and  $t_1$ ,  $\Delta t = t_1 - t_0$ , and  $Q(s)$  is the alongshore sediment transport. The volume of sand that is accreted or eroded between two consecutive positions of the shoreline is denoted by  $\Delta V$ .

The mass balance in the alongshore direction yields the following:

$$Q(s)\Delta t = \left( Q(s) + \frac{dQ(s)}{ds}\Delta s \right) \Delta t + \Delta V \quad (6.1)$$



Eq. (6.6) is the diffusion equation obtained by Pelnard-Considère (1956), and the diffusion coefficient  $\Gamma$  is called “diffusivity”. Considering the properties of the diffusion equation and the definition given for  $\Gamma$ , situations where  $\Gamma > 0$  will lead to shoreline smoothing, whereas situations where  $\Gamma < 0$  will lead to the growth of shoreline perturbations (Ashton and Murray, 2006b). Therefore, the analysis of the diffusivity  $\Gamma$  is a useful tool to analyze the potential behavior of the shoreline, and hence the potential results of the online model.

## 6.2 Diffusivity analysis

Analysis of the diffusivity were previously done by Falqués and Calvete (2005) and Ashton and Murray (2006b). The first authors used the CERC expression for the alongshore sediment transport, obtaining a diffusivity which is:

$$\Gamma_{\text{CERC}} \sim H_b^{5/2} \quad (6.7)$$

On the other hand, Ashton and Murray (2006b) expressed the alongshore sediment transport in term of deep-water quantities, obtaining the following expression:

$$\Gamma_{\text{A\&M}} \sim \left[ \cos^{1/5}(\alpha_{0p} + \phi) \left( \cos^2(\alpha_{0p} + \phi) - \frac{6}{5} \sin^2(\alpha_{0p} + \phi) \right) \right] \quad (6.8)$$

Under certain conditions, the sign of Eq. (6.8) changes, which led to the high-angle wave instability mechanism. Ashton and Murray (2006a) explained the presence of sand waves on rectilinear coastlines as the result of an instability mechanism based on the coupling between littoral drift and coastal morphology induced by high-angle waves (off-shore waves approaching at an angle greater than  $43^\circ$  with respect to the shoreline orientation). In the next paragraphs, the diffusivity is obtained for the two approaches defined in this Thesis for the alongshore sediment transport. It was done by obtaining an analytical expression for Eq. (6.4) replacing the expressions for  $Q(s)$  (Eqs. 4.17 and 4.28).

### 6.2.1 Diffusivity of the first approach for the alongshore sediment transport

When Eq. (4.17) is substituted in Eq. (6.4) and the chain rule is applied, it yields the following:

$$\begin{aligned} \frac{\partial \mu}{\partial t} = & -\frac{1}{D_a} \left[ \left( P_2(b(s)) \cos(2\phi(s)) - P_1(b(s)) \sin(2\phi(s)) \right) \frac{\partial \phi(s)}{\partial s} \right. \\ & \left. + \left( \frac{\partial P_1(b(s))}{\partial b} \cos(2\phi(s)) + \frac{\partial P_2(b(s))}{\partial b} \sin(2\phi(s)) \right) \frac{\partial b}{\partial s} \right] \end{aligned} \quad (6.9)$$

In this equation, the first term in the right member is proportional to the curvature of the coastline, whereas the second term includes the effect of the variation of energy conditions along the coastline. The former dependence is similar to that previously obtained by Ozasa and Brampton (1980), whereas the latter dependence resembles the one given by Ashton and Murray (2006a).

Eq. (6.9), which was obtained after considering sediment conservation, includes a term that depends on  $\partial\phi/\partial s$  as well as a new term that depends on the gradient of the energy conditions along the coast ( $\partial b/\partial s$ ). In a oneline model, Payo et al. (2008) also included a new term for the variation in wave height and direction of propagation along the coastline. In the formulation presented here, the term proportional to  $\partial b/\partial s$  is a function of  $T$ ,  $\phi(s)$ ,  $b(s)$ , and  $\alpha_{0p}$  and represents the variation in wave energy conditions along the coastline. Unlike the other formulations, Eq. (6.9) includes a term that depends on the gradient of the shoreline angle, in which no assumption or simplifications of the curvature are made.

If it is assumed that  $\tan\phi(s) = \partial\mu/\partial s$ , the first term in Eq. (6.9) is similar to the diffusive term in Eq. (6.6), obtained firstly by Pelnard-Considère (1956):

$$\frac{\partial\mu}{\partial t} = \Gamma_{LR12} \frac{\partial^2\mu}{\partial s^2} - \frac{1}{D_a} \left( \frac{\partial P_1(b(s))}{\partial b} \cos(2\phi(s)) + \frac{\partial P_2(b(s))}{\partial b} \sin(2\phi(s)) \right) \frac{\partial b}{\partial s} \quad (6.10)$$

with:

$$\Gamma_{LR12} = \frac{2}{1 + (\partial\mu/\partial s)^2} \left( P_2(b(s)) \cos(2\phi(s)) - P_1(b(s)) \sin(2\phi(s)) \right) \quad (6.11)$$

To compare this expression of the diffusivity with the obtained by Ashton and Murray (2006a), a constant  $b$  has to be considered to simplify Eq. (6.12) into:

$$\frac{\partial\mu}{\partial t} = \Gamma_{LR12} \frac{\partial^2\mu}{\partial s^2} \quad (6.12)$$

Fig. 6.3 shows the non-dimensional diffusivity ( $\Gamma/\max(\Gamma)$ ) for a curvilinear shoreline (with  $\phi(s)$  ranging from  $0^\circ$  to  $90^\circ$ ), which was calculated with Eq. (6.11) and (6.8) for a deep-water angle of  $\alpha_0 = 0^\circ$ . The behavior of the Ashton and Murray (2006a) expression and that of the proposed formulation are very similar and only differ in the zone with larger shoreline angles (close to  $\phi = 90^\circ$ ).

### 6.2.2 Diffusivity of the second approach for the alongshore sediment transport

If the expression of the second approach for the alongshore sediment transport (Eq. 4.28) is introduced in Eq. (6.4):

$$\frac{\partial\eta}{\partial t} = -\frac{1}{D_a} \frac{dQ}{ds} = -\frac{1}{D_a} \left( \frac{\partial Q}{\partial s} + \frac{\partial Q}{\partial \Psi} \frac{\partial \Psi}{\partial \phi} \frac{\partial \phi}{\partial s} + \frac{\partial Q}{\partial b} \frac{\partial b}{\partial s} \right) \quad (6.13)$$

Considering that  $\partial Q / \partial s = 0$  (Eq. 4.28), and  $\phi = \partial \mu / \partial s$ :

$$\frac{\partial \eta}{\partial t} = \Gamma_{\text{LR14}} \frac{\partial^2 \mu}{\partial s^2} - \frac{1}{D_a} \frac{\partial Q}{\partial b} \frac{\partial b}{\partial s} \quad (6.14)$$

This expression results in a diffusion term  $\Gamma_{\text{LR14}}$  and a new term that is proportional to the alongshore surf zone width gradient  $\partial b / \partial s$ . This new term depends on  $T$ ,  $\phi(s)$ ,  $b(s)$  and  $\alpha_{0p}$  and represents the variation in wave energy conditions along the coastline, and is equivalent to the obtained for the first approach for the alongshore sediment transport (Eq. 6.9). Considering the framework defined, it also represents the alongshore variations in the dissipation rate.

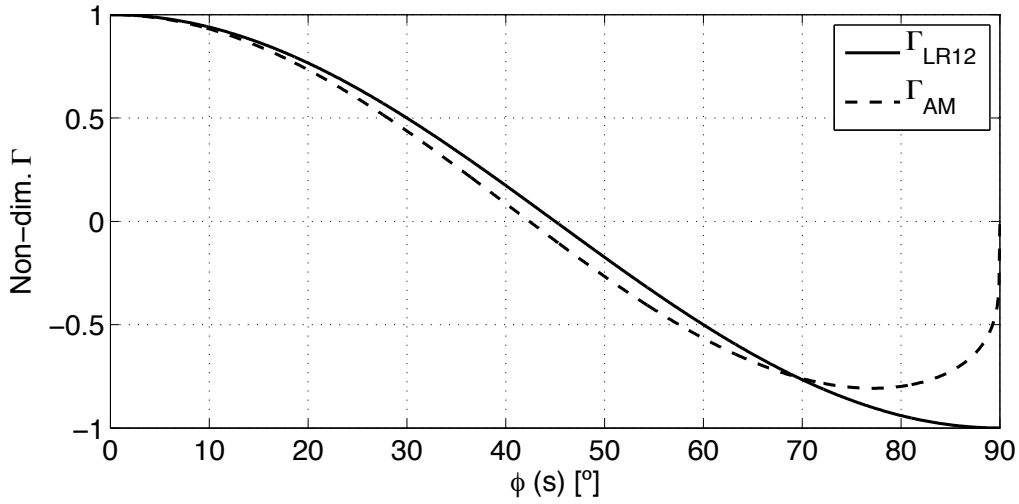


Figure 6.2: Non-dimensional diffusivity along a curvilinear shoreline for constant  $b$  and  $\alpha_0 = 0^\circ$  using the proposed formulation (Eq. 6.11) and the Ashton and Murray (2006a) expression (Eq. 6.8).

In this case, the obtained diffusivity was compared with the CERC and the Ashton and Murray (2006a) expressions (Eqs. 6.7 and 6.8). All the diffusivities were obtained for the cases 10 and 11 (Table 5.1) defined in Chapter 5. The first of these cases has a deep-water wave obliquity below the limit for high-angle waves (HAW) defined by Ashton and Murray (2006a), whereas the latter corresponds to

Fig. (6.3) shows the non-dimensional diffusivity ( $\Gamma / \max(\Gamma)$ ) for the two cases. For case 10,  $\Gamma_{\text{CERC}}$  and  $\Gamma_{\text{LR14}}$  behave similarly, being higher in the horns where the wave energy is concentrated. However, the expected shoreline evolution is not the same for the CERC and the LR14 expressions; our approximation considers the effect of the new term, which depends on  $\partial b / \partial s$ . Both diffusivities are  $\lambda/4$  out of phase with respect to  $\Gamma_{\text{A\&M}}$ , which only accounts for the shoreline and deep-water wave angles. For this value of  $\alpha_{0p}$ , all the diffusivities are positive.

For case 11,  $\Gamma_{\text{CERC}}$  and  $\Gamma_{\text{LR14}}$  behave similarly, but the maximum moves updrift, following the position of the wave concentration. More differences are observed for  $\Gamma_{\text{A\&M}}$  because it is negative throughout the domain. Ashton and Murray (2006a) related this change in the diffusivity sign with the development of shoreline sand waves. However, the

results obtained with the LR14 approach described in section 5.2.1 indicate that shoreline undulations can evolve for  $\alpha_{0p} < 45^\circ$ , although negative diffusivities are not obtained either for  $\alpha_{0p} > 45^\circ$ . Thus, the new term obtained in Eq. (6.14) seem to play an important role in alongshore sediment transport and hence in shoreline evolution.

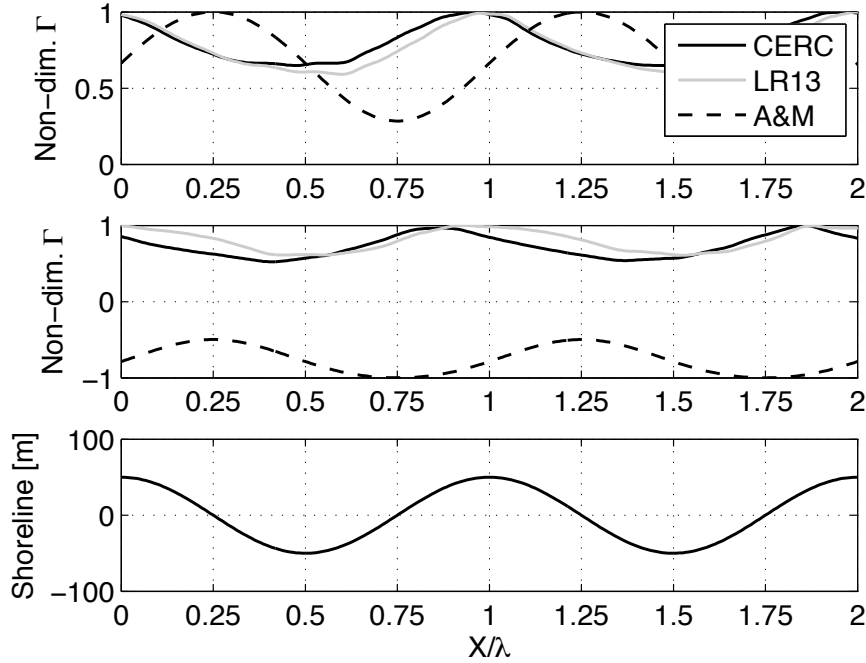


Figure 6.3: Non-dimensional diffusivity for the CERC formula (solid black lines), LR14 approach (solid grey lines) and Ashton and Murray (2006a) expression for cases 10 (upper panel) and 11 (intermediate panel). Shoreline is depicted in the lower panel.

### 6.2.3 Conclusions

After the analysis of the diffusivities obtained for the alongshore sediment transport expressions presented in Chapter 4, the following conclusions can be drawn:

- For both approaches, after the analytical application of the online model two different terms arise. One can be considered equivalent to the classical diffusivity obtained by Pelnard-Considère (1956). The second is a new term that depends on  $T$ ,  $\phi(s)$ ,  $b(s)$  and  $\alpha_{0p}$  and is proportional to  $\partial b / \partial s$ . If only the first is considered ( $b$  constant), the results are similar to previous expressions as the one by Ashton and Murray (2006a). This implies that the framework defined in Chapter 4 let consider new effects (mainly in the new term obtained) in the morphodynamic evolution of the coast that the previous approaches can not consider.
- With our framework, and after the analysis of the results in Section 6.2.2, it is not necessary the presence of high angle waves for the development of shoreline features, as their grow is not associated with a change in the sign of the diffusivity. Hence, the development of such features seems to be related with the combined effect of the two terms obtained in Eqs. (6.9) and (6.13).





---

## Chapter 7

# Applications

---

In this chapter, a numerical solution of the oneline model is applied to four different locations in the Spanish coast: 1) a circular spit front in Doñana, Huelva; 2) an elliptical spit front in El Puntal, Santander; 3) horn-embayment system in Carchuna Beach, Granada; and 4) an erosional stretch of coast in the Guadalfeo river mouth, Granada. The results show good agreement with observations and previous works.

### 7.1 Introduction

Through the next sections, the oneline model presented in Chapter 6 is solved numerically for four different locations. The governing equation (Eq. 6.4) was solved with an explicit finite differences scheme, using Neumann-type boundary conditions. After some tests, these boundary conditions proved to assure that no numerical oscillations were introduced in the solutions. The alongshore sediment transport expression used was the obtained for the first approximation of the nearshore wave angle, Eq. (4.17). The total time of the simulations vary for every location depending on the spatial and time scales of the features observed. However, it always remains between the short (weeks) and the mid term (5 years). For every time step, the wave forcing (surf zone width, wave period and deep-water wave angle, see Chapter 4) was previously obtained, together with the shoreline angle of the preceding time step.

### 7.2 Application to undulations on prograding spit fronts

The shape of the tip of a spit can be either circular (i.e. Sylt Spit, Fig. 2.1a) or elliptical (i.e. Cape Lookout Spit, Fig. 2.1c). In this work, two examples corresponding to a circular and an elliptical spit have been selected to study the evolution of the shoreline undulations: Doñana and El Puntal. Doñana characteristic dimensions are on the order of kilometers whereas El Puntal are on the order of hundreds of meters. Human influence during last decades has also been different at both sites. At the Guadalquivir estuary there has been massive occupation of wetlands that affects the equilibrium of the system. On the contrary, no significant interventions were done at El Puntal since late 80's of the past century. For both sites there are available data from previous studies (Medellín et al., 2008,

2009; Díez-Minguito et al., 2012). The reasons why a spit develops a curvilinear or elliptical shape or it has different characteristic dimensions are out of the temporal scale of the processes analyzed in this work, as this work deals with short (event) to medium-term evolution of shoreline features instead of the long-term evolution of the spit (Rodríguez-Ramírez et al., 1996). By applying the formulation proposed, this section studies how the shape and dimensions of the spit front influences the generation and evolution of the undulations of the coastline.

## 7.2.1 Circular spit front: Doñana

### 7.2.1.1 Study zone

The Doñana spit is located at the Guadalquivir River mouth, in the Gulf of Cádiz, Southern Spain (Fig. 7.1). This river (560 km long) drains a catchment of 57 000 km<sup>2</sup>, and is partly blocked in the lower reach by sandy barriers, resulting in a large estuary (1800 km<sup>2</sup>). In the South-Western sector, this estuary includes the Doñana National Park, a UNESCO-MAB Biosphere Reserve. This site is one of the largest wet-lands (50 720 ha) in Europe and represents the last tract of relatively undisturbed marsh in this system (Ruiz et al., 2004).

Wave action, drift currents, fluvial regime and tidal flux control the hydrodynamic processes, although the last two will be neglected in this study in order to focus on the along-shore sediment transport effects on morphodynamics. The tidal regime is mesotidal and semidiurnal, with an average tidal range of approximately 3.6 m. Dominant waves associated with the Atlantic circulation come from the southwest, with a medium wave energy because 75% of the waves do not exceed 0.5 m in height. These conditions favor the development of broad lowlands, usually sheltered by spits, where tidal flats and freshwater marshes extend several kilometers inland. Littoral drift currents transport sand-size sediments from the Portuguese coast to the Spanish nearshore zone, determining the large-scale form of the coastal plan-view (Ruiz et al., 2004, Díez-Minguito et al., 2012).

However, the observation of aerial and satellite images reveals the presence of shoreline undulations in the tip of the spit, with a smaller spatial scale, that are superimposed to the large-scale shape of the coast (Fig. 7.1). These features have a wavelength of  $\lambda = 500 - 2000$  m and a crest-trough amplitude of  $a \simeq 150$  m. The aim of applying the methodology described in Section 7.1 is to study if the effects of the wave propagation over a curvilinear bathymetry, such as the present in the Doñana spit, play a key role in the formation of these small-scale features.

Since the beginning of the 18th century and specially after the middle of the past century, the natural course of the estuary has been modified several times. It has been dammed, and the width and depth of the main channel have been enlarged. Currently, the estuary is being periodically dredged from its mouth to where it accesses the Port of Seville in order to guarantee a minimum navigation channel depth of 6.5 m (Díez-Minguito et al., 2012). For this reason, to avoid the effects of the human interventions in the spit morphodynamics (out of the scope of this work), the results of the online model are compared with the more ancient data of the shoreline position available: aerial photographs taken in 1956.



Figure 7.1: Doñana spit, Southern Spain. The dashed lines indicate the shoreline undulations identified in the prograding spit front.

### 7.2.1.2 Shoreline simulations

The aerial photographs taken since 1956 show that the undulations at the Doñana Spit seem to be permanently present though their location, shape, and dimensions vary. Consequently, the generation and evolution of these undulations are not linked to the occurrence of a single storm event. Regarding the dimensions of the spit, it appears that at least a few years of climate forcing are required for these undulations to develop (Falqués and Calvete, 2005). Accordingly, we analyzed the evolution of the shoreline position after five years of wave climate forcing, using the online model (Eq. 6.4) as well as the methodology in Baquerizo and Losada (2008). This procedure assumes that since morphologic changes in coastal areas are cumulative processes, their response to a certain state is the initial condition for the next sea state. The process can be reproduced for a certain period of time by using the local climate as the forcing mechanism. The local climate is thus simulated as a series of consecutive states and as a morphodynamic model that runs under stationary input climatic conditions.

Wave climate conditions were simulated by using the methodology devised by Solari and Losada (2011). For significant wave height,  $H_0$ , a non-stationary parametric probability model is used for seasonal variability and a copula-based model for time dependence. The wave peak period and mean direction were obtained with a Vector Autoregressive (VAR) model on the basis of the simulated wave height and the available wave climate data (Solari and Losada, 2011). The methodology for the wave climate simulation is described in Appendix A

The wave climate forcing was provided to the model as a series of three-hour sea states, the first of which started with the initial shoreline. In each subsequent wave state, the shoreline position used was that predicted for the previous state. For each sea state the surf zone width was calculated as proportional to the wave height, whereas the shape of the surf zone depended on the incoming wave direction. According to the results pre-

sented in Chapter 3, a different shape was defined for each  $10^\circ$  interval of the deep-water wave angle. Furthermore, it was assumed that during the sea state, the possible changes in bathymetry did not significantly affect wave propagation. After repeating the experiment  $N$  times, a sample space consisting of  $N = 500$  equally likely outcomes of the shoreline was obtained and analyzed with probabilistic techniques.

This procedure was applied to a straight stretch of coastline, followed by a curved stretch (Fig. 7.2) of the same dimensions as the Doñana Spit front. Values for the slope of the surf zone ( $\tan \beta = 0.004$ ) and the sediment size ( $D_{50} = 0.17$  mm) were taken of previous studies of the zone (Ruiz et al., 2004, Díez-Minguito et al., 2012). For the wave climate simulations, we used the data obtained at hindcasting point WASA14718 ( $36.5^\circ$  N ,  $7^\circ$  W), provided by Puertos del Estado (Ministry of Public Works, Spain, WANA project).

Fig. 7.2 shows ten representative shorelines after 2.5 years of climate forcing, i.e. halfway through the five-year simulation. As can be observed, undulations are beginning to develop on all of the shorelines. The first undulation is located between longshore positions of 2500 and 3000 m, whereas the second undulation is located between longshore positions of 1000 and 2500 m. Although the location and wavelength of the features are almost deterministic, their amplitudes are variable. Moreover, this sequence of erosion-sedimentation stretches is similar to that obtained in laboratory experiments by Petersen et al. (2008) and to those observed at the Sylt Spit (Fig. 2.1a).

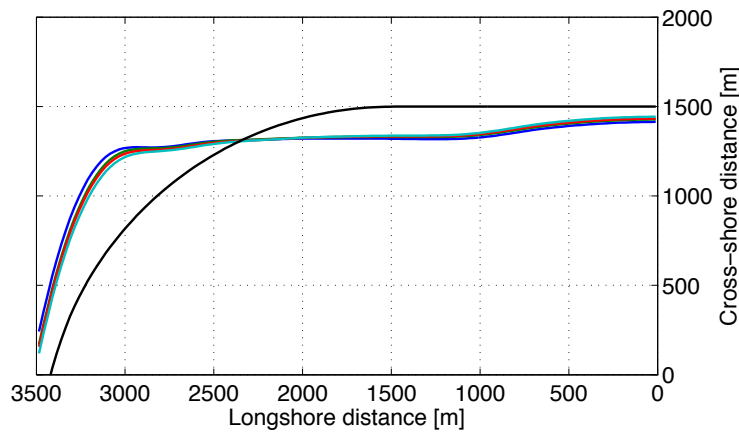


Figure 7.2: Some final shorelines for the Doñana spit after 2.5 years of wave climate forcing (colored lines). The black line represents the initial shoreline.

At the end of the simulations, the shoreline undulations are more pronounced although they remain in the same alongshore position (Fig. 7.3). The similarity between the shorelines obtained after 2.5 and 5 years of wave climate simulation, as well as the small variability between all the final shorelines, confirm that, in the short term, the model solutions tend to a quasi-steady geometry. Once again, the location and wavelength of the undulations are almost deterministic, and a certain variability is observed in their amplitudes, which range from 50 to 170 m. It was also found that the straight stretch of the coast was eroding, and that there was an accretion zone at the tip of the spit. In other words, the spit showed a net longitudinal growth.

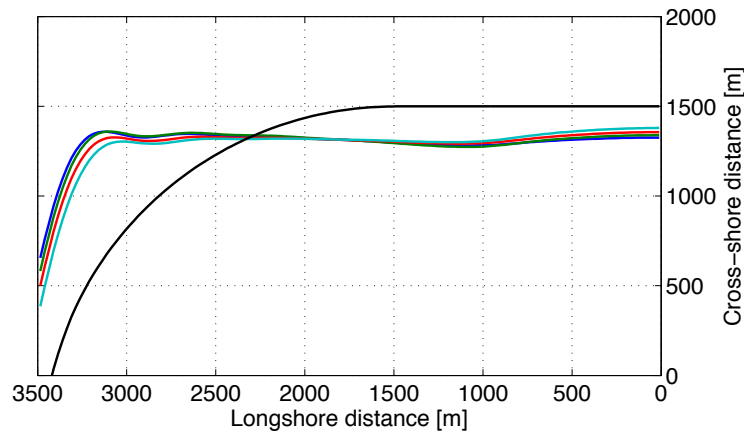


Figure 7.3: Some final shorelines for the Doñana spit after 5 years of wave climate forcing (colored lines). The black line represents the initial shoreline.

The analysis of the shoreline positions obtained during the last year of the simulations show that the variations of the shoreline trough this period were small. Therefore, during the first 2.5 years of the simulations the initial shorelines experience great changes in their shape while they are adapting to the mean wave conditions, whereas at the end of the simulations the shoreline seems to be reached the equilibrium, and only small changes due to seasonal climate variability are observed.

### 7.2.1.3 Analysis of the results

To analyze the uncertainty of the shoreline predictions obtained with the one line model, the following scheme was applied (Baquerizo and Losada, 2008). From the climatic data base we performed a number of  $N$  5-years wave climate simulations. For these  $N$  experiments the shoreline evolution was simulated using the model described in the previous section, obtaining  $N$  different shorelines. With these shoreline solutions, the Empirical Orthogonal Functions (EOF) analysis and statistical inference can be done to obtain a higher number of experiments and the probability distribution function of some of the geometric characteristics of the coastline. Given the main objectives of this work, the variables studied were the amplitude and the wavelength of the shoreline undulations obtained.

Once the 100 final shorelines were obtained, the EOF analysis was used to obtain the values of the undulations wavelength and amplitude after 500 experiments. With the available data, this analysis is capable to explain the 95% of the shoreline evolution variance considering only the first eigenfunction and more than 99% considering the first three (Baquerizo and Losada, 2008).

The analysis of the 500 amplitudes and wavelengths of the undulations shows that the value of the wavelength is a quasi-deterministic parameter with  $\lambda_1 \simeq 2000$  m and  $\lambda_2 \simeq 700$  m. However, the amplitude shows certain variability and their cumulative probability functions can be obtained using statistical inference. They range approximately between 110m and 160m for the first one (Fig 7.4) and between 10m and 50m for the latter (Fig. 7.5).

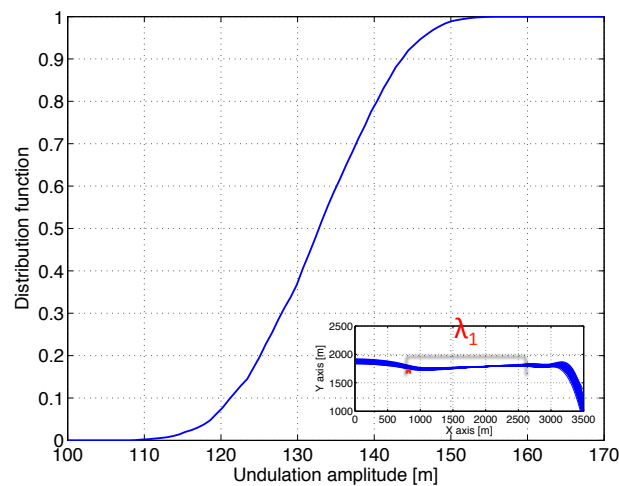


Figure 7.4: Distribution function of the first shoreline undulation amplitude obtained after the EOF analysis.

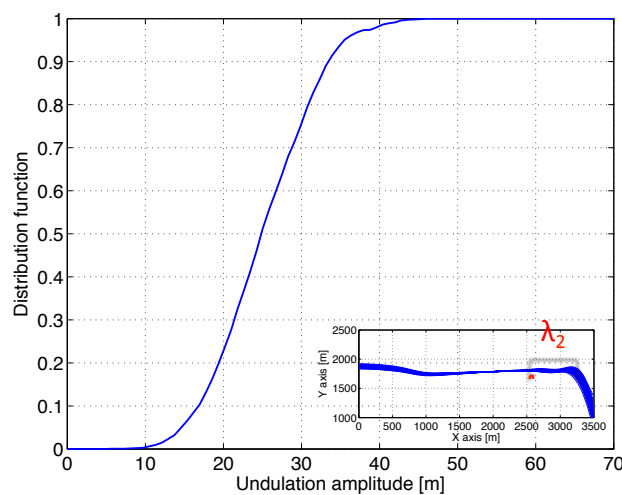


Figure 7.5: Distribution function of the first shoreline undulation amplitude obtained after the EOF analysis.

## 7.2.2 Elliptical spit front: El Puntal

### 7.2.2.1 Study zone

El Puntal spit is a 2.5 km long sand spit with a Western-Eastern orientation and located north of Santander Bay, on the Cantabrian coast of Spain, Gulf of Biscay (Fig. 7.6). The Cantabrian Coast, in Northern Spain, is divided into a series of pocket beaches and small inlets isolated between rocky headlands. Waves on the Gulf of Biscay approach mostly from the northwest with a mean significant wave height,  $H_s$ , of 1 m and a typical winter storm significant wave height of  $H_s \simeq 5$  m. The tides are semi diurnal with a mean tidal range of 3 m and a spring tidal range of 5 m. Mean grain size along the spit is 0.3 mm (Medellín et al., 2008). In contrast with Doñana spit, in this case the length (alongshore direction considering the main alignment of the coast) and width (cross-shore direction)



of the spit have different dimensions. That confers to the spit an elliptical shape. For detailed information about the El Puntal spit, the reader is referred to Medellín et al. (2008) and Medellín et al. (2009).



Figure 7.6: El Puntal spit, Northern Spain.

### 7.2.2.2 Shoreline features events

Medellín et al. (2008) identified two sand-wave formation events at the El Puntal spit with a duration of approximately two months. The wave climate for the phases of growth, saturation, and decay of these morphologies are different and are also influenced by the presence of the Magdalena Peninsula, which protects the prograding front of the spit from the severe wave conditions of the Cantabrian Sea (Medellín et al., 2008), see Fig. (7.6).

An initial coastline without undulations was defined with the same dimensions as the El Puntal spit and a slope of  $\tan \beta = 0.13$ . Although the tidal range in the area is 3-4 m, a representative constant mean level was considered for the simulation. The model was run with the mean wave conditions that occurred during the phases of sand wave development described by Medellín et al. (2008), with a total simulation time of 60 days ( $\sim 20$  days / phase). In each stage, high-angle waves from the origin to the tip of the spit were observed. Thus, the surf zone width was defined without an energy concentration in the transition from the straight stretch of the coast to the curved stretch, according to the results presented in Chapter 3

Fig. 7.7 shows the result after 20 days of simulation with a wave climate of  $H_0 = 0.8$  m,  $T_p = 12$  s, and  $\alpha_0 = 50^\circ$ , which is characteristic of the growth stage of the sand waves. The sediment transport pattern has only one maximum followed by a minimum, which results in a simple shoreline undulation with a wavelength smaller than that of at the Doñana spit.



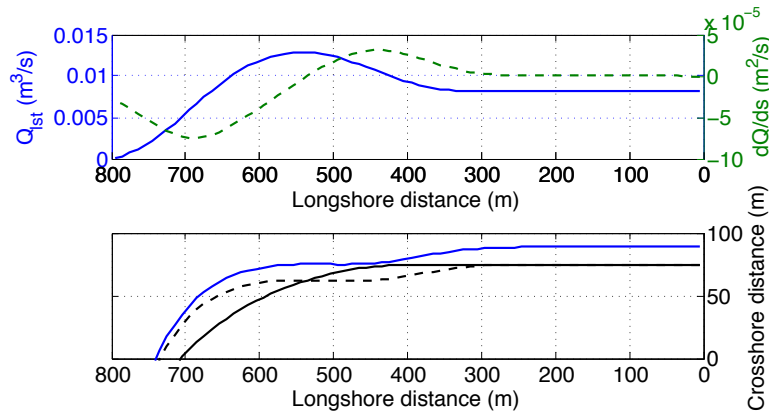


Figure 7.7: Evolution of the coastline for the El Puntal spit after the growth stage of the undulations. Upper graph: longshore sediment transport (LST) (solid line) and LST derivative (dashed line). Lower graph: initial shoreline (black line), breaker line (grey line), intermediate shoreline (dashed line).

Another 20-day simulation was performed using the final shoreline in Fig. 7.7 as the initial condition. In this case, the wave conditions defined were  $H_0 = 0.5$  m,  $T_p = 15$  s, and  $\alpha_0 = 60^\circ$ , typical of the saturation stage of the sand waves. The result (Fig. 7.8) shows the development of two shoreline undulations with a wavelength of approximately 200 m and an amplitude of 15 m. These features are very similar to those observed by Medellín et al. (2008) during the two sand-wave development events that were recorded.

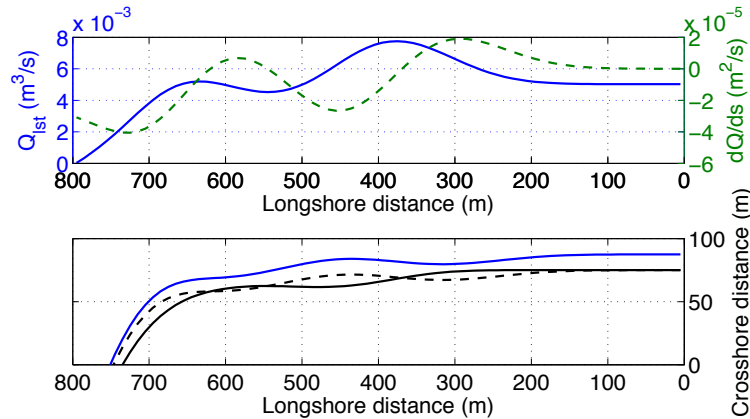


Figure 7.8: Evolution of the coastline for the El Puntal spit after the saturation stage of the undulations. Upper graph: longshore sediment transport (LST) (solid line) and LST derivative (dashed line). Lower graph: initial shoreline (black line), breaker line (grey line), intermediate shoreline (dashed line).

Finally, to study the possible disappearance of the shoreline undulations, we simulated the decay stage by forcing the system during 20 days and using the final shoreline obtained in Fig. 7.8 as the initial condition. The wave climate was defined as  $H_0 = 1$  m,  $T_p = 15$  s, and  $\alpha_0 = 70^\circ$ , which were the most energetic and oblique conditions recorded during the sand-wave development events. The results (Fig. 7.9) show a shoreline without undulations. Furthermore, there is a net longshore growth of the spit and a reduction of its width.

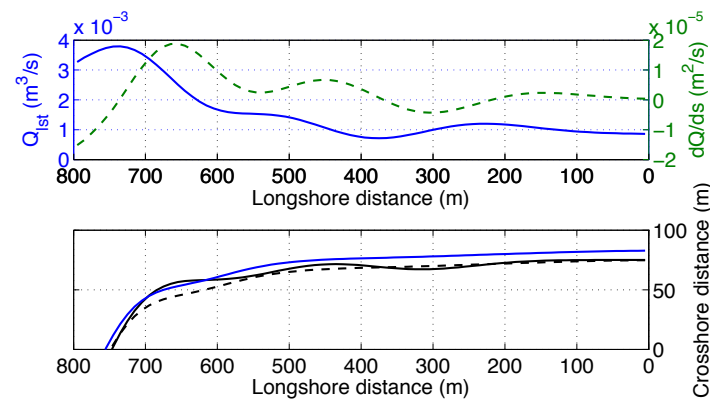


Figure 7.9: Evolution of the coastline for the El Puntal spit after the decay stage of the undulations. Upper graph: longshore sediment transport (LST) (solid line) and LST derivative (dashed line). Lower graph: initial shoreline (black line), breaker line (grey line), intermediate shoreline (dashed line).

### 7.2.3 Comparison with observations

Fig. 7.10 shows the comparison between model simulations and observations for the two sandy spits modeled. In the case of Doñana, the geometry of the obtained coastlines is similar to that observed in aerial photographs of Doñana spit in 1956, before the intense human interventions in the estuary (Díez-Minguito et al., 2012) (Fig. 7.10a); however, there are some differences. Although these differences are, in part, caused by model simplifications, they are mainly due to the fact that the effect of the river floods on river mouth dynamics was ignored. More specifically, this boundary was treated like a sink of sediment in a lagoon where no currents move the sediment.

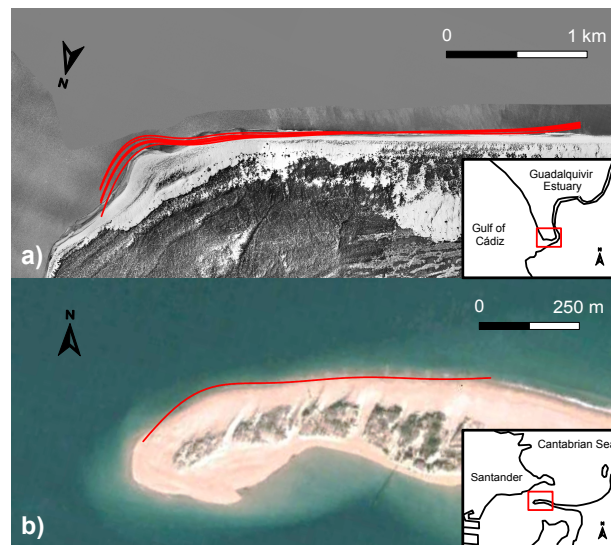


Figure 7.10: Comparison between the obtained shorelines (red lines) and the plan view of the study cases: a) Doñana spit with an aerial photograph taken in 1956; b) El Puntal spit, with a satellite image taken in 2006.

In the case of El Puntal spit, the available aerial image confirming the events observed by Medellín et al. (2008) in 2006 is compared with the results showed in Fig. 7.8. The differences between the model results and observations are again due to the model simplifications. For both study areas, the locations, the lengths and the amplitudes of the shoreline undulations are very similar to the observations.

## **7.3 Application to a horn-embayment system**

In this section, the online numerical solution is used to model the shoreline evolution of a horn-embayment system in Carchuna Beach, Southern Spain. This coastal system is characterized by a sequence of horns and embayments in the shoreline and by a group of submerged features. The aim of these simulations was to check if the presence of these features and their effects on wave propagations are the main responsible of the shoreline rhythmic shape.

### **7.3.1 Carchuna beach system**

#### **7.3.1.1 Coastal morphology**

Carchuna Beach is located on the southeastern coast of Spain and faces the Alborán Sea (Fig. 7.11). The beach exhibits a series of large-scale cusped features with an along-shore spacing of hundreds of meters. These features are bounded by a series of seaward-extending horns (H2-H6, Figs. 7.11 and 7.12). Analysis of aerial photographs taken since 1956 and images obtained from the video camera station installed in November 2002 has not revealed significant changes in either the coastline or the alongshore locations of the horns (Quevedo et al., 2008). The beach is bounded to the west by Cape Sacratif and to the east by the Punta del Llano Promontory (H6), which corresponds to the west side of the Calahonda Spit. The Calahonda Spit is composed of several beach ridge units (or landforms developed on prograded coasts with beach shorelines, according to Tamura, 2012). These beach ridges constitute major progradational phases separated by erosional gaps. This system has been prograding to the east during the Holocene in response to cyclic climatic conditions (Lario et al., 1999).

The beach slope varies along the length of the embayments from 0.04 (in the middle) to 0.3 (in the horns) due to the alongshore variations in the sediment grain size. The steeper-sloping zones are correlated with larger proportions of coarser sediments (Bramato et al., 2012). The steepest beach slope is located at H6 and corresponds to an old river outlet at that location.

#### **7.3.1.2 Submarine geomorphology and sediments**

The shelf adjacent to Carchuna Beach is dissected by the Carchuna Canyon (Fig. 7.11). Unlike the majority of the submarine canyons of the northern margin of the Alborán Sea (Ballesteros et al., 2008), the head of Carchuna Canyon is located a short distance from the coastline. The Carchuna Canyon trends N–S, paralleling the Motril Canyon located to the west (Muñoz et al., 2008). The canyon ends at a water depth of approximately 700 m

and has a total length of approximately 5 km. Although the major part of the canyon is located in deep water, the upper part of the western and eastern tributaries cut the shelf (Fig. 7.12). These tributaries, which extend to water depths from approximately 10 m to approximately 180 m, are relatively small in comparison with the main channel of the canyon.

To the east of Carchuna Canyon, a wedge-shaped sedimentary body exists that has been interpreted as an infralittoral prograding wedges (IPW) in previous studies (Fernández-Salas et al., 2009), see Fig. 7.11. These bodies are sandy bodies deposited beyond the shoreface in steep inner shelves. The physical continuity between the emerged beach ridge units and several marked increases in slope occurring over the Carchuna IPW have been interpreted as the result of a linked genetic mechanism with oblique or lateral progradation of successive IPWs rather than growth normal to the nearby coastline (Fernández-Salas et al., 2009).

The shelf is covered by mainly gravelly sands in the vicinity of the study area. The sand content decreases steadily seaward, ranging from more than 90% at a water depth of less than 20 m (landward of the well-marked increase in slope characterizing the Carchuna IPW) to approximately 70% in the vicinity of the shelf break. In contrast, the gravel content increases steadily from less than 5% at shallow depths to as much as 25% at the distal shelf margin (Bárcenas et al., 2011).

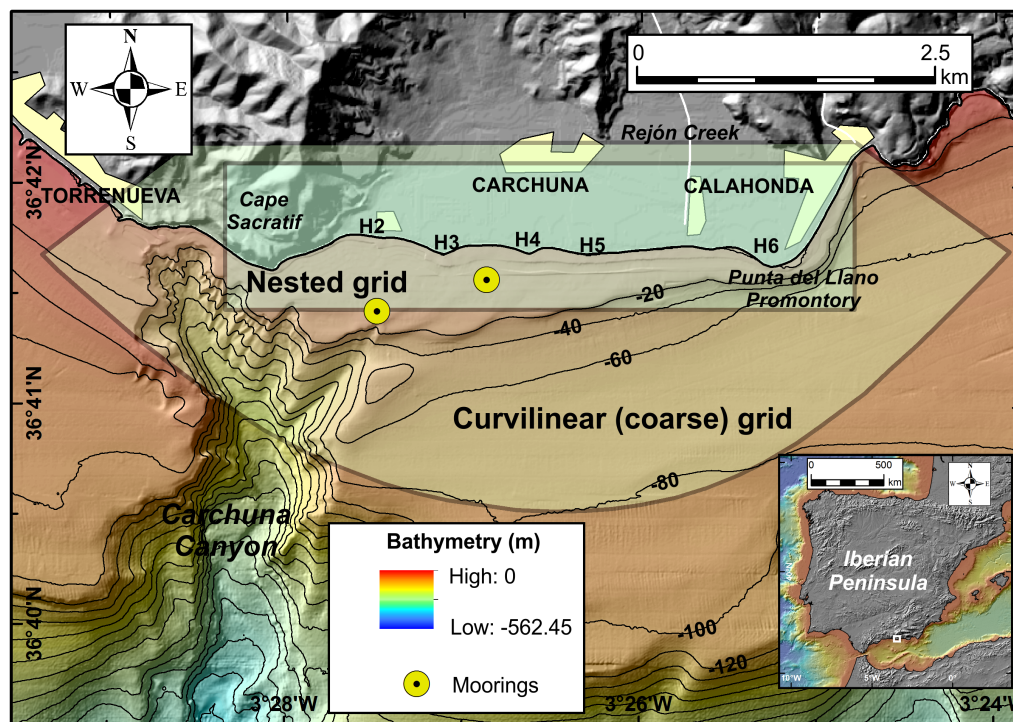


Figure 7.11: Shaded-relief bathymetry of the study area, comprising the littoral and adjacent sedimentary wedges, indicating the location of the grids (the curvilinear coarse grid and the nested grid) used in the numerical model and moorings. The bathymetric contours are given in meters below the present sea level.

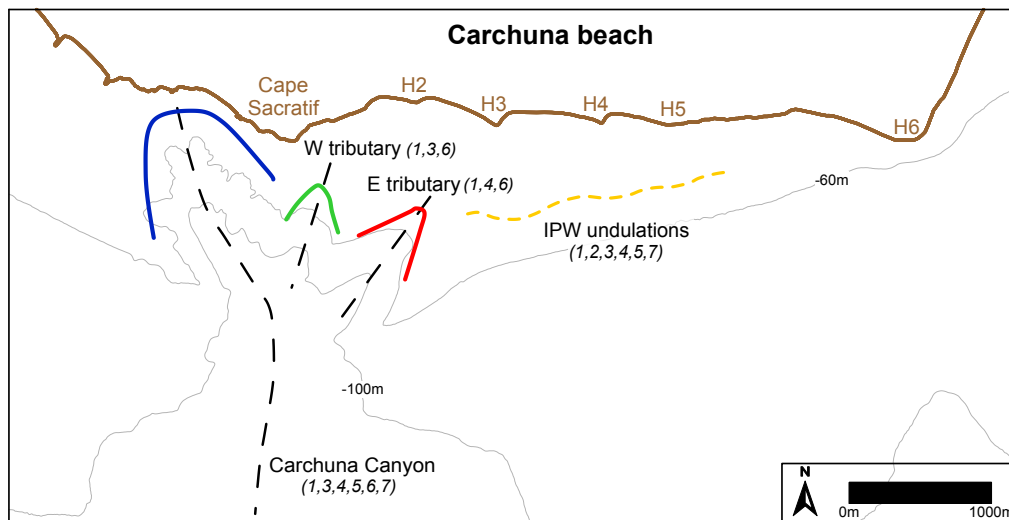


Figure 7.12: Scheme showing the main bathymetric elements. The blue line indicates the Carchuna Canyon. The green and red lines correspond to the western and eastern tributaries, respectively. The yellow dashed line indicates the position of the undulations of the IPW. The black dashed lines represent the mean alignment of the Carchuna Canyon and the tributaries. The numbers in parentheses indicate the scenarios in which the bathymetric element is present.

### 7.3.1.3 Oceanographic regime

The coasts of the Alborán Sea are subjected to low to moderate wave energy levels and microtidal conditions (a tidal range of approximately 0.5 m). The study area is subjected to the passage of extratropical Atlantic and Mediterranean storms (Quevedo et al., 2008). South Atlantic and south Mediterranean storms generate wind waves under limited fetch conditions (approximately 300 km) with average wind speeds,  $U_{10}$ , of 18 to 22 m/s.

The most energetic wave approaches are from the W, WSW, SW, ESE, and E directions. These waves are strongly oblique with respect to the mean alignment of the coastline. The shelf to the east of Carchuna Canyon is dominated by westward depth-averaged storm-induced flows with an average velocity of 0.15 m/s. Under the dominance of Westerlies, the eastward current flows reach velocities up to 0.1 m/s (Bárcenas et al., 2011).

## 7.3.2 Influence of the submarine canyon on wave propagation

The modeling is based on (a) the definition of various bathymetric scenarios, (b) the analysis of the wave propagation patterns for the different scenarios and (c) the characterization of the alongshore wave energy distribution near the coast.

### 7.3.2.1 Bathymetric scenarios

As waves propagate from deep water to the coast, they are affected by the seabed when they reach intermediate and shallow water regions. As a result, physical propagation processes, such as shoaling and refraction, are affected (Dean and Dalrymple, 1991). The main elements of the Carchuna shelf that transform wave characteristics, i.e., the canyon,

its western and eastern tributaries, and the geomorphological characteristics of the IPW are plotted in Fig. (7.12).

To analyze the influence of the different bathymetric elements on the coastal morphology, the wave energy distribution under different forcing conditions was analyzed for the actual situation and six synthetic scenarios that were created by removing or smoothing the bathymetric elements. The wave energy distribution was characterized by assessing the propagation coefficient along the study zone. The results were then compared to quantify how the bathymetric elements contribute to the alongshore wave energy modulation.

Scenario 1 (the actual situation) corresponds to a high-resolution bathymetry measured in 2010. In scenario 2, the canyon was eliminated. To achieve this, the original bathymetric contours were split up to remove the canyon and the remaining parts were joined to follow the natural curvature of the shelf. In scenarios 3 and 4, the western and eastern tributaries, respectively, were removed using the procedure described for scenario 2. In scenario 5, both tributaries were removed. In scenario 6, the undulatory pattern exhibited by the IPW offlap break was removed from the bathymetry by straightening the contour lines by smoothing. In scenario 7, both tributaries and the undulatory pattern were removed. A summary of all the scenarios defined is shown in Table (7.1), whereas Fig. (7.13) depicts the most representative scenarios, i.e., scenarios 1, 2, 5, and 6.

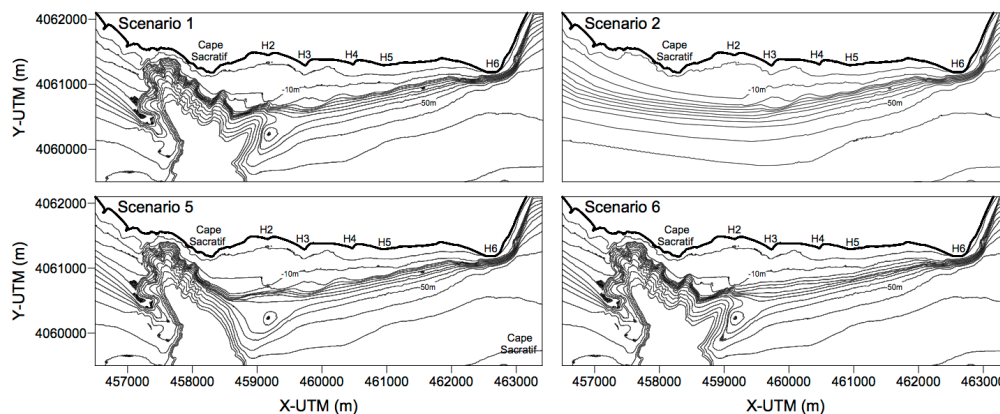


Figure 7.13: Bathymetries of scenarios 1, 2, 5, and 6 that were used for the wave propagation analyses (iso-baths are in meters).

### 7.3.2.2 Numerical model

For the different bathymetric scenarios, the waves were propagated from deep water to the nearshore using the third-generation wave model SWAN (Simulating WAVes Nearshore) (Booij et al., 1999). This model was designed to simulate random, short-crested waves in coastal regions (Lesser et al., 2004; Dan et al., 2011). The main processes included in the model are refraction due to bottom and current variations; shoaling, blocking, and reflections due to opposing currents; transmission/blockage through/by obstacles; wind effects; whitecapping; depth-induced wave breaking; bottom friction; and nonlinear wave-wave interactions.



Scenario	Canyon body	Western Tributary	Eastern Tributary	IPW Undulations
1	✓	✓	✓	✓
2	✗	✗	✗	✓
3	✓	✗	✓	✓
4	✓	✓	✗	✓
5	✓	✗	✗	✓
6	✓	✓	✓	✗
7	✓	✗	✗	✗

Table 7.1: Bathymetric scenarios defined for Carchuna beach.

Although refraction is the dominant propagation process (Magne et al., 2007), to accurately model the surface gravity waves propagating over the complex inner shelf bathymetry, combined refraction and reflection models are required. To this end, Gorrell et al. (2011) demonstrated that, although the SWAN assumptions include small bottom slopes, the alongshore variations of the nearshore wave field caused by refraction over steep canyons are predicted satisfactorily.

The model domain for Carchuna consists of two different grids, shown in Fig. (7.11). The first grid is a coarse curvilinear 244 x 73-cell grid covering the entire Carchuna region, with cell sizes that decrease with the depth from 38 x 55 to 16 x 24 m. The second grid is a nested grid covering the beach with 325 and 82 cells in the alongshore and cross-shore directions, respectively, and a cell size of 15 x 15 m. For the spectral resolution of the frequency space, 24 logarithmically distributed frequencies ranging from 0.05 to 1 Hz were used, whereas for the directional space, 72 directions covering 360° in increments of 5° were defined. Simulated data at isobaths of -5 m and -8 m were extracted for each scenario for further analysis.

Although the SWAN model was previously applied to Carchuna and validated with data captured during a 7-day field survey (Bramato et al., 2012), we also compared the model results with the data obtained with the instrument moored in 2010 (Fig. 7.11). Fig. (7.14) depicts the wave height measured by the instrument during the field survey and the equivalent wave height propagated with the SWAN model for the same location. The wave heights propagated by the model were shown to agree well with the measured wave heights.

As shown in the results section, WSW and E are the predominant incoming wave directions. Hence, to describe the general energy distribution on the beach, the following representative incoming wave cases were simulated: WSW and E directions, characteristic mild and storm wave heights (1 and 4 m, respectively), and short and long peak periods (6 and 10 s), based on the classification defined by Ortega-Sánchez et al. (2003b).

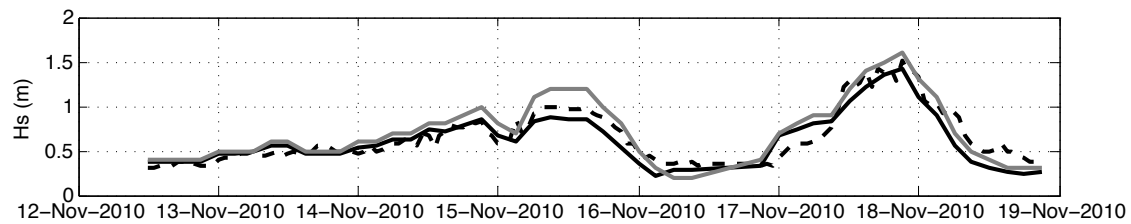


Figure 7.14: Comparison between the offshore WANA input wave data (the gray line), the propagated wave data measured by the ADCP (the dashed line), and the SWAN wave model results obtained for the same location of the ADCP (the black line). The wave model results correspond to the propagation over the real bathymetry (scenario 1)

### 7.3.2.3 General energy distribution and littoral drift trends

Based on the analysis of the data obtained at hindcasting point WANA204279, the wave directionality approaches result 47.70% and 45.64% of the time for the E-ESE and W-WSW-SW, respectively, with two main predominant directions: WSW (30.11%) and E (31.66%). The significant wave heights are predominantly less than 1 m (76.9%), whereas storms that are characterized by significant wave heights greater than 3 m occur more than once per year on average.

Fig. (7.15) shows an example of the SWAN model results for the real bathymetry (scenario 1) under storm conditions ( $H_s=4$  m,  $T_p=10$  s). For both incoming directions (WSW and E), the wave energy is modulated alongshore, with areas of concentration and divergence. The WSW waves concentrate energy between Cape Sacratif and H3 and in the western part of H4. The energy is significantly reduced in the rest of the beach. In contrast, although the results obtained for the E waves showed some areas of wave energy concentration, the energy content was generally significantly lower throughout the beach.

Fig. (7.16) represents the alongshore evolution of the propagation coefficient for these two cases. This coefficient is defined as the ratio between the wave height at a given depth (5 or 8 m) and the offshore wave height. An alongshore modulation pattern is clearly observed, and similar results were obtained for both mild ( $H_s=1$  m) and storm waves ( $H_s=4$  m). The waves approaching from the WSW are more energetic, with propagation coefficients close to 1 at the western boundary of the beach. These coefficients decrease to the east, but remain consistently greater than 0.6. In contrast, the waves approaching from the E have a coefficient of less than 0.6, with a minimum of 0.3 close to the canyon. The difference between the propagation coefficients in the west and the east of the study zone shows that the wave heights in the west of the study zone are approximately 20% higher than in the east of the study zone for the same offshore conditions.



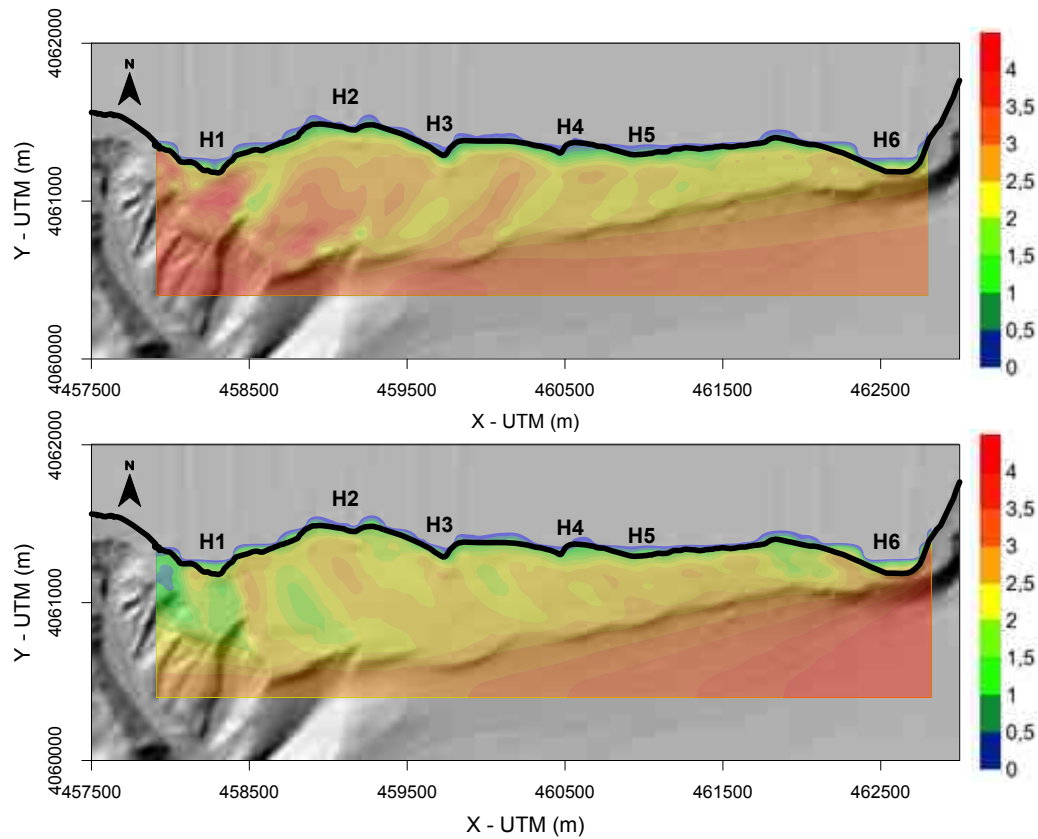


Figure 7.15: Graphs of the nearshore wave patterns for the actual bathymetry (sc1). Upper panel: W incoming waves (from the left lower corner of the figure). Lower panel: E incoming waves (from the right lower corner of the figure). Both cases correspond to storm conditions (a significant wave height of 4 m and a peak period of 10 s).

#### 7.3.2.4 Influence of the canyon

Because most of the wave energy modulates and concentrates near the canyon, its influence on the wave propagation was analyzed. The wave propagation results for bathymetric scenario 2 (no canyon) were compared with those obtained for scenario 1 (the actual bathymetry). Fig. (7.17) shows the difference in the propagation coefficients between the two scenarios for various forcing conditions. Positive values correspond to energy increases due to the canyon, whereas negative values indicate the opposite. The results show that the canyon concentrates wave energy between H1 and H3, whereas after H3, the nearshore waves behave in a similar manner for both scenarios 1 and 2, with no differences in the propagation coefficients. The presence of the canyon increases the nearshore wave heights up to approximately 25%, with a corresponding increase in the wave energy. Because the canyon is located along the western boundary of the beach, its influence is greater on western waves than on eastern waves.

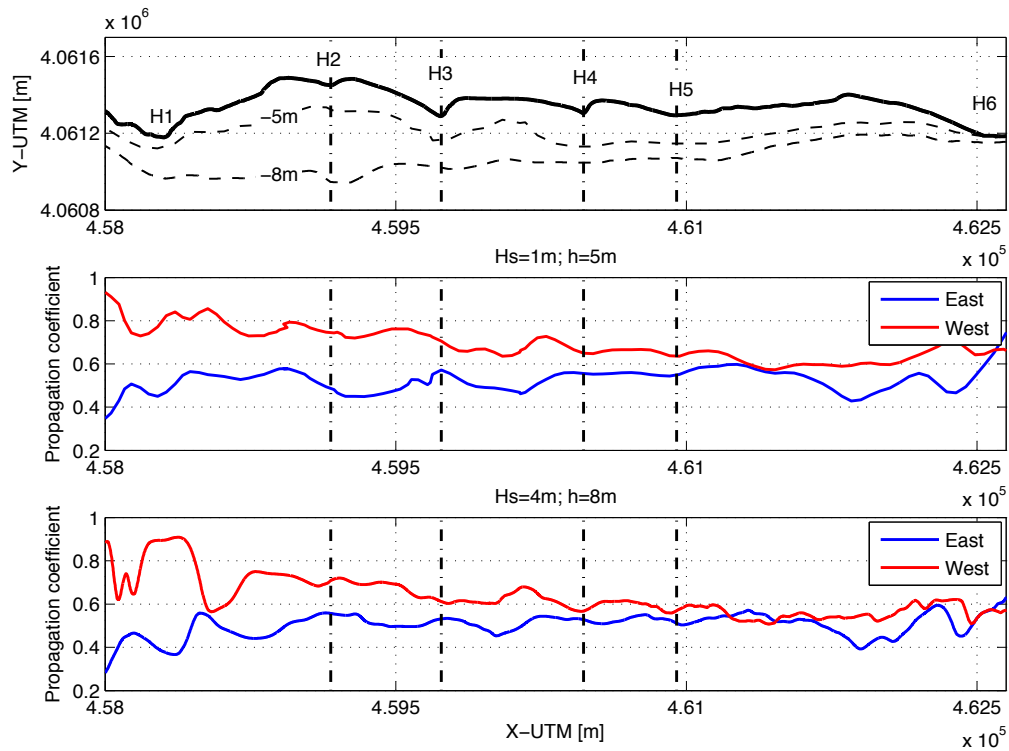


Figure 7.16: Graph of the evolution of the wave energy content for the actual bathymetry (sc1). The results correspond to an average period. The wave data were extracted for depths of 5 m and 8 m to avoid the influences of wave breaking and reflection near the shoreline. West refers to WSW waves.

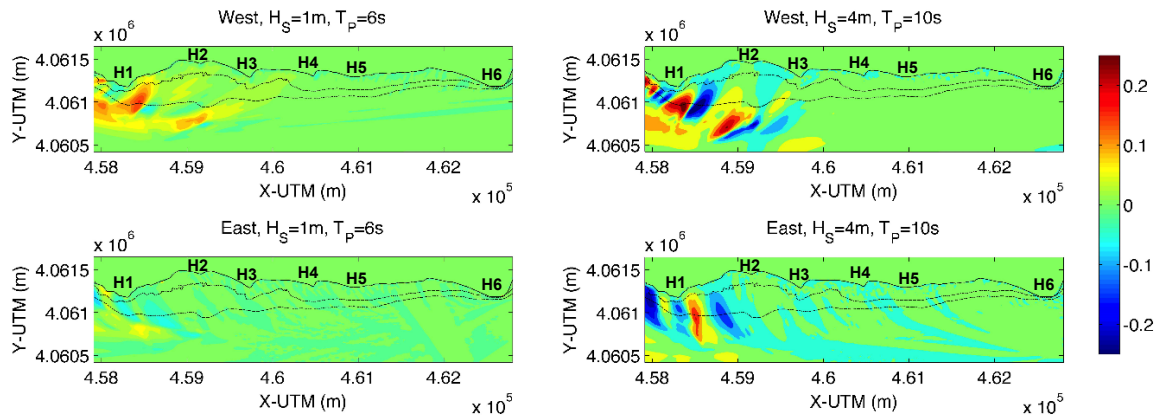


Figure 7.17: Differences in the propagation coefficients between scenarios 1 and 2. Positive (negative) values indicate increases (decreases) in the wave energy. The discontinuous contour lines correspond to the isobaths for depths of 5 and 8 m. West refers to WSW waves.

Fig. (7.18) shows the alongshore evolution of the propagation coefficients for scenarios 1, 3, 4, and 5. The western tributary of the canyon does not exert a significant influence on the wave patterns: the curves for scenarios 1 and 4 are coincident close to H1, and there are significant differences only in front of H2 (more significant at a depth of 8 m than at a depth of 5 m). In contrast, the eastern tributary has a greater influence

on the wave modulation: the reduction of the propagation coefficient off Cape Sacratif, which may be responsible for the circulation patterns, disappears. Very similar behavior was observed for the scenario in which both tributaries were eliminated (scenario 5), but some alongshore oscillations were observed. After H3, the influence of the tributaries disappears, and all of the propagation curves collapse into a single one.

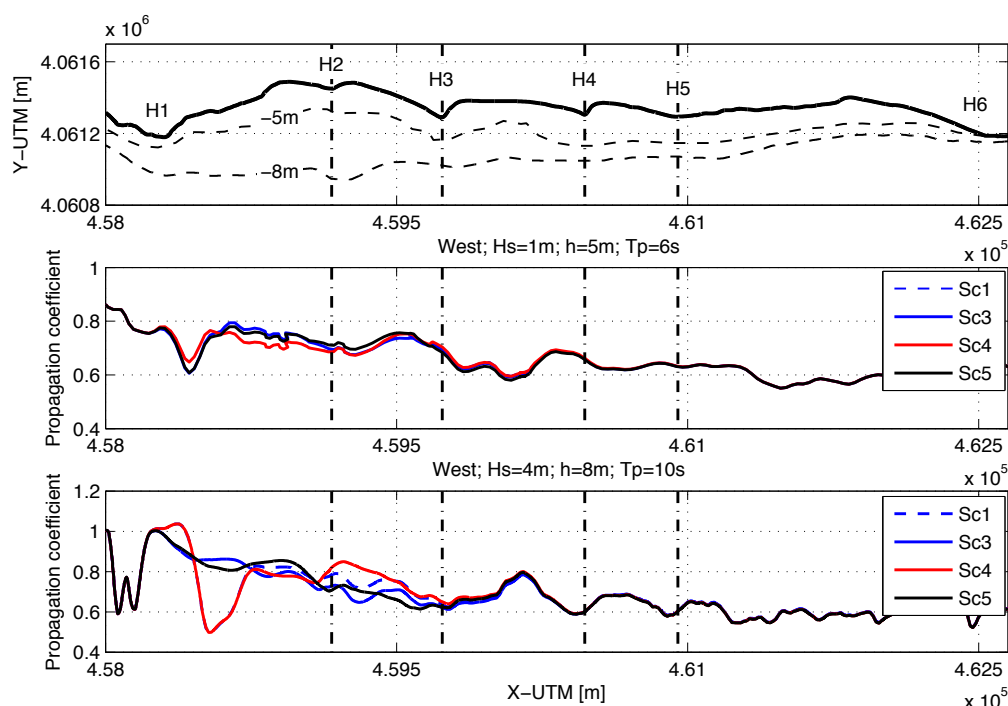


Figure 7.18: Graph of the evolution of the wave energy content for the actual bathymetry (sc1) and the scenarios with the canyon tributaries (sc3, sc4, and sc5). West refers to WSW waves.

### 7.3.2.5 Influence of the submerged IPW undulations

Despite the previous studies on the morphology of Carchuna Beach, it is still unclear how the peculiar non-rhythmic large-scale shoreline features are formed. The presence of Carchuna Canyon results in a concentration of wave energy between H1 and H3 (Figs. 7.15 and 7.16), but the canyon does not affect nearshore waves between H3 and H6 for WSW waves (Fig. 7.17), where some of those large-scale cusped features are found. The possible influence of the submerged IPW undulations was therefore analyzed.

Fig. (7.19) presents the alongshore evolution of the difference between the propagation coefficients for scenarios 1 and 6 (no submerged undulations) under the predominant wave conditions. For both western and eastern waves, an alongshore variation in the wave height on the order of 5–10% was observed. The maxima were found between the horns of the large-scale shoreline features, although higher values were obtained for the western waves than for the eastern waves. At a depth of 8 m, the maxima and minima for the W and E waves are not at the same locations, whereas at a depth of 5 m, the waves are more refracted and shoaled, and both the amplitude and locations are similar for the W and E waves.

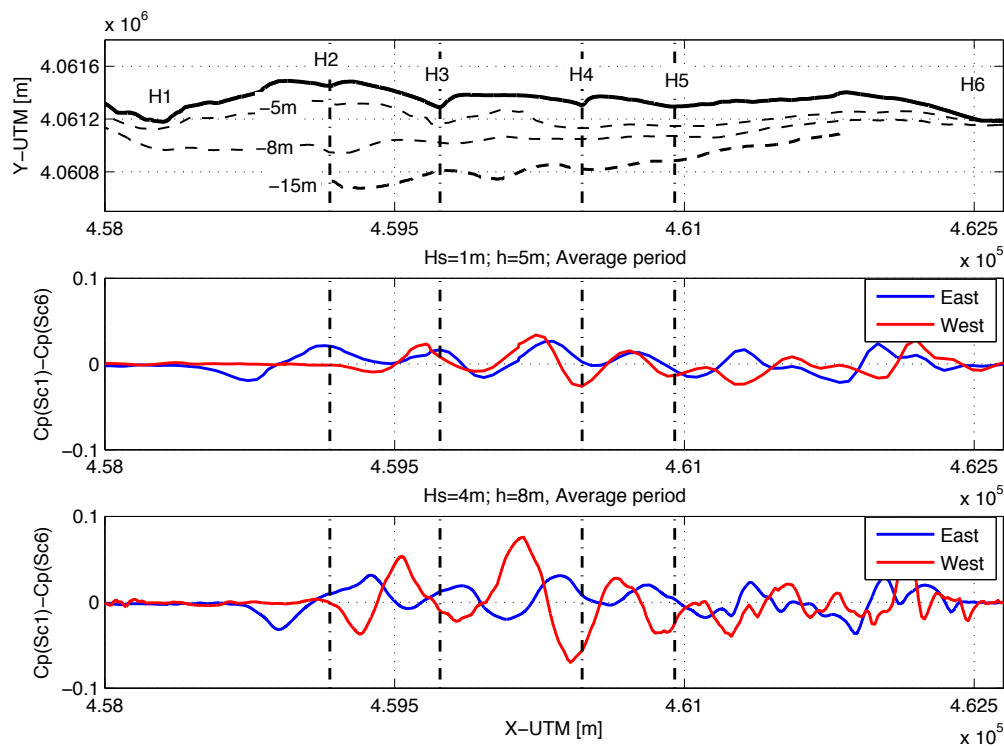


Figure 7.19: Alongshore evolution of the differences in the propagation coefficients between sc1 and sc6. Positive (negative) values indicate increases (decreases) in the wave height due to undulations. For clarity, the -15m bathymetric line, where the shape of the undulations is more pronounced, was included in the upper graph of the figure. West refers to WSW waves.

### 7.3.2.6 Conclusions

As demonstrated by the SWAN model, the Carchuna Canyon favors wave height increases and consequently wave energy concentration in the western part of the system, particularly under the influence of western waves. The enhanced wave activity would have led to significant coastline erosion between Cape Sacratif and H3, generating a coastal embayment. Energy concentration would also cause erosion in the shoreface and inner shelf, as indicated by erosional truncation of the sediment wedge in the canyon head. The widespread erosion in the western part of the system would provide a sediment source that would likely tend to be transported laterally (i.e., eastward).

Although both nearshore WSW and E waves have the potential obliquity (Fig. 7.15) to induce an alongshore drift, the western waves are more energetic and have higher propagation coefficients. These results are also consistent with the field measurements that showed that western storms produce more changes in the profile of Carchuna Beach than eastern storms (Bramato et al., 2012). The morphological development of the Carchuna IPW, which decreases in width and size toward the east, is consistent with the hydrodynamically induced sediment transport trends. The continued process would have favored the lateral growth of the entire submarine sediment body, through the stacking of successive attached progradational wedges, concomitant with the eastward development of the coastal plain through the accretion of beach ridge deposits. This set of evidence supports the hypothesis that the IPW could have been formed as the result of (a) the long-term

coastal erosion associated with extreme energy events focused by the Carchuna Canyon and (b) the growth led by predominant sediment transport in the east direction, in consonance with the development of the onshore beach.

### 7.3.3 Interaction between the submarine and coastline morphologies

Carchuna Beach is characterized by a coastline morphology with non-rhythmic large-scale alongshore features (H2-H6) of different cross-shore extents. The shelf-indenting Carchuna Canyon and the undulating IPW modulate the wave energy in the nearshore. Our results confirm that the concentration and divergence wave patterns are the main mechanisms responsible for the formation of the large-scale shoreline features (Ortega-Sánchez et al., 2003b). In particular, the canyon is mainly responsible for the morphology in the western part of the beach (H1-H3), whereas the submerged IPW undulations modulate the alongshore wave energy and reinforce horns H4-H5-H6. Other mechanisms, such as the atmospheric-hydrodynamic coupling in the nearshore induced by Cape Sacratif (Ortega-Sánchez et al., 2008a), may reinforce this morphology.

Ortega-Sánchez et al. (2003b) reported the existence of rhythmic shoreline features spaced on the order of 102 m between H5 and H6. These researchers showed that one possible mechanism responsible for the formation of these features is the partial reflection of edge waves at the horns. Quevedo et al. (2008) presented a hydrodynamic model that also predicts the generation of these beach lobes by turbulent wind vortices blowing over the sea surface on the lee side of geographic obstacles. Fig. (7.20) shows that the IPW undulations between H5 and H6 induce an alongshore wave height modulation that may reinforce the formation of these beach lobes. The smaller cross and longshore dimensions of these beach lobes, compared with the dimensions of the horns H1-H6, may be due to the smaller propagation coefficients of both the WSW and E waves in this part of the beach.

The fact that the wave energy increases in the embayments of the large-scale features, regardless of the direction of the incoming predominant waves, in combination with the obliquity of the waves in the nearshore (Fig. 7.15), leads to the hypothesis that the submerged IPW undulations may play a key role in the formation of the shoreline morphology. This hypothesis is consistent with the results reported by Ortega-Sánchez et al. (2003b), although they did not identify the bathymetric element causing the modulation. Whereas other studies have quantified the importance of the complexity of the inner shelf bathymetry in the nearshore hydrodynamics (Apotsos et al., 2008; Gorrell et al., 2011), our results show that the adjacent bathymetry also has a strong influence on the evolution of the shoreline morphology.

Although the alongshore distribution of the wave energy may explain the formation (and location) and the irregular spacing of horns H2-H6, the main processes responsible for their different shapes remain unknown. As a first approximation, Ortega-Sánchez et al. (2008c) applied the model developed by Ashton and Murray, 2006a,b and found good general agreement between the large-scale features of Carchuna Beach and the results obtained using the Ashton and Murray (2006a) model. According to this model, instabilities and rhythmic features tend to appear on coastlines where the waves impinge with

an obliquity greater than  $45^\circ$  with respect to the shore-normal orientation. Nevertheless, there were some aspects that were not reproduced by the model: 1) the protruding horns do not have a symmetric shape, 2) there is a general alongshore variation in the shape of the features, and 3) the relative orientation of the shoreline changes between features. Ortega-Sánchez et al. (2008c) concluded that nearshore wave energy modulation should be considered to fully explain the morphology of Carchuna Beach.

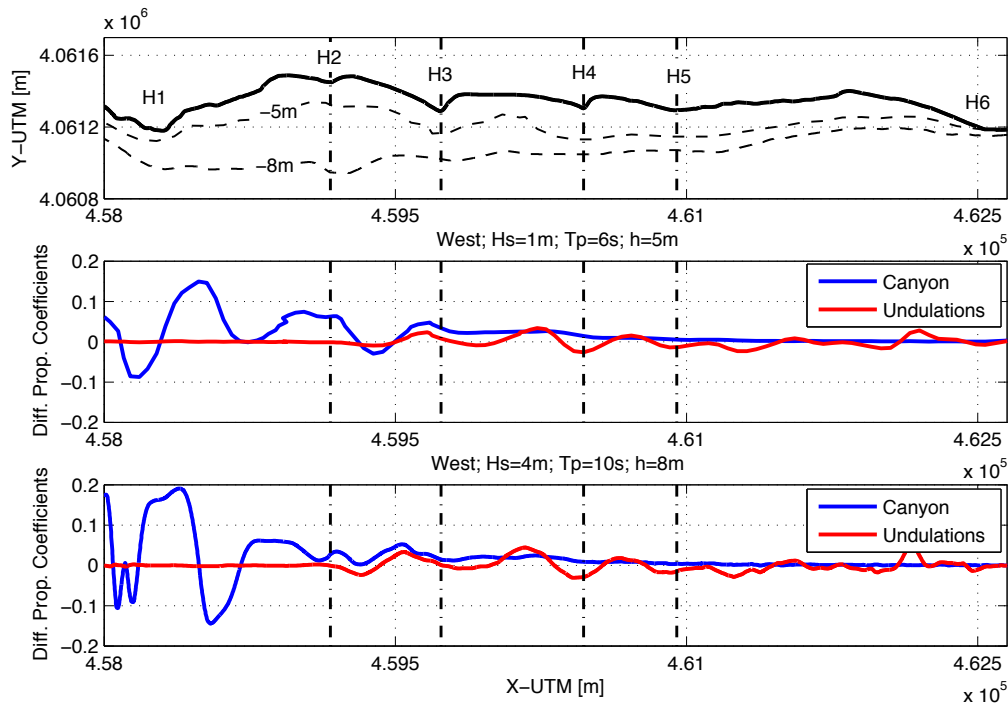


Figure 7.20: Alongshore evolution of the differences in the propagation coefficients between sc1-sc2 (the blue line) and sc1-sc6 (the red line). Positive (negative) values indicate increases (decreases) in the wave height due to the canyon (blue) or to the effect of undulations (red), respectively. West refers to WSW waves.

The complexity of the nearshore wave propagation patterns at Carchuna Beach, in combination with the curvature of the shoreline, results in an alongshore variation in the wave properties (i.e. Fig. 7.20). López-Ruiz et al. (2012a) developed a one-line-type model that considers the effects of the alongshore variation in the wave properties and the curvature of the shoreline. This model was applied to an initially rectilinear beach of the same length as Carchuna Beach. The wave forcing consisted of a modeled surf zone width that varied according to the wave propagation results described in the previous sections. Considering that the canyon is located in the western part of the beach and that western waves induce greater alongshore energy variations than eastern waves, only storm WSW waves were simulated.

Fig. (7.21) shows the simulation results for the shoreline after 50 days of constant storm conditions. A series of horns with alongshore spacings very similar to those observed in Carchuna Beach were obtained. Moreover, the resulting features have an asymmetric shape: the side exposed to the more energetic western waves was larger than the

protected side. The horns also have a non-uniform configuration in the alongshore direction, with changes in the relative orientation of the shoreline between the features due to the alongshore variation in wave energy.

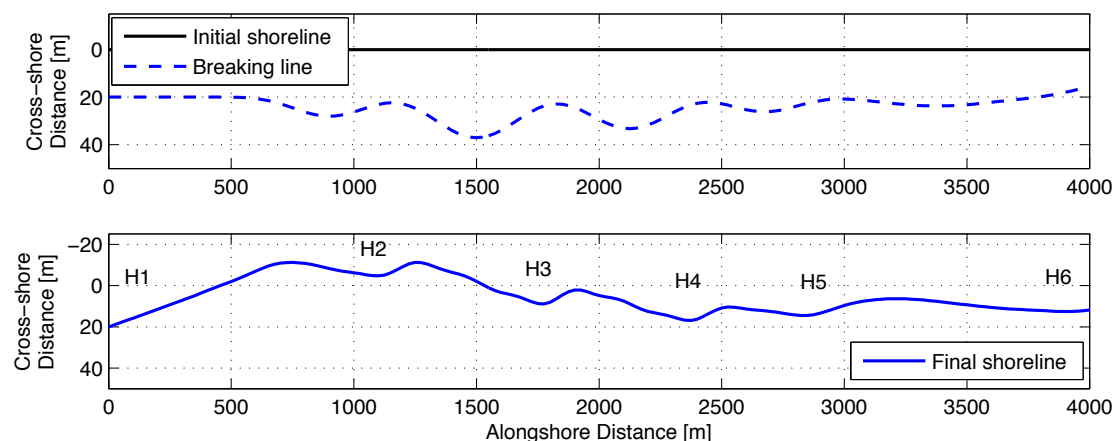


Figure 7.21: Upper panel: Initial shoreline for the one-line simulation (the solid black line) and surf zone width used during the simulation (the dashed blue line). Lower panel: Shoreline obtained after the simulation.

Although the model captures the main geometric characteristics of the shoreline features, the shoreline evolution must be simulated using real variable climate forcing to reproduce the cross-shore length of the horns (López-Ruiz et al., 2012a). So, these qualitative results appear to confirm the hypothesis that the nearshore wave energy modulations induced by the presence of the submerged features under the prevailing waves can explain the development of the shoreline horns at Carchuna Beach. Moreover, these qualitative results appear to confirm that complex bathymetries exhibiting submerged large scale sedimentary features, i.e., IPW, or shelf-indenting canyons can play a key role in the formation of asymmetrical and/or irregular shoreline shapes, such as observed at Carchuna beach. Simple shoreline evolution models (i.e., one-line type models) can be of significant use in the study of such shoreline shapes because they generally include both the wave energy patterns induced by the complex bathymetry and the changes in shoreline orientation as the coastline evolves.

## 7.4 Application to an erosional stretch of coast

Preliminary results of the model were also obtained for an erosional coastal stretch of a beach adjacent to the Guadalfeo river mouth, located in Southern Spain. This beach has a curvilinear nearshore bathymetry (Fig. 7.22) due to the deposition of the Guadalfeo river sediment that took place mainly before the construction of dam in the river basin in 2004. The weak sediment contribution of the river after that time, and the channelization of its mouth that acts as a barrier for the alongshore sediment transport, have produced during the last years, severe erosion in the downdrift part (right side in Fig. 7.22). Available aerial images of this stretch of the beach frequently show shoreline undulations with wavelengths 250 m.



To analyze the role that the curvilinear bathymetry and the presence of a barrier in the alongshore sediment transport play in the development of shoreline undulations in this type of coast, the one-line type model was applied to a straight coast with two dikes that do not allow sediment transport to occur from one side to the other. For the wave forcing, SWAN propagations were carried out using the real bathymetry of the study zone (Fig. 7.22). The results show that the concave-type nearshore bathymetry produces a wave energy concentration downdrift the river mouth (considering the direction of the main littoral drift, see Fig. 7.23).

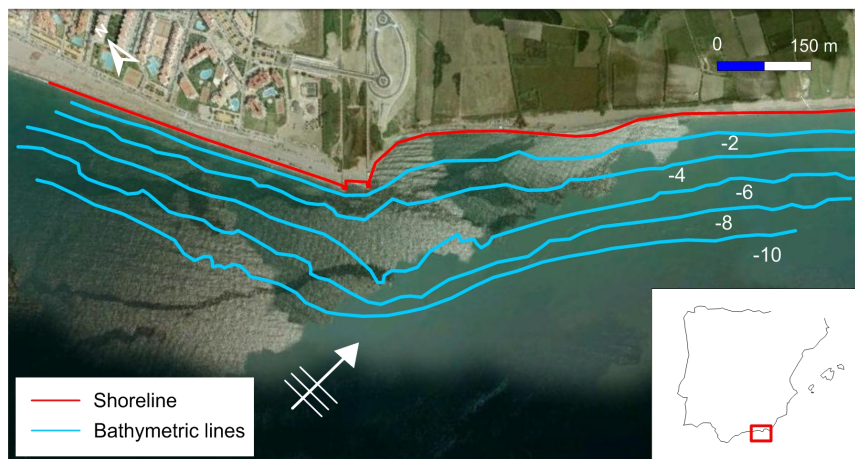


Figure 7.22: Plan view of the Guadalfeo river mouth, Granada, Southern Spain. Bathymetry (blue lines) and direction of the predominant waves are superposed.

The one-line type model developed is forced with the surf zone width obtained from SWAN propagations. Fig. (7.23) presents the results after three months of predominant wave forcing and shows the formation of shoreline undulations in the downdrift part of the beach, as well as the accretion of the updrift part. Results are qualitatively in agreement with the observations. However, a more intensive analysis that includes the variability of the wave climate is necessary to properly validate the simulations and to obtain more accurate values of wavelengths and amplitudes.

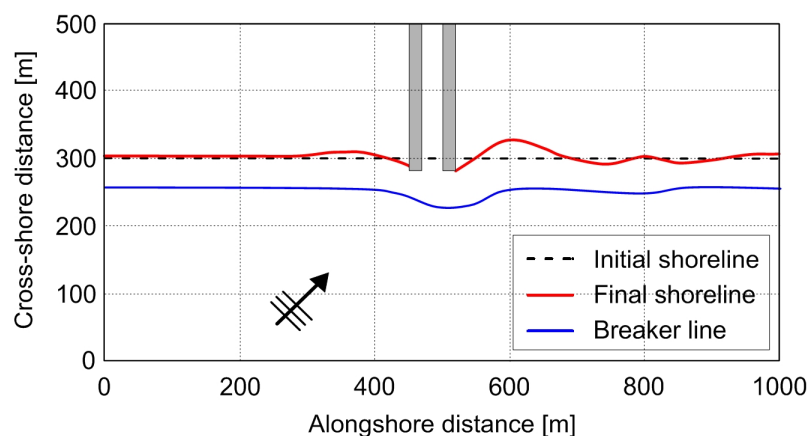


Figure 7.23: Results obtained with the one line model for the Guadalfeo river mouth.



Results seems to confirm that the combined effect of wave energy gradients due to the propagation of waves over curvilinear bathymetry and the presence of obstacles for the alongshore sediment transport, drive the formation and development of shoreline undulations in beaches adjacent to river mouths. Thus, these undulations seem to be related to erosional stretches of coast.

---

# **Conclusions and future research**

---

## **8.1 Main conclusions**

Coastlines around the world are complex systems that develop a wide range of shoreline features. How these features form and evolve and what conditions favor their growth are questions that still remain unanswered. To gain insight into the previous questions, this Thesis has mainly focused on (1) the identification and characterization of shoreline features that are frequently found on curvilinear coasts and (2) to present analytical approaches to quantify the importance of different hydrodynamic and morphological variables on the evolution of weakly curvilinear shorelines.

The main objective of this Thesis was “to derive an updated formulation for the alongshore sediment transport rate on curvilinear coasts that will be used to study the morphological evolution of the coast”. To make this derivation, the effects of the presence of curvilinear bathymetries were identified. An averaged energetic expression for the alongshore sediment transport was adapted to consider these effects by considering local quantities of the nearshore wave magnitudes and then integrating the resulting expression through the surf zone. Two different solutions for this integration were obtained depending on the wave angle approximation defined. Both are able to consider alongshore variations in beach slope, sediment size, wave properties and shoreline orientation. To study the morphological evolution of a curvilinear coasts with these formulations, a one-line model was defined. An analytical analysis of the model was performed to compare the implications of the new approach on coastal morphology with those obtained with previous works, whereas a numerical solution of the model was applied to four different locations where shoreline features on curvilinear coasts appear.

The most important conclusions of the Thesis are summarized by presenting the conclusions obtained for the specific objectives that were formulated in Section 1.2.2:

1. To establish a formal definition of the shoreline undulations and find under what conditions they are more likely to occur and if there are a relationship between the presence of curvilinear bathymetries and the development of such undulations.

Shoreline undulations are defined as “medium to large spatial scale shoreline features with alongshore dimensions ranging from hundreds to thousands of meters and amplitudes from tens to hundreds of meters”. After the realization and analysis of an European database along 50.000 km and 15 countries, it is noticed that the

majority of the shoreline undulations exhibit less than 4 undulations. In these cases they are clearly related to curvilinear coasts or river mouth/outlets. More than 50% of the sites identified have a constraint located nearby the undulations. Hence, it can be concluded that the presence of a curvilinear or at least irregular bathymetry is a very common characteristic of the locations where SU are identified. Moreover, the analysis of the presence of SU in combination with the wave forcing agents for the Spanish coast reveals that their formation is favored under mild wave conditions and micro or mesotidal conditions.

2. To analyze and quantify the effects of the presence of curvilinear coasts on wave propagation, mainly on the variables that drive the alongshore sediment transport.

The results obtained with a numerical wave propagation model shows that the presence of curvilinear bathymetries generates important alongshore wave variations in the breaking wave height, and hence, in the wave energy. These gradients in wave energy can be of 45% in the case of a prograding spit front, whereas for a undulating shoreline they can reach more than 20%. In the case of the nearshore wave angle, differences of 30° and 20° are observed along the shoreline for the prograding spit and the undulating shoreline, respectively. Since the wave energy and the nearshore wave angle are the main variables usually considered to calculate the sediment transport rates, their gradients may induce important changes in the sediment transport pattern along the coast.

3. To find an expression for the alongshore sediment transport that considers all the effects identified in the previous specific objective, and also other important characteristics in the morphodynamics of the sandy beaches (sediment size, beach slope, etc.).

The alongshore sediment transport expression was obtained as a modification of the Inman and Bagnold (1963) energy approach. The resulting expression only requires deep-water wave data (the significant wave height, peak period and angle), geometric data (the beach orientation and slope) and nearshore data (the width of the surf zone). The expression also considers the effect of alongshore grain size variations, alongshore beach slope gradients, and variations in the type of wave breaking. Two different and simple analytical expressions were obtained depending on the nearshore wave angle approximation. Therefore, they are useful tools in the management of curvilinear coasts and the study of the formation of some shoreline features, such as shoreline undulations.

4. To analyze how changes in the wave conditions and beach configurations modify the alongshore sediment transport defined and the potential evolution of the shoreline.

Numerical experiments with the alongshore sediment transport previously obtained were analyzed, in which the deep-water wave angle, the wave period, the deep-water wave height, the geometry of the shoreline and the alongshore distribution of the beach slope in undulating beaches were varied. The results show that three different shoreline movements can be driven: (1) variations in the deep-water

wave angle may induce the updrift migration of the shoreline undulations, (2) an increase in the deep-water wave height or wave period and a decrease in the relation between the wavelength and the amplitude of the shoreline undulations can trigger the formation of steeper undulations without changes in their wavelength, and (3) changes in the alongshore distribution of the beach slope and grain size may cause a change in the wavelength and symmetry of the undulations. Alongshore variations in wave energy dissipation and wave setup were also analyzed. When the beach slope is higher in the beach horns than in the embayments, variations in setup may induce alongshore currents that enhance the currents generated by the wave breaking. Hence, the generation of closed circulation cells is favored under such conditions. If the beach slope is larger in the embayments than in the horns, this effect is not produced.

5. To define a morphological evolution model for the plan view of the coast (oneline type model) and compare it with other solutions obtained previously.

The oneline equation was presented, and an analytical development was performed to compare the implications on coastal morphology of the defined approach with those of previous works. For the two analytical expressions of the alongshore sediment transport obtained through this Thesis, two different terms arise in the oneline equation. One can be considered equivalent to the classical diffusivity obtained by Pelnard-Considère (1956). The second is a new term that depends on wave period, shoreline angle, surf zone width and deep-water wave angle and is proportional to alongshore gradient in surf zone width. This implies that the framework defined in this work let consider new effects (mainly in the new term obtained) in the morphodynamic evolution of the coast that the previous approaches can not consider. Moreover, with this framework it is not necessary the presence of high angle waves for the development of shoreline features, as their growth is not associated with a change in the sign of the diffusivity. Hence, the development of such features seems to be related with the combined effect of the two terms obtained for the analytical expression of the oneline equation.

6. To apply this model to different locations with curvilinear coasts where rhythmical shoreline features develop to establish if the new processes considered in this work are decisive in the formation of such features.

A numerical solution of the oneline model was applied to four different locations. In the case of Doñana spit (Southern Spain), the two undulations present in the circular-shaped prograding spit front were reproduced in the 500 shorelines modeled with 5 year of wave climate simulation. Results are in good agreement with observations for the location, wavelength and amplitude of the undulations. For El Puntal spit (Northern Spain), three events of shoreline undulations development were reproduced using the wave climate registered during the events. Again, results are in good agreement with observations. For the horn-embayment system of Carchuna beach (Southern Spain), the shoreline was modeled considering the combined effects of the presence of submerged undulations and a submarine canyon. The model reproduced the asymmetric shape of the features and the non-uniform

alongshore configuration, which are the main characteristics of the beach. Changes in the relative orientation of the shoreline between the features is attributed to alongshore variation in wave energy. Finally, preliminary results of the model were also obtained for an erosional stretch of coast in the vicinity of a river mouth in which shoreline undulations appear. These results seem to confirm that the consideration of wave energy gradients along the coasts can drive these features.

## 8.2 Future research

After the analysis of the results, many questions remain concerning how the undulating shorelines are generated, grow and evolve. This Thesis provides simple tools and increases our understanding of the physics involved so that we can address those questions in further studies. After the realization of this work, these studies should focus on 3 main lines:

1. The first line should focus on how the formation of the undulating coasts initiates. Shorelines tend to be in dynamic equilibrium when the alongshore sediment transport rate is nearly constant. When this equilibrium is not satisfied, erosion-accretion patterns appear, and the shape of the shoreline changes. This is generally due to changes in the sediment supply (i.e., river discharges) or due to modifications in the alongshore wave energy distribution due to the offshore bathymetry. López-Ruiz et al. (2012a) show how even a slight curvature of the shoreline, in combination with oblique waves, induces changes in the alongshore wave energy distribution.

In this study, we have reinforced those results and show that other variables, such as the amplitude and wavelength of the undulations, the beach slope variations, and the size of the sediment also have strong influences on the sediment transport patterns and consequently on the shape of the shoreline. However, more detailed studies are necessary to analyze what deviations from equilibrium in the alongshore sediment transport trigger the transformation of a rectilinear coast into an undulating coast.

2. The next research line should focus on the relationship between the hydrodynamic conditions and the presence and geometry of undulations in the coast. The results presented in this work show that there is a relation between the changes in those variables and the potential evolution of the coast. This can lead to considering whether it is possible to know somehow the mean hydrodynamic conditions of a beach by simply observing the shape of the shoreline, that is, whether the undulations are a script in the beach related to their hydrodynamic condition history.

This line should also analyze the nearshore circulation system for coastlines with shoreline undulations. Undulating shorelines and the associated systems of nearshore circulation are based on a predominant alongshore current and can be

considered an intermediate step before the development of a system with independent cells of circulation between horns. It is still not well understood how this transition may occur and when the alongshore circulation studied in this work degenerates into a nested circulation system with closed cells. Hence, the velocity field in the nearshore should be studied for shoreline undulations with different relationships between beach slope, amplitude and wavelength of the undulations.

3. The last line should focus on the inclusion of cross-shore processes in the model. In this work, it has been assumed that the alongshore processes dominates the morphodynamics and the coastal evolution. However, on curvilinear coasts the cross-shore effects may be more important than on rectilinear coasts and they must introduce variations in the beach profile. In that sense, it would be of major importance the definition of a nearshore bathymetry evolution model that accounts for not only spatial, but also temporal variations in beach slope. The approach should be similar to the work of Wolinsky (2009), where a unifying framework for shoreline migration is presented using the Exner equation, what led the inclusion of both alongshore and cross-shore processes of different temporal scales.



## Conclusiones

---

Las costas de todo el mundo son sistemas complejos en los que pueden identificarse una gran variedad de morfologías en la línea de costa. Cómo estas morfologías se forman y evolucionan y qué condiciones favorecen su crecimiento son cuestiones que aún no tienen una respuesta clara. Para poder responder a estas cuestiones, esta tesis se ha centrado principalmente en (1) la identificación y caracterización de las morfologías costeras que se encuentran con frecuencia en las costas curvilíneas y (2) un estudio analítico para cuantificar la importancia de las diferentes variables hidrodinámicas y morfológicas en la evolución de la línea de costa en playas con curvatura suave.

El objetivo principal de esta tesis es “obtener una formulación para el transporte longitudinal de sedimentos en costas con curvatura suave y utilizarla para estudiar la evolución morfológica de la costa”. Para hacer este estudio, se han identificado los efectos de la presencia de batimetrías curvilíneas en la propagación del oleaje. Después, se ha adaptado una expresión conocida del transporte longitudinal de sedimentos para tener en cuenta estos efectos, considerando cantidades locales de las magnitudes del oleaje en la zona de rompientes y luego integrando la expresión resultante a lo largo de la zona de rompientes. Se han obtenido dos soluciones diferentes para esta integral en función de la aproximación del ángulo del oleaje definida. Ambas son capaces de considerar variaciones longitudinales en la pendiente de la playa, tamaño del sedimento, características del oleaje y la orientación de la costa. Para estudiar la evolución morfológica de un tramo de costa curvilínea con esta formulación, se ha definido un modelo de una línea. Asimismo, se ha realizado un análisis analítico del modelo para comparar las implicaciones que tiene este nuevo enfoque en la morfología costera, comparando los resultados con los obtenidos en trabajos previos. Además, se ha aplicado una solución numérica del modelo a cuatro lugares diferentes en donde aparecen morfologías de la línea de costa en costas curvilíneas.

Las conclusiones más importantes de la Tesis se resumen a continuación como respuesta a los objetivos específicos que se formularon en la sección 1.2.2:

1. Establecer una definición formal de las ondulaciones de la línea de costa y encontrar en qué condiciones es más probable que aparezcan y si hay una relación entre la presencia de batimetrías curvilíneas y el desarrollo de estas ondulaciones.

Las ondulaciones de la línea de costa (SU) se definen como “morfologías costeras de media a gran escala con dimensiones longitudinales que van desde cientos a miles de metros y amplitudes de decenas a cientos de metros”. Después de la realización y el análisis de una base de datos europea a lo largo de 50.000 kilómetros y



15 países, se ha observado que la mayoría de las ondulaciones de la línea de costa presentan menos de 4 ondulaciones. En estos casos, están claramente relacionadas con costas curvilíneas o desembocaduras fluviales. Más del 50 % de los sitios identificados tienen una obstáculo en las cercanías. Por lo tanto, se puede concluir que la presencia de una batimetría curvilínea o al menos irregular es una característica muy común de los lugares en los que se identifican SU. Por otra parte, el análisis de la presencia de SU en combinación con el forzamiento climático a lo largo de la costa española revela que su formación se ve favorecida por oleajes suaves a medios y condiciones mesomareal.

2. Analizar y cuantificar los efectos de la presencia de costas curvilíneas en la propagación del oleaje, principalmente en las variables que determinan el transporte longitudinal de sedimentos.

Los resultados obtenidos con un modelo numérico de propagación de oleaje muestran que la presencia de batimetrías curvilíneas genera importantes variaciones longitudinales en la altura de ola de rotura y, por tanto, en la energía del oleaje. Estos gradientes de energía pueden llegar al 45 % en el caso de frentes de flechas litorales, mientras que para una costa ondulada puedan llegar a más del 20 %. Para el ángulo del oleaje cerca de la costa, se han observado variaciones de 30° y 20° a lo largo de la costa para frentes de flechas litorales y costas onduladas, respectivamente. Dado que la energía y el ángulo del oleaje cerca de la costa son las principales variables que se consideran para el cálculo de las tasas de transporte de sedimentos, sus gradientes pueden producir cambios importantes en el patrón de transporte de sedimentos a lo largo de la costa.

3. Obtener una expresión para el transporte longitudinal de sedimentos que considere todos los efectos señalados en el objetivo específico anterior, y también otras características importantes de la morfodinámica de playas arenosas (tamaño del sedimento, pendiente de la playa, etc.).

Se ha obtenido una expresión del transporte longitudinal de sedimentos como una modificación de la formulación de Inman and Bagnold (1963). La expresión resultante sólo requiere datos del oleaje en profundidades indefinidas (altura significativa de ola, periodo de pico y ángulo), datos geométricos (orientación de la playa y pendiente) y la anchura de la zona de rompientes. La expresión también considera el efecto de las variaciones longitudinales del tamaño de grano, los gradientes de pendiente de la playa, y las variaciones en el tipo de rotura del oleaje. Se han obtenido dos expresiones analíticas sencillas distintas en función de la aproximación del ángulo del oleaje cerca de la costa. Por lo tanto, son herramientas útiles en la gestión de costas curvilíneas y el estudio de la formación de algunas de las morfologías litorales, como las ondulaciones de la línea de costa.

4. Analizar cómo los cambios en las condiciones del oleaje y en la configuración de la playa modifican el transporte longitudinal de sedimentos definido y la posible evolución de la línea de costa.

Se han realizado distintos experimentos numéricos con el transporte longitudinal de sedimentos obtenido previamente, en los se han variado el ángulo del oleaje en

profundidades indefinidas, el período, la altura de ola en indefinidas, la geometría de la línea de costa y la distribución de pendiente de la playa en distintas costas onduladas. Los resultados muestran tres movimientos distintos de la línea de costa: (1) las variaciones en el ángulo del oleaje en profundidades indefinidas pueden inducir la migración en la dirección de la corriente longitudinal del oleaje de las ondulaciones de la línea de costa, (2) un aumento en la altura de la ola o el periodo del oleaje y una disminución de la relación entre la longitud de onda y la amplitud de las ondulaciones puede desencadenar la formación de ondulaciones más pronunciadas sin cambios en su longitud de onda, y (3) los cambios en la distribución de la pendiente de la playa y del tamaño de grano pueden causar un cambio en la longitud de onda y la simetría de las ondulaciones.

También se analizaron las variaciones longitudinales en la disipación de energía de las oleaje y en el setup. Cuando la pendiente de la playa es mayor en las puntas que en las bahías, las variaciones en el setup pueden inducir corrientes longitudinales que se suman a las corrientes generadas por la rotura del oleaje. Por lo tanto, la generación de células de circulación cerradas se ve favorecida bajo tales condiciones. Si la pendiente de la playa es mayor en las bahías que en las puntas, este efecto no se produce.

5. Definir un modelo de evolución morfológica de la forma en planta de la costa (modelo tipo oneline) y compararlo con otras soluciones obtenidas previamente.

Se ha obtenido la ecuación del modelo de una línea y se ha realizado un análisis analítico para comparar las implicaciones en la morfología costera del transporte longitudinal de sedimentos definido en esta Tesis con los de trabajos anteriores. Para las dos expresiones analíticas del transporte de sedimentos obtenidas en este trabajo, dos términos diferentes aparecen en la ecuación del modelo de una línea. Uno se puede considerar equivalente a la difusividad clásica obtenida por Pelnard-Considère (1956). El segundo es un nuevo término que depende de periodo del oleaje, ángulo de línea de costa, anchura de la zona de rompientes y el ángulo del oleaje en profundidades indefinidas y es proporcional al gradiente longitudinal de la anchura de la zona de rompientes. Esto implica que el esquema definido en este trabajo permite considerar nuevos efectos (principalmente en el nuevo término obtenido) en la evolución morfodinámica de la costa que los trabajos anteriores no pueden tener en cuenta. Por otra parte, con este esquema no es necesaria la presencia de oleaje muy oblicuo para el desarrollo de ondulaciones de la línea de costa, ya que su desarrollo no está asociado con un cambio en el signo de la difusividad. Por lo tanto, el desarrollo de las ondulaciones parece estar relacionado con el efecto combinado de los dos términos obtenidos para la expresión analítica de la ecuación del modelo de una línea.

6. Aplicar este modelo a diferentes costas curvilíneas donde aparecen morfologías rítmicas para establecer si los nuevos procesos considerados en este trabajo son decisivos en la formación de tales morfologías.

Se ha aplicado una solución numérica del modelo de una línea a cuatro lugares distintos. En el caso de la flecha de Doñana (Sur de España), los dos ondulaciones

presentes en la punta de la flecha litoral de forma circular se han reproducido en las 500 líneas de costa modeladas con 5 años de simulación del oleaje climático. Los resultados son muy similares a las observaciones realizadas en la zona para la longitud de onda y la amplitud de las ondulaciones. Para la flecha del El Puntal (norte de España), tres eventos de formación de ondulaciones de la línea de costa han sido reproducidos utilizando el clima marítimo registrado durante esos intervalos temporales. Una vez más, los resultados son muy similares a las observaciones. Para el sistema punta-bahía de la playa de Carchuna (sur de España), la línea de costa se ha modelado teniendo en cuenta el efecto combinado de la presencia de ondulaciones sumergidas en la batimetría y un cañón submarino. El modelo reproduce la forma asimétrica de las ondulaciones de la costa y la falta de uniformidad en las separaciones longitudinales de la puntas, que son las principales características de la playa. Por último, se han obtenido resultados preliminares del modelo para un tramo de costa erosivo en las proximidades de la desembocadura de un río en el que aparecen ondulaciones de la línea de costa. Estos resultados parecen confirmar que los procesos que considera el modelo pueden ser los principales responsables de la formación de estas ondulaciones.

## **Wave climate simulation**

---

The simulation of time series of climate agents is an important tool in Civil Engineering, particularly in the application of Monte Carlo techniques for probabilistic designs. Hence, to study the temporal evolution of the shoreline, as well as the analysis of the associated uncertainty, it is important to simulate certain climatic variables that influence the morphodynamics of the coastal stretch under study. Within these variables, the most important are the significant wave height, peak wave period and the mean wave direction. In this appendix, the method used for the simulation of these climatic variables is described.

Among the applications of simulation models for climatic variables, it is important to distinguish between those that require the simulated series retains the same characteristics in terms of the time dependence as the original series and those that do not. The latter are those in which systems without memory or where the persistences are not relevant are studied (Solari and Losada, 2011). When persistences are studied or when the system has memory, as in the case of the morphodynamic evolution of a coast, it is necessary to take into account the time dependence of the series. The method described here focus on this type of simulations.

Moreover, when the interest is concentrated in the extreme behavior of the variables, the most common approach is to simulate time series of storms without simulating the average values of the variables (Callaghan et al., 2008; Payo et al., 2008). On the contrary, if the interest is on all the range of values of the variable, various authors propose methods to simulate complete series (Guedes Soares and Ferreira, 1996; Cai et al., 2007, among others). However, the latter tend to focus on the autocorrelation of the series, and not perform a rigorous check of the persistence and the extreme behavior of the simulated series.

In this appendix the application of a simulation model based on the work of Solari and Losada (2011) is described. These authors propose a parametric model to simulate complete series of wave height. The model consists of two parts: (1) the definition of a non-stationary probability distribution function that takes into account seasonal and from year to year variations, and (2) the study of the time dependence of the variable using copulas. After simulating the significant wave height, peak wave period and mean wave direction are simulated using an autoregressive vector model (VAR) in which these variables are defined from values of wave height and simulated values in previous instants of  $T_p$  y  $\theta_m$ . The fit of both models by studying a known time series, allows the simulation

of  $H_s$ ,  $T_p$  and  $\theta_m$  with a properly representation both the main-mass and the extreme regimes, and as temporal dependencies between these variables.

## A.1 Significant wave height

The parametric model of Solari and Losada (2011) for the simulation of wave height obtains temporal series with the following characteristics: (1) have the same marginal probability distribution of the original series, (2) account for the seasonal and year to year variations of the variable, (3) maintain the autocorrelation (4) maintain the persistence regime, and (5) maintain the storm regime, the peaks over threshold (POT) regime and the rate of annual maximum. This model has two main phases. The first consists in obtaining a non-stationary distribution function which varies throughout the year and from year to year. The second is to fit a model of copulas to account for the relationship between the value taken by the variable in a given instant and those that were taken in previous instants. To do that, it is assumed that the time series is a continuous Markov process of order  $k$  to be determined.

### A.1.1 Non-stationary distribution function

For the non-stationary distribution function a mixed parametric model is used. It is formed by a log-normal (LN) distribution for the central values, and two generalized Pareto distributions (GPD) for the extremal values.

$$f(x) = \begin{cases} f_m(x)F_c(u_1) & x < u_1 \\ f_c(x) & u_1 \leq x \leq u_2 \\ f_M(x)(1 - F_c(u_2)) & x \geq u_2 \end{cases} \quad (\text{A.1})$$

$$F(x) = \begin{cases} F_m(x)F_c(u_1) & x < u_1 \\ F_c(x) & u_1 \leq x \leq u_2 \\ F_c(u_2)F_M(x)(1 - F_c(u_2)) & x \geq u_2 \end{cases} \quad (\text{A.2})$$

where  $F_c$  is the LN distribution function and  $F_m$  and  $F_M$  are the minimum and maximum GPD, respectively. The parameters  $u_1$  and  $u_2$  are the thresholds for mean and extreme wave conditions, respectively. Their values are defined as dependent on time, so the seasonal variations in wave climate can be considered. In this work, these thresholds are normalized,  $Z_1$  and  $Z_2$ , so that  $F_c(u_1) = \Phi(Z_1)$  and  $F_c(u_2) = \Phi(Z_2)$ , being  $\Phi$  the standard normal distribution. Imposing continuity of the distribution and that the lower limit of the minimum GPD is zero, the five model parameters are  $(\mu_{LN}, \sigma_{LN}, \xi_2, Z_1, Z_2)$ , where  $\mu_{LN}, \sigma_{LN}$  are the mean and the standard deviation of the LN and  $\xi_2$  is the shape parameter of the minimum GPD.

To account for annual and year to year cycles, the parameters  $(\mu_{LN}, \sigma_{LN}), \xi_2$  are approximated by a Fourier series with a main period equal to the period of the estimated

variation:

$$\mu_{LN}(t) = \mu_{a0} + \sum_{k=1}^N (\mu_{ak} \cos(2\pi k t) + \mu_{bk} \sin(2\pi k t)) \quad (\text{A.3})$$

$$\sigma_{LN}(t) = \sigma_{a0} + \sum_{k=1}^N (\sigma_{ak} \cos(2\pi k t) + \sigma_{bk} \sin(2\pi k t)) \quad (\text{A.4})$$

$$\xi_2(t) = \xi_{a0} + \sum_{k=1}^N (\xi_{ak} \cos(2\pi k t) + \xi_{bk} \sin(2\pi k t)) \quad (\text{A.5})$$

where  $t$  is time in years. The parameters are set using maximum likelihood functions minimizing the negative log-likelihood functions (NLLF). It has been observed that increasing the order of the Fourier series always improves the fitting (Solari and Losada, 2011). To assess when this increase of the order brings no significant improvement of the fitting, the Bayesian Information Criterion (BIC) is used:

$$BIC = -2\log(L) + \log(N_d)p \quad (\text{A.6})$$

where  $L$  is the value of the likelihood function,  $N_d$  is the number of data available and  $p$  is the number of model parameters. Thus, the model chosen is the one with lowest BIC, being penalized the number of parameters to be estimated.

Once the parameters are estimated, the cumulative probability function for the period  $(t, t + T)$  is estimated as follows:

$$P(H \leq H^*) = \frac{1}{T} \int_t^{t+T} P(H \leq H^* | t) dt \quad (\text{A.7})$$

where  $P(H \leq H^* | t)$  is given by the non-stationary LN-GPD model (NS-LN-GDP), which is the non-stationary version of A.1:

$$P(x_t | t) = \begin{cases} F_m(x_t | t) \Phi(Z_1) & x < u_1(t) \\ F_c(x_t | t) & u_1(t) \leq x_t \leq u_2(t) \\ \Phi(Z_2) F_M(x_t | t) (1 - \Phi(Z_2)) & x \geq u_2(t) \end{cases} \quad (\text{A.8})$$

### A.1.2 Temporal dependence

With the NS-LN-GPD model (Eq. A.8), the non-stationary wave height series  $H_t$  is transformed into a stationary series with a uniform distribution  $P_t \sim \mathcal{U}(0, 1)$ , so that  $P_t =$

$Prob[H \leq H_t | t]$ . This allows the use of the copulas theory to model the joint distribution of  $(P_t, P_{t+1}, \dots, P_{t+n})$ , and therefore, the temporal dependence of the variable.

The use of copulas to define multivariate distribution functions is based on the Skalar theorem: ‘‘Given a joint distribution  $F_{XY}$  with marginal distributions  $F_X$  y  $F_Y$ , then there is a copula such that  $F_{XY} = Prob[X \leq x, Y \leq y] = C(F_X(x), F_Y(y))$ ’’. For details about the copulas theory, the reader is referred to Joe (1997) and Nelsen (2006).

#### A.1.2.1 Markov model of first order

To analyze the temporal dependence between to following term of the series, the bi-variate vector  $(P_{t-1}, P_t)$  is defined. The dependence between both variables is assessed with the Kendall's ( $\tau_k$ ) or Spearman's ( $\rho_s$ ) statistics (Solari and Losada, 2011). If this dependence exists, the joint probability of  $(P_t, P_{t+1})$  can be obtained with a copula:

$$C_{12}(u, v) = Prob[P_t \leq u, P_{t+1} \leq v] \quad (A.9)$$

with  $u, v \in [0, 1]$ . With this copula, the conditioned probability function that defines the distribution of  $P_{t+1}$  given  $P_t$ , and the first order Markov process can be obtained.

#### A.1.2.2 Markov model of second and higher orders

To study if the order of the Markov chain has to be increased, it is necessary to analyze the temporal dependence between  $P_t$  y  $P_{t+2}$  that is not explained for the dependence between  $P_t$  and  $P_{t+1}$ . If this dependence (assessed though  $\tau_k$  or  $\rho_s$ ) exists, then a trivariate copula  $C_{123}$  has to be built:

$$C_{123}(u, v, w) = Prob[P_t \leq u, P_{t+1} \leq v, P_{t+2} \leq w] \quad (A.10)$$

With the same methodology can be applied to obtain the Markov chains of higher orders by analyzing the dependence between the variables  $P_t$  and  $P_{t+3}$ ,  $P_t$  and  $P_{t+4}$  and so on. The process has to be repeated until the dependence between  $P_t$  and  $P_{t+k}$  which is not explained by  $C_{1\dots k}$  is negligible, obtaining a Markov chain of order  $k$ .

### A.1.3 Application to the Gulf of Cádiz

This methodology for the wave climate simulation was applied to the area of the Guadalquivir river mouth. Particularly, a fit of the model was performed using a 13 years wave climate series of the hindcasting point WANA 1052046 (Puertos del Estado, Spanish Ministry of Public Works).

The fit of the non-stationary distribution function was done by obtaining the distribution parameters  $\mu_{LN}$ ,  $\sigma_{LN}$  and  $\xi_2$  with Eqs. (A.3 to A.5) for the orders 1 to 12. After fitting the temporal series and obtaining the BIC, the chosen model is the [411], being 4, 1 and 1 the approximation orders of  $\mu_{LN}$ ,  $\sigma_{LN}$  and  $\xi_2$ , respectively. Fig. (A.1) shows the evolution

during t  
rest of th

than the

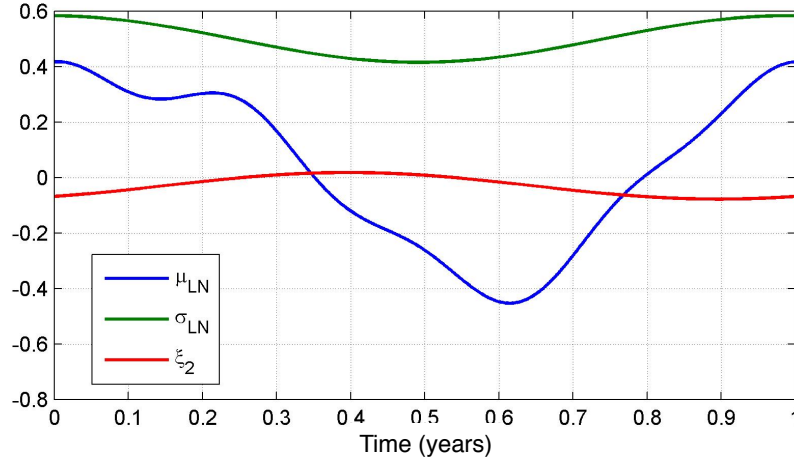


Figure A.1: Time evolution of  $\mu_{LN}$  (blue),  $\sigma_{LN}$  (green),  $\xi_2$  (red)

Regarding the analysis of the temporal dependence, different types of copules were studied for the zone. Finally, a asymmetric Gumbell-Hougaard copula was chosen for the Markov chain of order 1, and two Frechet copulas were chosen for the orders 2 and 3. The choice between the different types of copulas was done by a visual evaluation of the fit and the assessment of the log-likelihood function (LLF). Table (A.1) shows a summary of the parameters obtained for the different copulas.

$C_{12}$			$C_{13}$		$C_{14}$	
G-H Asim			Frechet		Frechet	
$\theta$	$\theta_1$	$\theta_2$	$\alpha$	$\beta$	$\alpha$	$\beta$
5.697	0.995	0.971	0	0.194	0.005	0

Table A.1: Fitted parameters of the copulas obtained with the NS-LN-GPD [4 1 1] distribution

Once the copulas are defined, the process to obtain a time series of simulated wave heights is the following:

1. Three probability values are generated randomly, as they are necessary to obtain a fourth value with a Markov chain of order 3.
2. With these three values ( $P_{t-1}, P_{t-2}, P_{t-3}$ ),  $P_t$  is obtained with the defined copulas. Thus, the probability values of a complete time series can be obtained using previously calculated values.
3. Once all the probability values are generated, the complete wave height series is obtained using the inverse distribution function of the NS-LN-GPD (Eq. A.7). This series has the same temporal dependences and seasonal and year to year variations as the original series.



## A.2 Peak wave period and mean wave angle

With the simulated series of wave height, the series for the peak wave period and mean wave direction can be obtained using previous values of these two series, and also previous and subsequent values of the wave height. With this method, the temporal dependence between consecutive values is kept and the final series have better statistical parameters than those obtained with conventional simulation methods. To do that, vector autoregressive models (VAR) are used, in which a linear relationship between the variables needed to calculate the period and wave direction at any given moment is assumed. The coefficients of the resulting system are adjusted using the known time series by least squares.

The methodology has three main steps:

1. Estimation of the non-stationary distribution functions of the peak wave period and the mean wave direction, and normalization of these functions with a univariate standard normal distribution.
2. Fitting of the VAR model, used to explain the temporal dependence and the interdependency of the normalized variables.
3. Simulation of the time series. This step has two phases: (1) simulations of the normalized variables  $Z_i$  through the fitted VAR, and (2) transformation of the normalized variables into the original ones with the non-stationary distributions fitted before.

### A.2.1 Non-stationary distribution functions and normalization of the variables

#### A.2.1.1 Peak period

For the wave peak period, a mixed model with two log-normal distributions (LN) was defined:

$$f(x) = \alpha f_{LN1}(x) + (1 - \alpha) f_{LN2}(x) \quad (\text{A.11})$$

The parameters of the distribution are  $(\mu_1, \sigma_1, \mu_2, \sigma_2, \alpha)$ , with  $\sigma_1, \sigma_2 > 0$  and  $0 \leq \alpha \leq 1$ . These parameters are time dependent and are expressed in terms of a Fourier series (Eqs. A.3 to A.5).

#### A.2.1.2 Mean direction

For the wave mean direction, the fitted probability function is a mixed model with 4 stationary normal distributions truncated on  $0^\circ$  and  $360^\circ$ :

$$f(x) = \sum_{i=1}^4 \alpha_i f_{Ni}(x) [F_{Ni}(360) - F_{Ni}(0)]^{-1} \quad (\text{A.12})$$

where  $f_N$  and  $F_N$  are the density and distribution functions of the normal distribution, respectively, and  $\sum_{i=1}^4 \alpha_i = 1$ . The position and shape parameters of the distributions are  $\mu_{Ni}$  and  $\sigma_{Ni} > 0$ .

### A.2.1.3 Normalization of the variables

To perform the normalization of variables, a process in which the series is converted into a stationary one, the time series of values of significant wave height, peak period and mean direction are transformed into series of probabilities through the functions distribution defined for each variable. Subsequently, these likelihood vectors are normalized by a univariate normal probability distribution, with mean  $\mu = 0$  and standard deviation  $\sigma = 1$

## A.2.2 Vector Autoregressive (VAR) Model

The VAR models of order  $p$  are given by (Lütkepohl, 2005):

$$y_t = v + \sum_{i=1}^p A_i y_{t-i} + \sum_{i=1}^q B_i v_{t-i-d} + u_t \quad (\text{A.13})$$

where  $y_t$  is the vector of normalized variables to be determined in the instant  $t$ ,  $v$  is the vector with the mean values of the variables,  $p$  is the order of the model (number of previous data of peak period and mean direction that are accounted for the assessment of the variables in every instant),  $A_i$  is the matrix of autoregressive coefficients,  $q$  is the number of values of an external variable (wave height) accounted for the calculation of  $y_t$ ,  $d$  is the delay with which these values are taken into account ( $d < 0$  take into account values of  $v$  in subsequent instants to  $t$ ),  $v$  is the external variable, and  $u_t$  is the *white noise*. The latter has a mean equal to zero ( $E(u_t) = 0$ ), and fulfills  $E(u_t u_t') = \Sigma_u$  and  $E(u_t u_s') = 0$  for  $s \neq t$ , being  $\Sigma_u$  the covariance matrix of the errors of the registered data series, obtained as the difference between the estimated values and the original wave climate series.

To fit the model, the values of  $A_i$  y  $B_i$  have to be fitted using the original data series. In this case, a least squares fit was used, and the following matrix system was defined:

$$Y = BZ + U \quad (\text{A.14})$$

After the fitting, the matrix of autocorrelation coefficients  $B$  is obtained:

$$\hat{B} = YZ^{-1}(ZZ')^{-1} \quad (\text{A.15})$$

On the other hand, the parameters  $(p, q, d)$  of the VAR model have to be defined. To do that, the BIC (Eq. A.6) is used again, obtaining its value for every combination of  $(p, q, d)$ . The chosen model (the optimum) is the one with a smaller value of BIC.

For the simulation of the peak period and the mean direction in the Guadalquivir river mouth, the VAR model was fitted using the hindcasting point WANA 1052046 (Puertos del

Estado, Spanish Ministry of Public Works). The optimum model defined after the BIC calculations has the parameters  $p = 6, q = 9, d = -6$ . Hence, to start the simulation, once the complete series of wave height is obtained, 6 random values for the normalized peak period and mean direction have to be generated. With these values and the wave height series, the complete series of the normalized variables of  $T_p$  y  $\theta_m$  is generated through the system defined in Eq. (A.13). From these values the associated probabilities are calculated with the cumulative probability function corresponding to the normal distribution. The values of the simulated variables are obtained with the inverse of the non-stationary distribution functions adjusted to each variable.

# Bibliography

---

- Allard, J., Bertin, X., Chaumillon, E., and Pouget, F. (2008). Sand spit rhythmic development: A potential record of wave climate variations? Arçay Spit, western coast of France. *Marine Geology*, 253(3-4):107–131.
- Apotsos, A., Raubenheimer, B., Elgar, S., and Guza, R. T. (2008). Wave-driven setup and alongshore flows observed onshore of a submarine canyon. *Journal of Geophysical Research*, 113(C7):1–9.
- Ashton, A. and Murray, A. B. (2006a). High-angle wave instability and emergent shoreline shapes: 1. Modeling of sand waves, flying spits, and capes. *Journal of Geophysical Research*, 111(F04):F04011.
- Ashton, A. and Murray, A. B. (2006b). High-angle wave instability and emergent shoreline shapes: 2. Wave climate analysis and comparisons to nature. *Journal of Geophysical Research*, 111(F04012).
- Ashton, A., Murray, A. B., and Arnoult, O. (2001). Formation of coastline features by large-scale instabilities induced by high-angle waves. *Nature*, 414(6861):296–300.
- Bakker, W. and Edelman, T. (1965). The coastline of river deltas. *Coastal Engineering Proceedings*, 1(9).
- Ballesteros, M., Rivera, J., Muñoz, a., Muñoz Martín, a., Acosta, J., Carbó, a., and Uchupi, E. (2008). Alboran Basin, southern Spain-Part II: Neogene tectonic implications for the orogenic float model. *Marine and Petroleum Geology*, 25(1):75–101.
- Baquerizo, A. and Losada, M. (1999). Wave height to depth ratio in front of coastal structures. *Proceedings of Coastal Structures*.
- Baquerizo, A. and Losada, M. A. (2008). Human interaction with large scale coastal morphological evolution. An assessment of the uncertainty. *Coastal Engineering*, (55):569–580.
- Bárcenas, P., Lobo, F., Macías, J., Fernández-Salas, L. M., and Díaz del Río, V. (2011). Spatial variability of surficial sediments on the northern shelf of the Alboran Sea : the effects of hydrodynamic forcing and supply of sediment by rivers. *Journal of Iberian Geology*, 37(2):195–214.
- Bird, E. (2010). *Encyclopedia of the World's Coastal Landforms*. Springer.

- Booij, N., Ris, R. C., and Holthuijsen, L. H. (1999). A third-generation wave model for coastal regions 1. Model description and validation. *Journal of Geophysical Research*, 104(C4):7649–7666.
- Bosboom, J., Aarninkhof, S., Reniers, A., Roelvink, J., and Walstra, D. (1997). Unibest-tc 2.0. *Overview of model formulations. Delft Hydraulics report H*, 2305:42.
- Bramato, S., Ortega-Sánchez, M., Mans, C., Losada, M. A., and . (2012). Natural Recovery of a Mixed Sand and Gravel Beach after a Sequence of a Short Duration Storm and Moderate Sea States. *Journal of Coastal Research*, 279:89–101.
- Bruun, P. (1954). Migrating sand waves or sand humps, with special reference to investigations carried out on the Danish North Sea Coast. In *Fifth conference on coastal engineering*, pages 269–295. ASCE.
- Cai, Y., Gouldby, B., Dunning, P., and Hawkes, P. (2007). A simulation method for flood risk variables. In *2nd IMA Intl. Conf. Flood Risk Assessment, Institute of Mathematics and its Applications, Southend, UK*, pages 85–95.
- Callaghan, D., Nielsen, P., Short, a., and Ranasinghe, R. (2008). Statistical simulation of wave climate and extreme beach erosion. *Coastal Engineering*, 55(5):375–390.
- Carter, R., Woodroffe, C., and 274, I. P. (1997). *Coastal Evolution: Late Quaternary Shoreline Morphodynamics*. Cambridge University Press.
- Coco, G. (2004). The role of tides in beach cusp development. *Journal of Geophysical Research*, 109(C4):C04011.
- Coco, G. and Murray, A. B. (2007). Patterns in the sand: From forcing templates to self-organization. *Geomorphology*, 91(3-4):271–290.
- Corniero, M. A. and Giménez-Curto, L. A. (2012). Discussion of “A note on wave-induced set-up by obliquely incident waves” by T.T. Janssen and I.S. Jones, *Coastal Engineering*, 58, 812-814, 2011. *Coastal Engineering*, 68:103–104.
- Dabees, M. and Kamphuis, J. W. (1998). ONELINE, A numerical model for shoreline change. In *Coastal Engineering Proceedings*, pages 2668–2681.
- Dan, S., Walstra, D.-J. R., Stive, M. J., and Panin, N. (2011). Processes controlling the development of a river mouth spit. *Marine Geology*, 280(1-4):116–129.
- Davidson-Arnott, R. G. D. and Heyningen, A. G. V. (2003). Migration and sedimentology of longshore sandwaves, Long Point, Lake Erie, Canada. *Sedimentology*, 50:1123–1137.
- Davis, R. and Fitzgerald, D. (2003). *Beaches and Coasts*. Wiley.
- Dean, R. and Dalrymple, R. (2002a). *Coastal Processes with Engineering Applications*. Cambridge University Press.
- Dean, R. G. (2002). *Beach Nourishment: Theory and Practice*. Wiley-Interscience, New York.

- Dean, R. G. and Dalrymple, R. A. (1991). *Water wave mechanics for engineers and scientist*. World Scientific.
- Dean, R. G. and Dalrymple, R. A. (2002b). *Coastal processes with engineering applications*. Cambridge University Press.
- del Valle, R., Medina, R., and Losada, M. (1993). Dependence of coefficient  $k$  on grain size. *J. Waterw. Port Coast. Ocean Eng.*, 5:568–574.
- Díez-Minguito, M., Baquerizo, A., Ortega-Sánchez, M., and Losada, M. A. (2012). Tide transformation in the Guadalquivir estuary (SW Spain) and process-based zonation. *Journal of Geophysical Research*, in press.
- Dodd, N., Stoker, A. M., Calvete, D., and Sriariyawat, A. (2008). On beach cusp formation. *J. Fluid Mech.*, 597.
- Falqués, A. and Calvete, D. (2005). Large-scale dynamics of sandy coastlines: Diffusivity and instability. *Journal of Geophysical Research*, 110(C03007).
- Fernández-Salas, L., Dabrio, C., Goy, J., Díaz del Río, V., Zazo, C., Lobo, F., Sanz, J., and Lario, J. (2009). Land-sea correlation between Late Holocene coastal and infralittoral deposits in the SE Iberian Peninsula (Western Mediterranean). *Geomorphology*, 104(1-2):4–11.
- Foster, T. and Skou, A. (1992). Litpack, an integrated modelling system for littoral processes and coastline kinetics. *3rd International Software Exhibition for Environmental Science & Engineering, Como, Italy*.
- Gorrell, L., Raubenheimer, B., Elgar, S., and Guza, R. (2011). SWAN predictions of waves observed in shallow water onshore of complex bathymetry. *Coastal Engineering*, 58(6):510–516.
- Gravens, M., Kraus, N., and Hanson, H. (1991). GENESIS: Generalized model for simulating shoreline change. Technical Report 2009, USACE, CERC.
- Guedes Soares, C. and Ferreira, A. M. (1996). Representation of non-stationary time series of significant wave height with autoregressive models. *Probabilistic Engineering Mechanics*, 11(3):139–148.
- Holloway, G. and Sou, T. (1996). Measuring the skill of an ocean model under eddy-topographic effects, based on a global inventory of long-term current meters. In *8th Topographic effects in the ocean; Hawaiian winter workshop*, pages 253–256. School of Ocean and Earth Science and Technology.
- Inman, D. L. and Bagnold, R. A. (1963). *Littoral processes*. In: *The sea*, volume 3. Wiley-Interscience, New York.
- Iribarren, C. and Nogales, C. (1949). Protection des ports. *XVII Int. Nav. Cong. Lisbon*, pages 180–193.

- Joe, H. (1997). *Multivariate models and dependence concepts*. Chapman & Hall/CRC.
- Kaergaard, K. and Fredsoe, J. (2013a). Numerical modeling of shoreline undulations part 1: Constant wave climate. *Coastal Engineering*, 75:64–76.
- Kaergaard, K. and Fredsoe, J. (2013b). Numerical modeling of shoreline undulations part 2: Varying wave climate and comparison with observations. *Coastal Engineering*, 75:77–90.
- Kaergaard, K., Fredsoe, J. r., and Knudsen, S. r. B. (2012). Coastline undulations on the West Coast of Denmark: Offshore extent, relation to breaker bars and transported sediment volume. *Coastal Engineering*, 60:109–122.
- Kamphuis, J. W. (1991). Alongshore sediment transport rate. *J. Waterw. Port Coastal Ocean Eng.*, 117:624–640.
- Komar, P. D. (1998). *Beach processes and sedimentation*. Prentice-Hall, Upper Saddle River, NJ, 2nd edition.
- Lario, J., Zazo, C., and Goy, J. (1999). Fases de progradacion y evolucion morfosedimentaria de la flecha litoral de Calahonda (Granada) durante el Holoceno. *Estudios Geológicos*, 250:247–250.
- Larson, M., Hanson, H., and Kraus, N. C. (1997). Analytical solutions of one-line model for shoreline change near coastal structures. *Journal of Waterway, Port, Coastal, and Ocean Engineering*, 123(August):180–191.
- LeMehaute, B. and Soldate, M. (1977). Mathematical Modeling of Shoreline Evolution. Technical Report 2009, USACE, CERC.
- Lesser, G., Roelvink, J., van Kester, J., and Stelling, G. (2004). Development and validation of a three-dimensional morphological model. *Coastal Engineering*, 51(8-9):883–915.
- Lindhorst, S., Fürstenau, J., Hass, H. C., and Betzler, C. (2010). Anatomy and sedimentary model of a hooked spit (Sylt, southern North Sea). *Sedimentology*, 57(4):935–955.
- Longuet-Higgins, M. S. (1970). Longshore current generated by obliquely incident sea waves. 1. *Journal of Geophysical Research*, 75(33):6778–6789.
- López-Ruiz, A., Ortega-Sánchez, M., Baquerizo, A., and Losada, M. (2012a). Short and medium-term evolution of shoreline undulations on curvilinear coasts. *Geomorphology*, 159-160:189–200.
- López-Ruiz, A., Ortega-Sánchez, M., Baquerizo, A., Navidad, D., and Losada, M. (2012b). Nonuniform alongshore sediment transport induced by coastline curvature. In *33th Coastal Engineering Conference*, pages 3046–3052. Electronic edition, Texas Digital Library.
- Losada, M. A. (2009). *Recommendations for maritime works 1.0-09*. Puertos del Estado, Spanish Ministry of Public Works.

- Losada, M. A., Baquerizo, A., Ortega-Sánchez, M., and Ávila, A. (2011). Coastal Evolution , Sea Level , and Assessment of Intrinsic Uncertainty. *Journal of Coastal Research*, 59(59).
- Lütkepohl, H. (2005). *New introduction to multiple time series analysis*. Springer.
- Magne, R., Belibassakis, K. a., Herbers, T. H. C., Ardhuin, F., O'Reilly, W. C., and Rey, V. (2007). Evolution of surface gravity waves over a submarine canyon. *Journal of Geophysical Research*, 112(C1):C01002.
- Marinone, S. (1998). Effect of the topographic stress on the tide- and wind-induced residual currents in the Gulf of California. *Journal of Geophysical Research: Oceans*, 103:18437–18446.
- Martínez, M., Intralawan, A., Vázquez, G., Pérez-Maqueo, O., Sutton, P., and Landgrave, R. (2007). The coasts of our world: Ecological, economic and social importance. *Ecological Economics*, 63(2-3):254–272.
- Masselink, G. (2004). Test of edge wave forcing during formation of rhythmic beach morphology. *Journal of Geophysical Research*, 109(C6):C06003.
- Masselink, G. and Short, A. (1993). The Effect of Tide Range on Beach Morphodynamics and Morphology: A Conceptual Beach Model. *Journal of Coastal Research*, page 500.
- Medellín, G., Falqués, A., Medina, R., and González, M. (2009). Coastline sand waves on a low-energy beach at El Puntal spit, Spain: Linear stability analysis. *Journal of Geophysical Research*, 114(C03022).
- Medellín, G., Medina, R., Falqués, A., and González, M. (2008). Coastline sand waves on a low-energy beach at El Puntal spit, Spain. *Marine Geology*, 250(2-4):143–156.
- Muñoz, A., Ballesteros, M., Montoya, I., Rivera, J., Acosta, J., and Uchupi, E. (2008). Alborán Basin, southern Spain-Part I: Geomorphology. *Marine and Petroleum Geology*, 25(1):59–73.
- Nam, P. T., Larson, M., Hanson, H., and Hoan, L. X. (2009). A numerical model of nearshore waves, currents, and sediment transport. *Coastal Engineering*, 56(11-12):1084–1096.
- Nelsen, R. (2006). *An introduction to copulas*. Springer Verlag.
- Noda, E. K. (1974). Wave-induced nearshore circulation. *Journal of Geophysical Research*, 79(27):4097–4106.
- Nolan, T., Kirk, R., and Shulmeister, J. (1999). Beach cusp morphology on sand and mixed sand and gravel beaches, South Island, New Zealand. *Marine Geology*, 157:185–198.
- Nordstrom, K. F., Allen, J. R., Sherman, D. J., and Psuty, N. P. (1978). Management considerations for beach nourishment at Sandy Hook, New Jersey, U.S.A. *Coastal Engineering*, 2:215–236.
- Olabarrieta, M., Warner, J. C., and Kumar, N. (2011). Wave-current interaction in Willapa Bay. *Journal of Geophysical Research*, 116(C12):C12014.



- Ortega-Sánchez, M., Bramato, S., Quevedo, E., Mans, C., and Losada, M. (2008a). Atmospheric-hydrodynamic coupling in the nearshore. *Geophysical Research Letters*, 35, L23601 doi:10.1029/2008GL036043(L23601).
- Ortega-Sánchez, M., Fachin, S., Sancho, F., and Losada, M. A. (2008b). Relation between beachface morphology and wave climate at Trafalgar beach (Cádiz, Spain). *Geomorphology*, 99(1-4):171–185.
- Ortega-Sánchez, M., López-Ruiz, A., Baquerizo, A., and Losada, M. (2015). Shoreline undulations. In Kennish, M. J., editor, *Encyclopedia of Estuaries*. Springer (in press).
- Ortega-Sánchez, M., Losada, M., and Baquerizo, A. (2003a). On the development of large-scale cusped features on a semi-reflective beach: Carchuna beach, Southern Spain. *Marine Geology*, 198(3-4):209–223.
- Ortega-Sánchez, M., Losada, M., and Baquerizo, A. (2003b). On the development of large-scale cusped features on a semi-reflective beach: Carchuna beach, Southern Spain. *Marine Geology*, 198(3-4):209–223.
- Ortega-Sánchez, M., Quevedo, E., Baquerizo, A., and Losada, M. A. (2008c). Comment on “High-angle wave instability and emergent shoreline shapes: 1. Modeling of sand waves, flying spits, and capes” by Andrew D. Ashton and A. Brad Murray. *Journal of Geophysical Research*, 113(F1):1–2.
- Ozasa, H. and Brampton, A. H. (1980). Mathematical modelling of beaches backed by seawalls. *Coastal Engineering*, 4(1968):47–63.
- Park, J.-Y. and Wells, J. T. (2007). Spit growth and downdrift erosion: Results of longshore transport modeling and morphologic analysis at the Cape Lookout cusped foreland. *Journal of Coastal Research*, 3(23):553–568.
- Payo, A., Baquerizo, A., and Losada, M. (2002). One-line model with time dependent boundary conditions. In *28th Coastal Engineering Conference*, pages 3046–3052. World Scientific.
- Payo, A., Baquerizo, A., and Losada, M. (2008). Uncertainty assesment: application to the shoreline. *Journal of Hydraulic Research*, 46:94–104.
- Pelnard-Considère (1956). Essai de theorie de lévolution des formes de rivage en plages de sable et de galets. *4th Journees de l'Hydraulique, Les Energies de la Mer, III*, pages 289–298.
- Petersen, D., Deigaard, R., and Fredsøe, J. (2008). Modelling the morphology of sandy spits. *Coastal Engineering*, 55(7-8):671–684.
- Pethick, J. (1984). *An introduction to coastal geomorphology*. Edward Arnold.
- Pocinki, L. S. (1950). The application of conformal transformations to ocean wave refraction problems. *Trans. Am. Geophys. Union*, 31:856–860.

- Price, W., Tomlinson, K., and Willis, D. (1972). Predicting changes in the plan shape of beaches. *Coastal Engineering Proceedings*, 1(13).
- Quevedo, E., Baquerizo, a., Losada, M., and Ortegasanchez, M. (2008). Large-scale coastal features generated by atmospheric pulses and associated edge waves. *Marine Geology*, 247(3-4):226–236.
- Reis, A. H. and Gama, C. (2010). Sand size versus beachface slope - An explanation based on the Constructal Law. *Geomorphology*, 114(3):276–283.
- Rodríguez-Ramírez, A., Rodríguez-Vidal, J., Cáceres, L., Clemente, L., Belluomini, G., Manfra, L., Improta, S., and de Andrés, J. (1996). Recent coastal evolution of the Doñana national park (SW Spain). *Quaternary Science Reviews*, 15(8-9):803–809.
- Ruiz, F., Rodríguez-Ramírez, A., Cáceres, L. M., Rodríguez-Vidal, J., Carretero, M. I., Clemente, L., Muñoz, J. M., Yañez, C., and Abad, M. (2004). Late Holocene evolution of the southwestern Doñana National Park (Guadalquivir Estuary, SW Spain): a multivariate approach. *Palaeogeography, Palaeoclimatology, Palaeoecology*, 204(1-2):47–64.
- Schwartz, M. L. (2006). *Encyclopedia of coastal science*. Springer.
- Short, A. (2001). *Handbook of beach and shoreface morphodynamics*. John Wiley & Sons.
- Solari, S. and Losada, M. A. (2011). Non-stationary wave height climate modelling and simulation. *Journal of Geophysical Research*, 116(C9):1–18.
- Stewart, C. J. and Davidson-Arnott, R. G. D. (1988). Morphology, formation and migration of longshore sandwaves; Long Point, Lake Eire, Canada. *Marine Geology*, 81(1-4):63–77.
- Tamura, T. (2012). Beach ridges and prograded beach deposits as palaeoenvironment records. *Earth-Science Reviews*, 114(3-4):279–297.
- Thevenot, M. M. and Kraus, N. C. (1995). Longshore sand waves at Southampton Beach, New York: observation and numerical simulation of their movement. *Marine Geology*, 126:249–269.
- Todd Holland, K. (1998). Beach cusp formation and spacings at Duck, USA. *Continental Shelf Research*, 18(10):1081–1098.
- USACE (1984). Shore protection manual. *Coastal Engineering Research Center, Government Printing Office, Washington DC*.
- Verhagen, H. J. (1989). Sand waves along the dutch coast. *Coastal Engineering*, 13(2):129–147.
- Wolinsky, M. A. (2009). A unifying framework for shoreline migration: 1. Multiscale shoreline evolution on sedimentary coasts. *Journal of Geophysical Research*, 114(F1):1–12.
- Wood, D. J., Muttray, M., and Oumeraci, H. (2001). The {SWAN} model used to study wave evolution in a flume. *Ocean Engineering*, 28(7):805 – 823.

---

Woodroffe, C. (2002). *Coasts: Form, Process and Evolution*. Coasts: Form, Process, and Evolution. Cambridge University Press.